Atomic Layer Deposition and Lithium-ion Batteries: Studies on new materials and reactions for battery development

Miia Mäntymäki

Department of Chemistry
Faculty of Science
University of Helsinki
Helsinki, Finland

ACADEMIC DISSERTATION

To be presented, with the permission of the Faculty of Science of the University of Helsinki, for public criticism in Auditorium A110 of the Department of Chemistry (Chemicum), A. I. Virtasen aukio 1, on June 9th at 12 o'clock noon.

Helsinki 2017

Supervisors

Professor Mikko Ritala
Professor Markku Leskelä
Department of Chemistry
University of Helsinki
Helsinki, Finland

Reviewers

Professor Fred Roozeboom
Department of Applied Physics
Eindhoven University of Technology
Eindhoven, the Netherlands

Assistant Professor Neil Dasgupta
Department of Mechanical Engineering
University of Michigan
Ann Arbor, U.S.A.

Opponent

Professor Ola Nilsen
Department of Chemistry
University of Oslo
Oslo, Norway

ISBN 978-951-51-3253-6 (paperback)
ISBN 978-951-51-3254-3 (PDF)
http://ethesis.helsinki.fi/

Unigrafia
Helsinki 2017

Bang my head against the wall
Though I feel light-headed, now I know I will not fall
I will rise above it all
Found what I was searching for
Though I feel light-headed
I should have failed, and nailed the floor
Instead I rose above it all
David Guetta feat. Sia & Fetty Wap, Bang my head

Abstract

The increasing interest in both portable electronic devices and electric vehicles has given rise to a new wave of research into lithium-ion batteries. Lithium-ion batteries are the technology of choice for these applications, as they offer both high power and high energy densities. However, much research on this subject is still needed to answer the technology demands of future applications. For example, the safety concerns related to liquid electrolytes in the batteries of electric vehicles could be resolved by moving to all-solid-state batteries, which would not combust in the case of an accident. In addition, all-solid-state batteries could be manufactured into 3D structures, which would decrease the footprint area of the battery without sacrificing the amount of material. Thus, these structures would make even higher energy densities possible, which is important for example for laptops and cellphones. In addition, by combining smaller batteries with energy harvesters, such as solar cells, integrated autonomous devices could be realized.

Atomic layer deposition, or ALD, is a thin film deposition method based on sequential, saturative reactions of gaseous precursors with a substrate surface. ALD generally produces highly pure films with very good thickness uniformity also in difficult, 3D substrates. Therefore, ALD should be well-suited for the deposition of Li-ion battery materials for future applications.

The deposition of lithium containing materials is a fairly new avenue for ALD, the first paper being published only in 2009. It has been found that the Li-ion often bends the basic rules of ALD with its high reactivity and mobility during film growth, resulting in both unexpected reactions and film stoichiometries.

This thesis provides a comprehensive review on the atomic layer deposition of lithium containing materials with a focus on the behavior of lithium in the growth process. In the experimental part, new ALD processes were developed for potential Li-ion battery materials LiF and AlF_3. Both processes show reasonable ALD characteristics and produce pure films in proper deposition temperatures. In addition, conversion reactions taking place in ALD conditions were studied, and both LiF and Li_3AlF_6 were deposited using these reactions. The conversions were very clean, illustrated by the low impurity contents of the converted films. Lastly, the deposition of lithium containing ternary oxides was studied by heating atomic layer deposited film stacks in air. This ALD-solid state reaction -procedure resulted in pure, crystalline films of $LiTaO_3$, $LiNbO_3$ and Li_2TiO_3.

Preface

The work summarized in this thesis was performed in the Laboratory of Inorganic Chemistry of the University of Helsinki between 2010 and 2016. I wish to thank ASM Microchemistry Oy for their financial support during these years. I would also like to thank Kemian Päivien Säätiö and Walter Ahlströmin Säätiö for personal grants.

I am thankful to Professors Mikko Ritala and Markku Leskelä for giving me the opportunity to work in their group and learn ALD and ALD precursor synthesis from the very best. I am also grateful for their support for my other activities, namely teaching. I have not only been able to teach others, but also learn a lot myself.

I would like to thank the pre-examiners of this work, Professor Fred Roozeboom and Assistant Professor Neil Dasgupta, for their feedback and encouragement. Professor Ola Nilsen is thanked for taking on the task of being the opponent of this work.

The research papers comprising this thesis were the effort of many people besides myself. Dr. Jani Hämäläinen is thanked for teaching me so much about ALD and reactor related things. It was always a pleasure discussing reactor issues (and general lab maintenance things) with you. I am especially thankful for the elastic recoil detection analysis work of Dr. Kenichiro Mizohata, Prof. Timo Sajavaara, and Dr. Frans Munnik: without your contributions, I wouldn't have known where my lithium was. Dr Benoît Marchand is thanked for the XPS measurements, and Prof. Jyrki Räisänen for the smooth co-operation between our laboratory and the Ion Beam Division of the Department of Physics. Mr. Mikko J. Heikkilä is thanked for all the X-ray related help over the years (and the strange music you exposed me to during our discussions and experiments). Dr. Esa Puukilainen and Mr. Miika Mattinen are thanked for the AFM measurements. Lastly, I would like to thank Ms. Elisa Atosuo for all her hard work and dedication to her master's thesis project.

In addition to the names in the manuscripts, many others have contributed greatly to my work. I would like to thank Mr. Timo Hatanpää for teaching me about synthesis work and the related analysis methods. Dr. Marianna Kemell is thanked for all her help with the FESEM and EDX and for always having time for my stupid questions. Dr. Marko Vehkamäki is thanked for his help in evaporating metals for use in electrical measurements and discussions on the subject. Mrs. Sanni Seppälä is thanked for providing me with zirconia films. Mr. Mikko Nisula is

thanked for spending his valuable time looking at my samples with EIS (maybe someday one will actually work…) Lastly, Dr. Kjell Knapas is thanked for all the fun times spent on teaching. Ten years well spent.

I wouldn't have made it through these years without some therapeutic help from a bunch of great people. Leo, Emma, Heikkilä, Elina, and Maarit, it has been a pleasure working with you and also hanging out with you outside of work. Without you I would have surely gone insane. And Tiina, you are the best "työvaimo" a girl could have!

Lastly, I am ever so grateful for all the love and support I have always received from my family. Finally, I must also thank Dr. Esko and Kylli the Cat for making the past year fun as hell.

Helsinki, May 2017

Miia Mäntymäki

List of publications

This thesis consists of a literature summary and publications, which are listed below. In the text the publications are referred to by their Roman numerals. The author's contributions are listed below each paper.

I **Double metal alkoxides of lithium: Synthesis, structure and applications in materials chemistry**
Miia Mäntymäki, Mikko Ritala, and Markku Leskelä
Coord. Chem. Rev. 256 (**2012**) 854–877.
The author compiled the literature and wrote the review, taking into account feedback from the co-authors.

II **Atomic layer deposition of LiF thin films from Lithd and TiF_4 precursors**
Miia Mäntymäki, Jani Hämäläinen, Esa Puukilainen, Frans Munnik, Mikko Ritala, and Markku Leskelä
Chem. Vap. Deposition 19 (**2013**) 111–116.
The author made the deposition experiments and did the UV-Vis, GIXRD and FESEM analyses, wrote the first draft of the paper and finalized it with M.R. and M.L.

III **Atomic layer deposition of LiF thin films from Lithd, $Mg(thd)_2$, and TiF_4 precursors**
Miia Mäntymäki, Jani Hämäläinen, Esa Puukilainen, Timo Sajavaara, Mikko Ritala, and Markku Leskelä
Chem. Mater. 25 (**2013**) 1656–1663.
The author made the deposition experiments and did the UV-Vis, GIXRD and FESEM/EDX analyses, wrote the first draft of the paper and finalized it with M.R. and M.L.

IV **Atomic layer deposition of AlF_3 thin films using halide precursors**
Miia Mäntymäki, Mikko J. Heikkilä, Esa Puukilainen, Kenichiro Mizohata, Benoît Marchand, Jyrki Räisänen, Mikko Ritala, and Markku Leskelä
Chem. Mater. 27 (**2015**) 604–611.
The author made the deposition experiments and did the UV-Vis, GIXRD, XRR and FESEM analyses, wrote the first draft of the paper and finalized it with M.R. and M.L.

V **Studies on Li_3AlF_6 thin film deposition utilizing conversion reactions of thin films**
Miia Mäntymäki, Kenichiro Mizohata, Mikko J. Heikkilä, Jyrki Räisänen, Mikko Ritala, and Markku Leskelä
Submitted.
The author made the deposition experiments and did the UV-Vis, GIXRD and FESEM analyses, wrote the first draft of the paper and finalized it with M.R. and M.L.

VI **Preparation of lithium containing oxides by the solid state reaction of atomic layer deposited thin films**
Elisa Atosuo, Miia Mäntymäki, Kenichiro Mizohata, Mikko J. Heikkilä, Jyrki Räisänen, Mikko Ritala, and Markku Leskelä
Chem. Mater. 29 (**2017**) 998–1005.
The author supervised the experimental work of E. A., made some of the GIXRD, XRR and FESEM analyses, analyzed the results, wrote the first draft of the paper and finalized it with M.R. and M.L.

VII **Studies on solid state reactions of atomic layer deposited thin films of lithium carbonate with hafnia and zirconia**
Miia Mäntymäki, Elisa Atosuo, Kenichiro Mizohata, Mikko J. Heikkilä, Jyrki Räisänen, Mikko Ritala, and Markku Leskelä
Manuscript.
The author supervised the experimental work of E. A., deposited some of the films, made some of the GIXRD measurements and FESEM analyses, analyzed the results, wrote the first draft of the paper and finalized it with M.R. and M.L.

Other publications by the author

1. **Growth and phase stabilization of HfO_2 thin films by ALD using novel precursors**
J. Niinistö, M. Mäntymäki, K. Kukli, L. Costelle, E. Puukilainen, M. Ritala, and M. Leskelä
J. Cryst. Growth 312 (**2010**) 245–249.

2. **Cycloheptatrienyl-cyclopentadienyl heteroleptic precursors for atomic layer deposition of group 4 oxide thin films**
J. Niinistö, T. Hatanpää, M. Kariniemi, M. Mäntymäki, L. Costelle, K. Mizohata, K. Kukli, M. Ritala, and M. Leskelä
Chem. Mater. 24 (**2012**) 2002–2008.

3. **Nuclear reaction analysis for H, Li, Be, B, C, N, O and F with an RBS check**
W.A. Lanford, M. Parenti, B.J. Nordell, M.M. Paquette, A.N. Caruso, M. Mäntymäki, J. Hämäläinen, M. Ritala, K.B. Klepper, V. Miikkulainen, O. Nilsen, W. Tenhaeff, N. Dudney, D. Koh, S.K. Banerjee, E. Mays, J. Bielefeld, and S.W. King
Nucl. Instrum. Meth. B 371 (**2016**) 211–215.

4. **Vapor Deposition of LiF Thin Films**
U.S Patent 9,382,615
M. Mäntymäki, J. Hämäläinen, M. Ritala, M. Leskelä

5. **Atomic Layer Deposition of Aluminum Fluoride Thin Films**
U.S Patent 9,394,609
M. Mäntymäki, M. Ritala, M. Leskelä

List of abbreviations and acronyms

2D	2-dimensional
3D	3-dimensional
a.u.	arbitrary unit
Ac	acetate, CH_3COO-
AFM	atomic force microscopy
ALD	atomic layer deposition
at%	atomic percent
C, C-rate	rate at which a battery is fully (dis)charged, 1 C = full discharge in 1 hour
CNT	carbon nanotube
CV	cyclic voltammetry
CVD	chemical vapor deposition
Cp	cyclopentadienyl, C_5H_5-
DEPA	diethyl phosphoramidate, $(CH_3CH_2O)_2(NH_2)PO$
DEZ	diethylzinc, $(CH_3CH_2)_2Zn$
dmae	dimethylaminoethoxy, $(CH_3)_2NCH_2CH_2O$-
EDX	energy-dispersive X-ray spectroscopy
EIS	electrochemical impedance spectroscopy
ERDA	elastic recoil detection analysis
EtCp	ethylcyclopentadienyl, $(CH_3CH_2)C_5H_4$-
eV	electronvolt
FAMD	N,N-di-*iso*-propylformamidinate, $[(CH_3)_2CHN$-$]CH[$-$NCH(CH_3)_2]$
FESEM	field-emission scanning electron microscopy
FTIR	Fourier transform infrared spectroscopy
GIXRD	grazing incidence X-ray diffraction
hfac	1,1,1,5,5,5-hexafluoro-2,4-pentanedionato, hexafluoroacetylacetonato, $(CF_3CO$-$)CH(-OCCF_3)$
HMDS	hexamethyldisilazide, bis(trimethylsilyl)amido, $[(CH_3)_3Si]_2N$-
HQ	hydrokinone, benzene-1,4-diol, $C_6H_4(OH)_2$
HTXRD	high temperature X-ray diffraction
ICP-MS	inductively coupled plasma mass spectrometry
Li_2Q	dilithium 1,4-benzenediolate, $Li_2(C_6H_4O_2)$
LiBSO	lithium sulfate metaborate
LiPON	lithium phosphorus oxynitride
LISICON	lithium superionic conductor
LiSiPON	lithium silicon phosphorus oxynitride
LiSON	lithium sulfur oxynitride
LiTP	lithium terephthalate
LLT	lithium lanthanum titanate
LVSO	lithium vanadium silicate
MEMS	microelectromechanical systems

NASICON	sodium superionic conductor
Ni-MH	nickel-metal hydride
OEt	ethoxy, CH_3CH_2O-
O^{i}Pr	*iso*-propoxy, $(CH_3)_2CHO$-
O^{t}Bu	*tert*-butoxy, $(CH_3)_3CO$-
PEALD	plasma-enhanced atomic layer deposition
PLiON	plastic lithium-ion battery
ppm	parts per million
py	pyridine, C_5H_5N
QCM	quartz crystal microbalance
RBS	Rutherford backscattering spectrometry
rms	root-mean-square
RT	room temperature
SEI	solid-electrolyte interface
SIMS	secondary ion mass spectrometry
TDMA-Al	tris(dimethylamido) aluminum, $[(CH_3)_2N]_6Al_2$
TDMAH	tetrakis(dimethylamido) hafnium, $[(CH_3)_2N]_4Hf$
TDMAZ	tetrakis(dimethylamido) zirconium, $[(CH_3)_2N]_4Zr$
TEMAZ	tetrakis(ethylmethylamido) zirconium, $[(CH_3)(CH_3CH_2)N]_4Zr$
TEOS	tetraethyl orthosilicate, $(CH_3CH_2O)_4Si$
thd	2,2,6,6-tetramethyl-3,5-heptanedionato, $[(CH_3)_3CCO\text{-}]CH[\text{-}OCC(CH_3)_3]$
TMA	trimethylaluminum, $(CH_3)_3Al$
TMPO	trimethylphosphate, $(CH_3O)_3PO$
TMSO	trimethyl silanolate, $(CH_3)_3SiO$-
ToF-ERDA	time-of-flight elastic recoil detection analysis
TPA	terephthalic acid, benzene-1,4-dicarboxylic acid, $C_6H_4(COOH)_2$
UHV	ultra-high vacuum
UPS	ultraviolet photoelectron spectroscopy
UV	ultraviolet
UV-Vis	ultraviolet-visible
w%	weight percent
XANES	X-ray absorption near edge structure
XPS	X-ray photoelectron spectroscopy
XRD	X-ray diffraction
XRR	X-ray reflection
XRF	X-ray fluorescence
Å	Ångström, 10^{-10} m

Table of Contents

Abstract i

Preface ii

List of publications iv

Other publications by the author vi

List of abbreviations and acronyms vii

Table of Contents 1

1. Introduction 3

2. Lithium-ion Batteries 5

2.1 Concept 6

2.2 Inorganic materials for lithium-ion batteries 8

2.2.1 Electrodes 8

2.2.2 Solid electrolytes 11

2.3 Inorganic fluorides as lithium-ion battery materials 14

2.3.1 Electrodes 14

2.3.2 Solid electrolytes 16

3. Atomic Layer Deposition 18

3.1 Concept 18

3.1.1 Atomic layer deposition of binary materials 18

3.1.2 Atomic layer deposition of ternary and quaternary materials 22

3.2 Atomic layer deposition of metal fluorides 25

3.3 Atomic layer deposition of lithium containing materials 30

3.3.1 Binary materials 30

3.3.2 Ternary and quaternary materials 38
4. Experimental 50
4.1 Film deposition 50
4.2 Film characterization 51
5. Results and Discussion 52
5.1 Search for lithium containing double metal alkoxides 52
5.2 Exploring ALD chemistries for metal fluoride deposition 53
5.2.1 LiF 53
5.2.2 AlF_3 55
5.3 Conversion reactions for metal fluoride deposition 59
5.3.1 LiF 59
5.3.2 Li_3AlF_6 62
5.4 Combining ALD and solid state reactions for lithium containing ternary oxides 66
5.4.1 Studies on solid state reactions between ALD-made Li_2CO_3 and Ta_2O_5, TiO_2, and Nb_2O_5 films 66
5.4.2 Studies on solid state reactions between ALD-made Li_2CO_3 and HfO_2, and ZrO_2 films 69
6. Conclusions and Outlook 72
References 74

1. Introduction

The fast technical advancements taken place during the last few decades have created the need to store even more energy in ever smaller volumes. While in the 1980s alkaline batteries were enough to power one's Walkman, the mobile phones and laptops of today require more advanced batteries to function for a reasonable time. Lithium-ion batteries can provide larger energy and power densities than other battery technologies, making them especially suitable for small, light-weight portable electronics. In addition, due to a growing concern over climate change, and the dwindling fossil fuels, a move to renewable energy forms such as solar and wind is evident, resulting also in a need to store energy. Environmental concerns have also led to the rise of hybrid and all-electric vehicles, from the small and nimble Nissan Leaf[1] to the powerful Tesla Model S[2]. The developments in these fields of engineering have been powered by the developments in lithium-ion batteries. It is clear that the market for lithium-ion batteries will continue to increase in the years to come.[3, 4]

Despite currently being the technology-of-choice for multiple applications, lithium-ion batteries do suffer from a number of problems. There is still room for improvement, both in the battery capacity and energy density, because electric vehicles require higher capacity batteries in order to extent their operation range. At the same time, smaller batteries are sought for portable devices, because often the size of the battery can limit the size of the whole product. The biggest problem with these batteries is, however, related to their safety: it has become common knowledge that lithium-ion batteries can over-heat and even explode. This problem has become so worrying and large scale that it is affecting people's lives: for example, airlines are limiting the number of batteries per passenger,[5] and Samsung recently had to discontinue its flagship Galaxy Note 7 smartphone because the phones could explode, most likely because of a faulty lithium-ion battery.[6, 7] Thus, there is a clear need for clever materials engineering to increase both the capacity and safety of present day lithium-ion batteries.

Many enhancements in lithium-ion batteries can be achieved by utilizing thin films in various 3D constructions, as both active materials and protective layers on the active materials. During the 21st century, the thin film manufacturing method known as atomic layer deposition (ALD) has become a very important player in the field of microelectronics, and is now taking over battery research in a major way. The advantages of ALD, including high film uniformity and excellent conformality over various kinds of substrates, make it ideal for the deposition of materials for ever-smaller, more complicated batteries. Particularly, the deposition of solid electrolyte materials, instead of using the current liquid electrolytes, could solve many of the safety issues facing lithium-ion batteries today.

This thesis comprises 5 papers and 2 manuscripts, ranging from a literature review on precursors for ALD of battery materials to the study of new processes and materials for batteries. A special focus in this work was given to fluoride materials, which have not received

much attention in the battery community, and are an under-studied class of materials also in ALD research. In addition, the combination of simple ALD processes and solid state reactions was studied, producing interesting results related to the deposition of lithium containing multi-component oxide films. In order to properly review the results obtained, Chapter 2 provides a short introduction to lithium-ion batteries, including the concept and materials traditionally utilized therein. In Chapter 3, ALD is introduced, with examples of the deposition of both binary and ternary materials. Chapter 3 also provides a literature review on metal fluorides and lithium containing materials thus far deposited by ALD. Chapter 4 provides the experimental details related to papers I – VII, while Chapter 5 summarizes the experimental results. Conclusions based on this work are summed up in Chapter 6.

2. Lithium-ion Batteries

Lithium-ion batteries are used for energy storage in anything from cellphones and laptops to electric vehicles. The very basic concept of a lithium-ion battery is the same as for any other battery: chemical energy stored in the electrodes is converted into electrical energy via a chemical reaction.[8] Some of the battery types in use today are depicted in Figure 1. As can be seen, lithium-ion batteries have surpassed many of the older battery technologies both in energy and power density. This is related to the fact that lithium is small and light-weight, which makes it possible to obtain high energy densities from lithium containing materials. In addition, lithium forms compounds with large enough voltages to produce so-called "high quality" energy, or high power densities.[8] The small size of the lithium-ion is also an advantage in that lithium-ions can be highly mobile in many materials, ensuring only low energy losses due to kinetic effects. In the next subchapters, the basic concepts of both 2D and 3D Li-ion batteries are presented. Due to the vastness of this research area, only some of the most commonly used inorganic materials and their properties are reviewed. For example, polymer electrolyte materials will not be discussed. Even though most of the materials of interest today are multi-component oxide materials, special emphasis is also given to inorganic fluoride materials in lithium-ion batteries (Chapter 2.3).

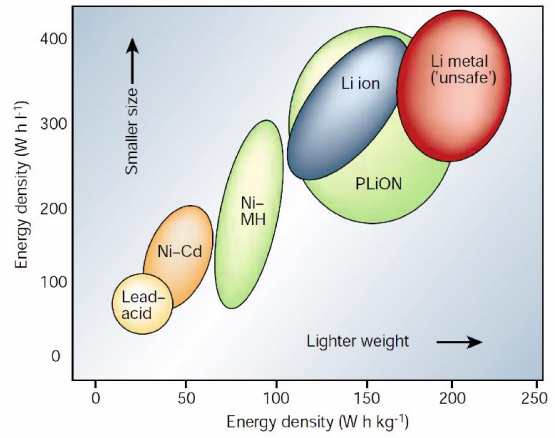

Figure 1: Comparison of energy densities in different battery types in use today.[9] Reprinted by permission from Macmillan Publishers Ltd: Nature, Vol. 414, pages 359–367, J.-M. Tarascon & M. Armand: "*Issues and challenges facing rechargeable lithium batteries*", Copyright (2001). www.nature.com

2.1 Concept

Figure 2 depicts the basic schematic of a lithium-ion battery. The battery consists of two electrodes (the positive cathode and the negative anode), an electrolyte and two current collectors. Because the active materials in the battery, the electrodes, are separated by an inert electrolyte, the energy liberated in the chemical reaction between the electrode materials can be converted into electrical work.[8] During battery operation, lithium-ions flow through the electrolyte from the anode to the cathode. At the same time, electrons flow in the outer circuit from the anode to the cathode, balancing the net charge flow. These electrons can be used to do work, such as operate a laptop.

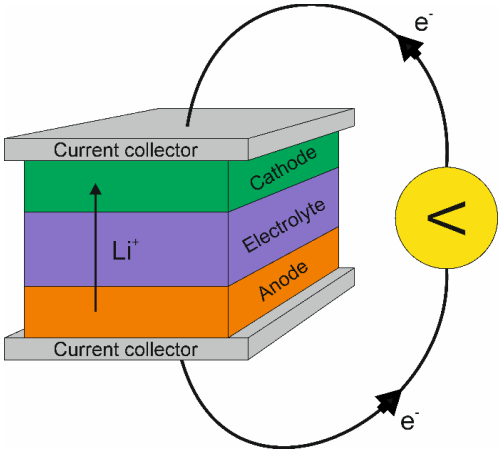

Figure 2: Basic concept of a lithium-ion battery, showing the flow of lithium-ions and electrons during discharge.

In addition to the high energy and power densities, interest in lithium-ion batteries derives from the fact that most of them can be recharged multiple times without losing much of the battery capacity. Batteries, which cannot be charged, are called primary batteries, whereas most lithium-ion batteries are rechargeable, or secondary. During recharging, a voltage is applied to the outer circuit, which reverses the flow of electrons and Li^+ ions, moving them from the cathode to the anode. During the charge-discharge cycling, the battery capacity should stay as constant as possible. Usually the capacity slowly degrades with increased cycling as a result of, for example, reactions between the electrolyte and the electrodes, and changes in the morphology of the electrodes, such as breakage or delamination.[8]

Most lithium-ion batteries employ an organic liquid electrolyte material, composed of organic carbonates such as ethylene, dimethyl and diethyl carbonates, lithium hexafluorophosphate, and different additives.[8, 10] Liquid electrolytes enable very high lithium-ion conductivities, which

are beneficial for the battery operation. At the same time, the electrolyte should be an electron insulator, so that no self-discharge takes place.[8] Liquid electrolytes can accommodate volume changes in the electrodes during cycling, which reduces stress in the battery. However, liquid electrolytes are also a major reason for the safety concerns of lithium-ion batteries: the electrolyte can decompose at the electrodes, most often on the anode, and form a solid-electrolyte interface layer, or SEI-layer.[8] Commonly the SEI-layer protects the electrodes from further reactions with the electrolyte, but in case of an incomplete SEI-formation, reactions can proceed further, with pressure building up inside the battery. Since the electrolyte materials are flammable, fiery explosions can occur.[11] Therefore, much research effort has been devoted to the study of solid lithium-conducting materials.

In addition to the safety benefits, another important reason for using solid electrolytes is that all-solid-state batteries can be easily integrated into, for example, microelectromechanical systems (MEMS) to achieve autonomous sensing devices. For integration, small batteries are generally required, because the size of the battery can easily limit the size of the whole device.[11, 12] Making a battery smaller by using thinner active layers is a viable solution for all-solid-state batteries because thinner layers result in smaller transport losses and over-potentials due to smaller diffusion length scales.[11–13] Particularly, the limitations of the much lower lithium-ion conductivities of solid electrolytes can thus be circumvented.[12] However, thin electrode layers limit the energy available from the battery. By making batteries smaller with 3D structures (Figure 3), gains in both energy and power density can be achieved due to simple geometrical reasons: more active material can be packed into smaller foot print areas, with the advantages of short diffusion lengths still present.[12]

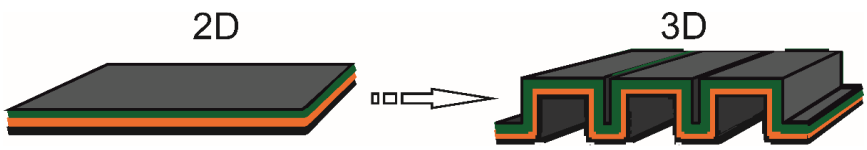

Figure 3: 3D battery constructions increase the amount of active material available per foot print area. These would be especially suitable for all-solid-state batteries.

2.2 Inorganic materials for lithium-ion batteries

2.2.1 Electrodes

As already mentioned, electrodes define the capacity and voltage of a battery. Since both lithium-ions and electrons move inside the electrodes, the materials need to be both ion and electron conductors. The reactions taking place in the electrodes can be roughly divided into conversion reactions, alloying reactions and insertion or intercalation reactions (Figure 4).[14] Conversion and alloying electrodes generally provide higher battery capacities, but often lead to problems with electrode degradation during cycling due to repeated volume changes associated with the conversion reaction. Thus, conversion and alloying electrodes have more often been used in primary batteries.

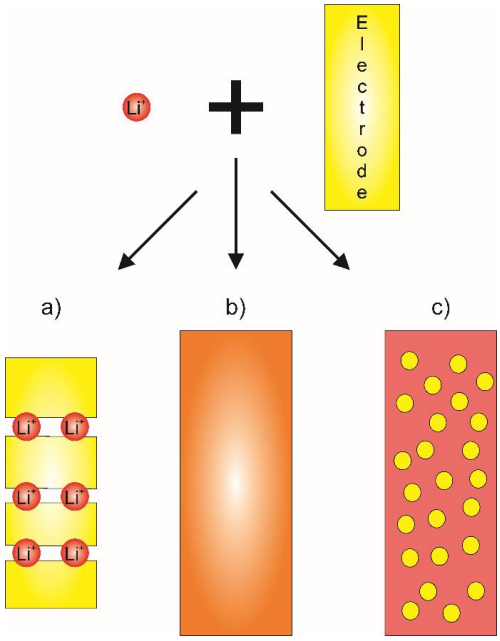

Figure 4: Schematic illustrating the different kinds of reactions possible with lithium ions and electrode materials. a) Intercalation b) Alloying c) Conversion. With alloying and conversion reactions, significant volume changes often take place in the electrode.

In secondary batteries, intercalation reactions are the most commonly used, with the $LiCoO_2$ – C_6 (graphite) battery being a prime example of this reaction. Even if intercalation electrodes do not generally suffer from volume changes of similar magnitude as conversion electrodes, they

still require care in the charging-discharging process: a too deep discharge can lead to irreversible changes in the electrode structure, which in turn can lead to a diminished battery capacity.

Intercalation cathode materials are most often lithium containing transition metal oxides, in which the insertion and extraction of lithium is made possible by the redox capabilities of the transition metal.[14, 15] Although $LiCoO_2$ is the most often used cathode material, oxides of, for example, manganese and nickel, and mixtures of these are gaining interest as possible future cathodes.[15, 16] Table 1 contains the voltages and capacities obtainable from some of the most studied cathode materials. Despite their common use in batteries today, transition metal oxide cathodes have some serious drawbacks. Firstly, the voltages obtainable from these materials are limited, which is a problem especially for high power density applications. Secondly, the capacities available from these materials are quite low as a result of the limited amount of lithium available before irreversible changes in the structures occur. For example, only half of the lithium-ions in $LiCoO_2$ can be reversibly utilized.[16] Lastly, liquid electrolytes are known to give rise to dissolution of the transition metal, thus decreasing the cathode capacity even further.[15] However, thin film methods such as atomic layer deposition can be used to deposit thin layers of, for example Al_2O_3 or AlF_3, onto cathode materials to protect them from side reactions such as transition metal dissolution (Chapter 2.3.1).[17] Some of these problems can also be circumvented by using mixture cathodes, such as $LiNi_{(1-y-z)}Mn_yCo_zO_2$, which can also produce slightly higher capacities.[10, 15, 16] In addition to oxides, sulfates and phosphates, such as $LiFePO_4$, have also been studied extensively.[16] Despite being cheaper and less toxic than most cathode materials, and providing a reasonable capacity, $LiFePO_4$ suffers from low electronic conductivity, limiting its applicability.[16]

For cathodes, alloying and conversion reactions have not gained much attention. Some transition metal fluoride conversion cathodes will be shortly discussed in Chapter 2.3.1.

Table 1: Operating voltages and capacities obtainable from some of the most studied lithium-ion battery cathode materials.

Material	Type	Voltage /eV (vs. Li/Li^+)	Specific capacity / mAh/g	Ref.
$LiCoO_2$	Intercalation	~3.9	140	14
$LiNiO_2$	Intercalation	2.7–4.1	140–200	14, 16
$LiMn_2O_4$	Intercalation	3.5–4.5	150	14
$LiFePO_4$	Intercalation	3.4	170	10, 14, 16
V_2O_5	Intercalation	3.2–3.4	120	14

Table 2 presents some potential anode materials for lithium-ion batteries. For an anode, a potential as low as possible (vs. Li^+/Li) is desired to reach a high cell voltage. As with the cathode materials, intercalation anodes are more common than the other types of anodes. However, a lot of work is now being put into studying materials such as silicon and tin as lithium-ion battery alloying anodes.[10, 14, 18]

Metallic lithium was the very first, ideal choice for the anode of a lithium-ion battery.[15] However, safety concerns, such as dendrite formation, have moved the interest towards anodes such as graphitic carbon C_6, which produces capacities of 370 mAh/g.[8, 10] Still, due to the very low electrode potential of carbon anodes, dendritic lithium deposition is also somewhat of a concern in these anodes. One possible replacement for carbon is the spinel lithium titanate $Li_4Ti_5O_{12}$, which has a reasonable capacity with a very small volume expansion during lithiation. In addition, the titanate is environmentally benign with a reasonable cost.[19] A major drawback of this material, and many insertion oxide anodes in general, is the high electrode potential, resulting in cells with low operation voltages.[10, 19]

Of the alloying anodes, elemental silicon has attracted much attention because of its low cost, abundance in nature and high specific capacity of over 3500 mAh/g.[19] However, alloying the maximum 3.75 lithium-ions per one Si atom produces volume changes of up to 300 % in the electrode, limiting the cycling ability of the anode.[10] Nanostructured Si is now studied in hopes of alleviating the problems with volume expansion.[10, 18] Similarly, elemental tin has attracted much attention, but suffers from the same problems as silicon.[18]

Attempts have been made to circumvent the volume change problem also by using conversion anodes composed of, for example SnO or SnO_2. In this anode, lithium first forms lithium oxide and metallic tin, which further alloys lithium and is responsible for the reversible capacity.[19] However, the problems related to volume changes still persist to some extent in these anodes.[19] Many transition metal oxides have also been studied as conversion anodes, with capacities ranging from 600 to 700 mAh/g.[20] In addition to the persisting volume change problem, conversion anodes often also suffer from large overpotentials.[18]

Table 2: Operating voltages and capacities obtainable from some of the most studied lithium-ion battery anode materials.

Material	Type	Voltage /eV (vs. Li^+/Li)	Specific capacity / mAh/g	Ref.
C_6	Intercalation	<0.6	370	10, 14
$Li_4Ti_5O_{12}$	Intercalation	1.5	175	14
Si	Alloying	0.1–0.3	3580	10, 14
Sn	Alloying	0.6–0.8	990	10, 14, 18
MO, M = Co^{2+}, Fe^{2+}, Cu^{2+}, Ni^{2+}	Conversion	~ 1.8–2.0	670–750	19–21

2.2.2 Solid electrolytes

Solid electrolyte materials are the enablers of all-solid-state Li-ion batteries. These materials have stringent property demands: they must be unreactive at the electrode potentials and have a high lithium-ion conductivity at room temperature.[8, 22] In addition, they must be good electron insulators to avoid self-discharge and short-circuits.[14] Despite the high demands for material properties, a vast number of possible solid electrolyte materials suitable for lithium-ion batteries have been reported in the literature.[22–25] In addition to inorganic ceramics, also composites and polymer mixtures can be used as solid electrolytes.[23, 25, 26]

Inorganic fast lithium-ion conducting materials can be single-crystalline, polycrystalline or amorphous, with many different structural types available for the crystalline materials (Table

3, Figure 5).[23, 24] Generally, an amorphous electrolyte material would be preferred, as grain boundaries in crystalline materials can lead to both impeded ion movement, and electron leakage, and thus poorer insulating properties.[25, 26] In addition, amorphous materials can provide isotropic lithium-ion conduction in a wide range of different compositions.[24]

Amorphous, or glassy electrolytes, can be roughly divided into oxide and sulfide glasses.[24] Probably the most studied amorphous solid electrolyte material is nitrogen doped lithium phosphate (lithium phosphorus oxynitride), or LiPON, which is in fact already in use in thin film lithium-ion batteries.[24, 25] The material is usually deposited with sputtering in a nitrogen atmosphere, and the resulting films have lithium-ion conductivities of the order of 10^{-6}–10^{-8} S/cm,[24] as compared to the ~ 10^{-2} S/cm for liquid electrolytes.[10] The success of LiPON comes not only from its reasonably high lithium-ion conductivity, but also from its excellent stability against electrode materials.[24] Sulfide glasses, on the other hand, have been studied much less than the corresponding oxides, mostly because of their reactivity in air, and corrosiveness.[24]

Out of crystalline materials, the perovskite (Li,La)TiO_3 (LLT) is known to show high bulk conductivities. However, reduction of Ti^{4+} and subsequent increase in electronic conduction are problems with this material.[23, 25] Titanium-free perovskites, such as (Li,La)NbO_3 have thus been studied, but no commercial batteries with a perovskite electrolyte are available.[24] Phosphates with the NASICON (sodium superionic conductor) structure are also known to show high lithium-ion conductivities.[24] In Table 3 $LiTi_2(PO_4)_3$ is given as an example, but many other +IV oxidation state metals can be substituted for titanium in the structure. LISICON (lithium superionic conductor) materials, on the other hand, are mixtures of lithium silicates or germanates, lithium phosphates or vanadates and lithium sulphates, and can produce similar conductivities as the NASICON structure.[24] In addition to these material classes, oxides such as $Li_6BaLa_2Ta_2O_{12}$ with the garnet structure have been studied extensively and shown to have reasonable ionic conductivities.[23] Another benefit of the garnet materials is their high chemical stability in contact with the electrodes.[24]

Table 3: Structures and ionic conductivities of some of the most studied solid inorganic lithium-ion conducting materials.

Material	Structure	Ionic conductivity at 25 °C / S/cm	Ref.
LiPON	Amorphous	10^{-6}–10^{-8}	23, 24
$Li_2O – SiO_2 – V_2O_5$, LVSO	Crystalline/Amorphous	10^{-5}–10^{-7}	24
$Li_2S – GeS_2 – Ga_2S_3$	Amorphous	10^{-4}	24
$(Li,La)TiO_3$, LLT	Perovskite	10^{-3}	23, 25
$LiTi_2(PO_4)_3$	NASICON	10^{-5}	23, 24
$Li_{14}ZnGe_4O_{16}$	LISICON	10^{-6}	25
$Li_6BaLa_2Ta_2O_{12}$	Garnet	10^{-5}	23

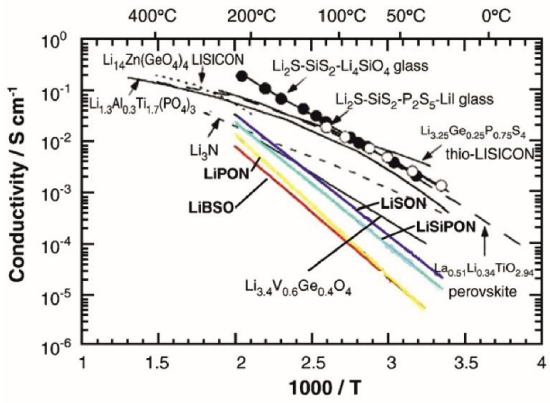

Figure 5: Bulk ionic conductivities of selected oxides and phosphates as a function of temperature.[25] Reprinted from Solid State Ionics, Vol. 180, pages 911–916, P. Knauth: "*Inorganic solid Li ion conductors: An overview"*, Copyright (2009), with permission from Elsevier. https://www.journals.elsevier.com/solid-state-ionics

2.3 Inorganic fluorides as lithium-ion battery materials

Inorganic fluorides can be utilized in lithium-ion batteries in many ways.[27] For the purpose of this thesis, this chapter will focus only on metal fluorides as electrodes, artificial SEI-layers and solid electrolytes. The reader is advised, however, that much work has also been done on other fluorinated materials in batteries, such as fluorinated salts as additives in liquid electrolytes,[27, 28] fluorinated solvents in batteries,[28] carbon fluorides as negative electrodes[27] and fluorinated binder materials.[27, 28] These fields will not be discussed further here.

2.3.1 Electrodes

Amatucci and Pereira note in their review on fluoride based electrode materials that "*The use of fluorides stems from the intrinsic stability of fluorinated materials and their ability to generate high electrochemical energy as electrodes.*".[27] Indeed, fluoride cathodes generally produce higher potentials than the corresponding oxides of the same redox-couple, leading to higher energy densities.[27] Thus, fluoride materials could be used in high voltage batteries, where the stability of active materials is especially important. Fluorides can be used as cathodes either as pure fluorides or as doped materials, such as oxyfluorides, fluorosulphates or fluorophosphates.[27, 28] Fluoride doping has been reported to improve capacity retention for intercalation cathodes such as lithium nickel oxide and lithium nickel cobalt oxide.[27] This could be related to a slower dissolution rate of transition metals into liquid electrolytes from the oxyfluorides.[27] For fluorophosphate cathodes, such as Li_2CoPO_4F, high potentials of over 5 V are obtainable, accompanied again by a slower dissolution of the transition metal.[27, 28] However, the performance of these cathodes is limited due to poor ionic and electronic conductivity and instability of liquid electrolytes at such high potentials.[28]

Pure metal fluorides are an interesting but understudied class of cathode materials for lithium-ion batteries. Fluorides were studied extensively in the 1960s and 1970s for use in primary batteries due to their high theoretical capacities (Figure 6) and energy densities.[27] It was hoped that these materials would act as conversion cathodes, with formation of lithium fluoride during discharge:

$$n\ Li^+ + n\ e^- + MF_n \rightarrow n\ LiF + M$$

However, the initial attempts on using materials such as CuF_2 and HgF_2 were not successful. Still, recently some work has been done to utilize these materials as reversible conversion electrodes in secondary batteries.[21, 27, 29–32] Unfortunately, metal fluorides suffer from the same

problem as other conversion electrodes, namely pulverization during cycling. In addition, fluorides are very poor electron conductors due to their high band gaps and often show high overpotentials, causing challenges in using them as reversible electrodes.[21] Despite this, much progress has been made in this area. For example, by utilizing nanocomposites of metal fluorides and conductive carbon, a capacity of 230 mAh/g was obtained for BiF_3, and 600 mAh/g for FeF_3.[31, 33]

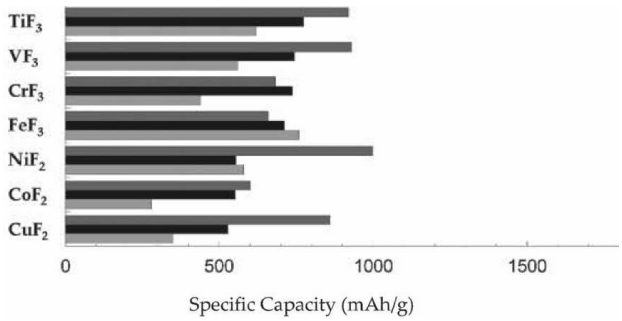

Figure 6: Theoretical (black), first discharge (dark grey) and charge (light grey) specific capacities of conversion fluoride cathode materials. Figure modified from ref [29]: Advanced Materials, vol. 22, pages E170–E192, J. Cabana *et al.*: "*Beyond Intercalation-Based Li-Ion Batteries: The State of the Art and Challenges of Electrode Materials Reacting Through Conversion Reactions"*, Copyright (2010), reproduced with permission from WILEY-VCH Verlag GmbH & Co. KGaA, Weinheim. http://onlinelibrary.wiley.com/doi/10.1002/adma.201000717/abstract

Due to the work on primary batteries, pure fluorides are generally considered only as conversion cathodes. However, some reports on intercalation fluorides also exist.[34–36] For example, Li_3FeF_6, a ternary fluoride resembling the structure of Li_3AlF_6, has been reported to show intercalation of 0.7–1 Li^+ ions per fluoride unit in a carbon nanocomposite form, resulting in a reversible capacity of 100–140 mAh/g.[34, 35] The capacity depends on the size of the Li_3FeF_6 particles, with smaller particles resulting in a higher capacity.[35] A deeper discharge of the material was reported to lead to LiF formation, indicating a conversion reaction at low potentials. Similarly, a nanocomposite of Li_3VF_6 was reported to reversibly intercalate up to one Li^+ per fluoride unit.[36] Calculations predict that fluorides such as $LiCaCoF_6$ could provide very high intercalation voltages.[37]

In addition to their potential as electrode materials, fluorides can also be utilized as solid-electrolyte interface layers on more conventional electrode materials. Especially AlF_3 has been studied extensively in this regard, on both cathodes[38–42] and anodes[43]. AlF_3 is suitable for electrode protection because it is rather inert, and aluminum cannot be reduced or oxidized in

battery conditions.[17] The material has been reported to, for example, decrease the irreversible capacity losses of electrodes and improve cycling stability,[38, 40] and increase the thermal stability of electrodes.[38, 39, 42] Figure 7 illustrates how a layer of AlF_3 can increase the capacity retention in a lithium cobalt nickel manganese oxide cathode. Using too much AlF_3, however, decreases the capacity considerably.

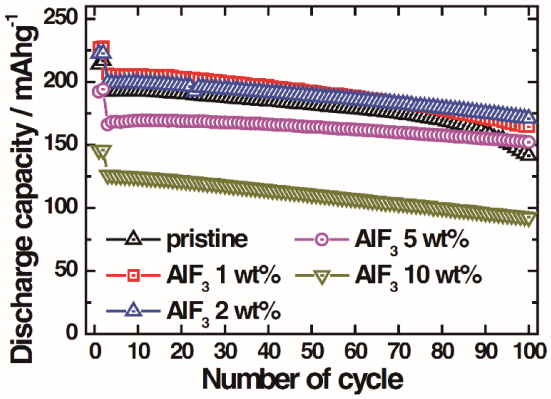

Figure 7: The effect of an AlF_3 coating on the discharge capacity of a lithium cobalt nickel manganese oxide cathode as a function of the number of charge/discharge cycles.[40] Reprinted from Advanced Materials, vol. 24, pages 1192–1196, Y.-K. Sun et al.: "*The Role of AlF_3 Coatings in Improving Electrochemical Cycling of Li-Enriched Nickel-Manganese Oxide Electrodes for Li-Ion Batteries*", Copyright (2012), reproduced with permission from WILEY-VCH Verlag GmbH & Co. KGaA, Weinheim. http://onlinelibrary.wiley.com/doi/10.1002/adma.201104106/abstract

2.3.2 Solid electrolytes

The applicability of metal fluorides as solid electrolytes for Li^+ ions has not been studied as extensively as their use as electrodes. However, some examples of potential electrolyte materials can be found in the literature. Li_3AlF_6, a mixture fluoride of LiF and AlF_3, has been reported to show high ionic conductivities of the order of 10^{-6} S/cm in thin film form.[44–47] In addition, milling this ternary fluoride with LiCl has been reported to lead to high conductivities.[48] Other fluorides, which also show high conductivities when mixed with LiF, include NiF_2, VF_3, CrF_3 and YF_3 (Figure 8).[45, 49] These materials have been deposited by thermal evaporation and fast quenching, resulting in amorphous thin films. The increased ionic conductivity in these mixtures is attributed to the formation of amorphous intermediate phases with high coordination numbers for lithium, such as in the Li_3AlF_6 phase.[45] Even more complicated fluoride mixtures have been studied as well,[44, 46, 50–52] such as the $LiF – AlF_3 – ScF_3$

system, which can reach similar conductivity values as the pure Li_3AlF_6.[44] For fluoride glasses of the type $LiF – ZrF_4 – LaF_3$ high lithium-ion conductivities can be obtained with high enough LiF molar ratios.[50]

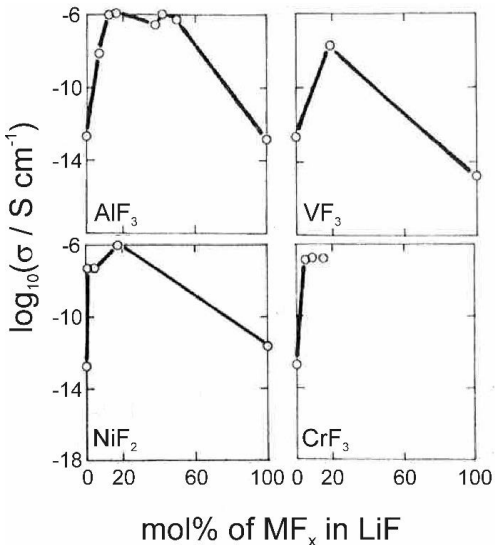

Figure 8: Room temperature ionic conductivities $\log_{10}\sigma$ of fluoride thin films composed of LiF and AlF_3, VF_3, NiF_2 or CrF_3. Figure modified from ref. [45]: Materials Research Bulletin, vol. 19, pages 451–457, T. Oi: "*Ionic conductivity of LiF thin films containing Di- or trivalent metal fluorides"*, Copyright (1984), with permission from Elsevier. https://www.journals.elsevier.com/materials-research-bulletin.

In addition to the applications in lithium-ion batteries, some metal fluoride mixtures can act as electrolytes for F^- ions, making high voltage fluoride-ion batteries a possibility.[53–57] To make things even more interesting, mixture fluoride glasses can, in some cases, produce both lithium- and fluoride-ion conductivities, depending on the molar ratios of the metal fluorides.[50, 52]

3. Atomic Layer Deposition

In this chapter, the basic features of atomic layer deposition are shortly discussed. The deposition of binary and ternary materials is covered in separate subchapters. The official definition of a binary material is a material that is composed of a metal and a non- or semimetal, such as TiO_2 or Al_2O_3. Ternaries are materials with three different kinds of ions, either two metals and a non-metal, as in $LiTaO_3$, or a metal and two non-metals as in TaO_2F. However, for the purpose of this thesis, the word "binary" is used to describe a material that only contains two ions, with lithium being one of them. Thus, materials such as lithium carbonate, Li_2CO_3, are defined as binary in this work because it is composed of two ions, Li^+ and CO_3^{2-}. Ternary materials will include other metals in addition to lithium.

After covering the basics of ALD, atomic layer deposition of metal fluorides and lithium containing materials are summarized. Because much of the fluoride thin film deposition has been covered in the theses of Dr. Tero Plvi[58] and Dr. Younghee Lee,[59] this subject will only be discussed shortly. More emphasis will be given to the deposition of lithium containing materials, due to both their high relevance to lithium-ion battery research, and interesting growth processes: as will be seen in Chapter 3.3, many of the basic rules of ALD outlined in Chapter 3.1 are tested in lithium containing chemistries, where the unusual reactivity and mobility of Li^+ play a strong role in the deposition processes, especially for ternary materials. The reader is advised that despite the novelty of this research area, review papers detailing the growth of lithium containing materials by ALD already exist.[60–62] In addition, reviews summarizing work on nanostructuring and surface modification of battery materials by ALD have also been published.[63–65]

3.1 Concept

3.1.1 Atomic layer deposition of binary materials

Atomic layer deposition (ALD) is a gas phase thin film deposition method, closely related to chemical vapor deposition (CVD). Whereas in CVD gaseous precursors are supplied simultaneously and decompose to react, in ALD precursor pulses are separated by purge gas pulses or evacuation periods, resulting in no gas phase reactions. Instead, the precursors react one at a time with the substrate or film surface groups in a digital manner.[66, 67]

Figure 9 is a representation of the simplest type of ALD reactions. First, one precursor adsorbs and reacts on a substrate surface. After all potential surface sites have reacted with the first precursor, excess precursor molecules and side products are purged away. In the next step, a second precursor reacts with the surface, forming a binary film. Also after this step a purge is applied. Generally, a film of one monolayer or less is formed in one ALD cycle.[68] The amount of material deposited depends both on the density of active surface groups and the size of the precursor molecules.[66, 68] The slowness of the deposition process is considered as one of the greatest weaknesses of ALD.[66] By repeating the four-step cycle, a film of desired thickness can be formed.[66] In ALD literature, the reaction type illustrated in Figure 9 has been traditionally called "ligand exchange":[68] For example in the case of Al_2O_3 deposition trimethylaluminum (TMA) and water react in a way that methane is produced as a side product. Thus, it can be viewed as methyl ligands changing their bonding from aluminum in TMA to hydrogen from water during the water pulse. In synthesis work, this type of reaction is commonly called metathesis. This broad definition of ligand exchange can be applied to most ALD reactions in use today. Other ALD-type reactions include combustion with ozone and oxygen radicals, an additive reaction with elemental precursors, and controlled decomposition of an adsorbed species.[69]

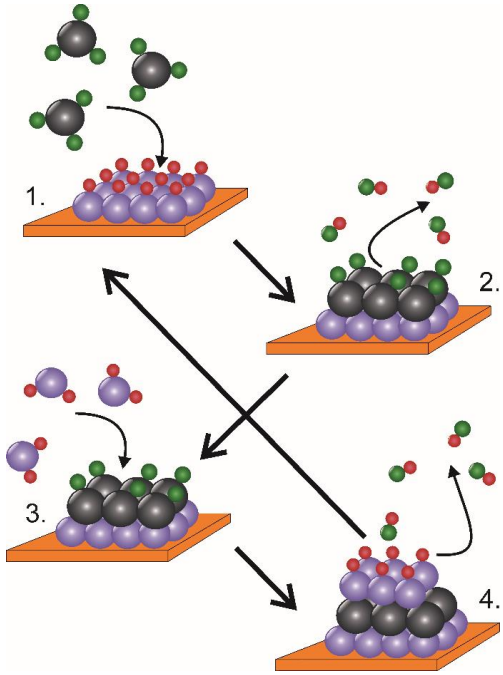

Figure 9: Schematic illustrating one cycle in ALD. 1. Precursor molecules react with a surface covered with active species. 2. Reaction side products are purged away. 3. Precursor 2 is introduced, and it reacts with the surface covered with precursor 1 molecules. 4. The reaction side products are again purged away, resulting ideally in one monolayer of material on the substrate.

ALD has different variations, including thermal ALD,[69] plasma-enhanced ALD (PEALD)[70] and photo-ALD,[71, 72] depending on how energy is provided to the deposition reaction. Thermal ALD refers to a process where the energy for the surface reactions is produced by heating. In PEALD, additional energy from radicals and, depending on the reactor configuration, possibly also ions and electrons, is used.[70] For the purposes of this thesis, mostly thermal ALD will be discussed in detail, although a few PEALD processes will be discussed in Chapter 3.3. The biggest advantage of using PEALD instead of thermal ALD is that lower deposition temperatures can often be used with plasma, and reactions, which are not possible thermally, can be realized with radicals.[67, 70] On the other hand, PEALD is not as conformal as its thermal sibling, caused by recombination of the active radical species on trench walls.[67, 70] However, the conformality achieved with PEALD depends on the radicals used, with hydrogen radicals showing the fastest recombination on metal surfaces and thus the poorest conformality.[70, 73] In contrast, oxide materials can be deposited in relatively high aspect ratio substrates, as long as high enough radical densities are obtained.[73] In addition to conformality issues, plasma damage induced by both energetic ions and also electromagnetic radiation can pose problems in PEALD processes.[70]

The temperature at which a film is deposited can strongly affect the reactions of the precursor on the surface and thus change the growth rate of the film (Figure 10a).[69] Ideal ALD-processes should show an ALD window, meaning a temperature region where the growth rate stays constant as a function of temperature. However, usually small deviations from this behavior are seen, because the number of active surface sites can be highly dependent on the deposition temperature.[69] At the low temperature end, the growth rate can either increase due to multilayer precursor adsorption or decrease due to limited reaction kinetics. At high temperatures, the growth rate can either decrease with temperature due to a decrease in sticking constant of one or both precursors, precursor desorption or a lack of active sites, or increase due to precursor decomposition and uncontrolled reactions.[67]

Because all reactions in ALD occur between surface groups and adsorbing gaseous precursors, the reaction becomes terminated when all the surface groups have reacted or when the steric hindrance from large precursor molecules prevents further precursor adsorbtion.[68] This results in self-limiting growth, which means that using higher precursor doses, often in practice meaning longer precursor pulse times, will not result in more growth, and that a constant amount of film is deposited in each cycle (Figure 10b).[66, 69] To achieve this self-limiting or saturative behavior, it is important that the precursor does not self-decompose. In addition, long enough purge times between precursor pulses are required to ensure no excess precursor is in the gas phase or adsorbed onto the surface when the second precursor is introduced. Self-limiting growth enables the large area uniformity, easy thickness control and good conformality of atomic layer deposited films: the growth per cycle is constant, which means that the film

thickness can be easily tuned by choosing a proper cycle number (Figure 10c). Thus, with ALD even demanding 3D structures can be covered with a film of constant thickness, when long enough precursor pulse times and purges (Figure 10d) are employed.[66]

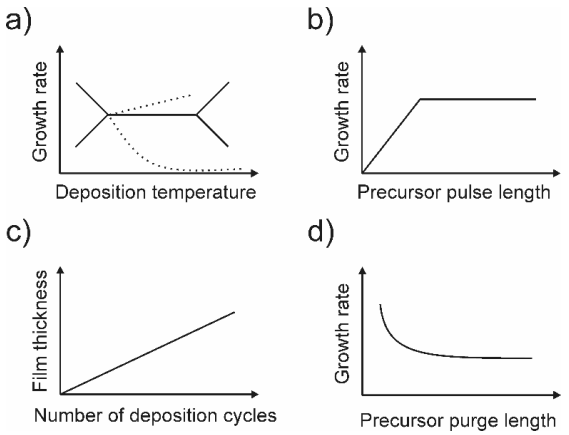

Figure 10: Schematic illustrating features of ALD. a) Often an "ALD window" can be found, in which the growth rate does not change as a function of temperature. b) ALD processes should show saturation, meaning the growth rate reaches a constant value when the precursor pulses are made longer. c) Because ALD processes are limited by the surface, a constant amount of film is deposited per cycle, resulting in a linear increase in thickness as a function of cycles. d) Purge times need to be long enough to avoid gas phase reactions and to obtain constant growth rates.

Gases, liquids and solids can all be used as precursors in ALD because the self-limiting growth mechanism does not demand that the rate of volatilization stays constant during the deposition process.[66, 69] Still, ALD places many other requirements for the precursors used to deposit a film. The precursors must be volatile and thermally stable, so that no gas phase decomposition or CVD-type growth occurs.[66, 69] Especially precursor decomposition destroys the self-limiting nature of ALD. At the same time, the precursors must be reactive enough to drive the reactions fast to completion during pulsing.[74] The side products formed should be inert, especially towards the forming film, and easy to remove with purging.[69] Secondary requirements include issues such as price, ease of handling, non-toxicity and non-corrosiveness.[69, 74] Precursors used in ALD include inorganic compounds such as halides, metal-organic complexes such as alkoxides, β-diketonates, and amidinates, and organometallic reactants such as alkyls and cyclopentadienyls.[74] For lithium containing materials deposition, a silylamide precursor is also widely used.[75–78] Water, oxygen and ozone are used as the second precursor for the deposition of oxides, whereas ammonia is used for nitrides, and hydrogen fluoride and transition metal fluorides have been used for fluoride deposition.[79–88] In this thesis, new processes for the deposition of two fluorides, $LiF^{II, III}$ and $AlF_3{}^{IV}$, were developed in an effort to deposit the ternary fluoride $Li_3AlF_6{}^{V}$.

3.1.2 Atomic layer deposition of ternary and quaternary materials

In addition to binary materials, ALD is also a convenient method for the deposition of ternary or even more complicated materials, most of which up until today have been oxides or chalcogenides.[74, 89, 90] All the same requirements for the deposition reactions and the precursors apply for ternary materials as for binaries. However, also many new challenges arise in more complicated systems, such as finding a common deposition temperature to accommodate all the different precursors and exchange reactions.[74, 90]

Generally, three different methods have been employed in the deposition of ternary materials. Firstly, the subcycle approach combines the deposition cycles of different binary materials one after another to intimately mix the two materials.[89] In this method, the stoichiometry of the ternary material is tuned by changing the pulsing ratios of the binary processes. This method can also be used for the deposition of nanolaminates, when the numbers of subcycles of the binary materials are increased (Figure 11).[91–93] The subcycle approach requires that the two materials to be mixed grow on top of each other in a controlled manner, meaning the growth rates should stay constant regardless of the starting surface.[68] In addition, the deposition temperature used should be applicable to both binary processes, although some exceptions to this rule do occur.[90, 94] Despite the digital nature of ALD, the metal stoichiometry of ternary materials deposited by the subcycle approach does not always linearly follow the pulsing ratios of the binaries: the amount of metal deposited in one subcycle depends on the size of the precursor molecules, the active sites on the surface, and also on the reaction mechanism.[89, 95] This can make obtaining the correct stoichiometry challenging, despite the inherent simplicity of this deposition method.[74] This is especially true for lithium containing ternaries and quaternaries, which will be covered in detail in Chapter 3.3.2.

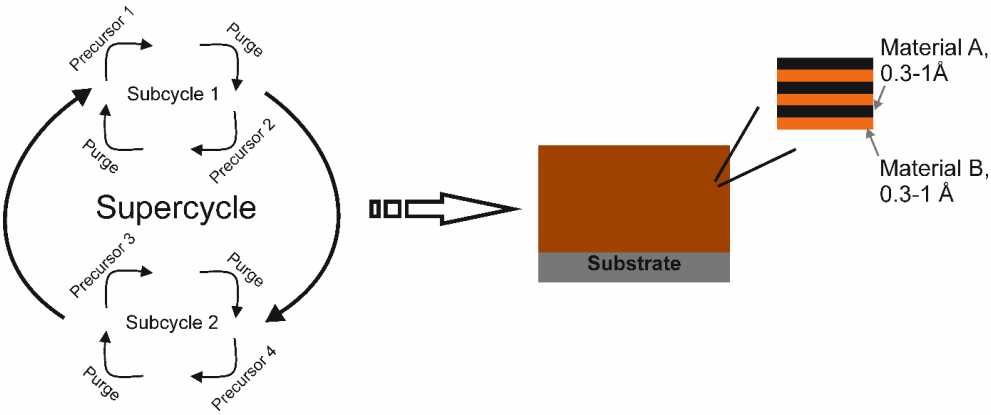

Figure 11: In the subcycle approach to deposit ternary materials by ALD, the ALD cycles of two different materials are applied after one another. The amounts of cycles for each subcycle can be tuned. As a result, a ternary material is deposited, with intermixed layers. If the numbers of subcycles are made large enough, nanolaminates are formed.

Ternary films deposited by the subcycle approach are most often amorphous as-deposited but can be crystallized with post-deposition annealing.[74, 90] In essence, annealing offers also another convenient route to produce ternary materials with ALD. Post-deposition annealing can be used to obtain a homogenous ternary material from nanolaminate film stacks (Figure 12).[92, 93] In an extreme case, only two thick layers of the corresponding binary materials are deposited and then exposed to high temperatures.[VI, 96–98] By using this bilayer method and solid state reactions induced by the post-deposition annealing, ternary materials can be obtained also in cases where, for example, the ALD windows of the two materials to be mixed do not overlap, or the growth of the two materials on top of each other is not completely linear.[96, 97] In addition, this method provides a convenient way to combine ALD with other thin film deposition processes for the deposition of ternaries.[99] Even stacks composed of films tens of nanometers in thickness can be made to react with sufficient annealing.[96, 98, 100, 101] One limitation of this method is the low diffusivity of many metal ions, especially in oxides. Still, higher annealing temperatures can often be used to counter-effect the low diffusivities. In addition to problems with the ion diffusivities, void formation as a result of the Kirkendal effect can occur with this method.[98, 100] Mobile metal ions, for which this method can be especially useful, include for example lithium,[VI, VII] copper(I),[97, 101] and bismuth.[92, 102] In this work, papers VI and VII report our findings on the deposition of lithium containing ternary oxides by the combination of atomic layer deposition and solid state reactions.

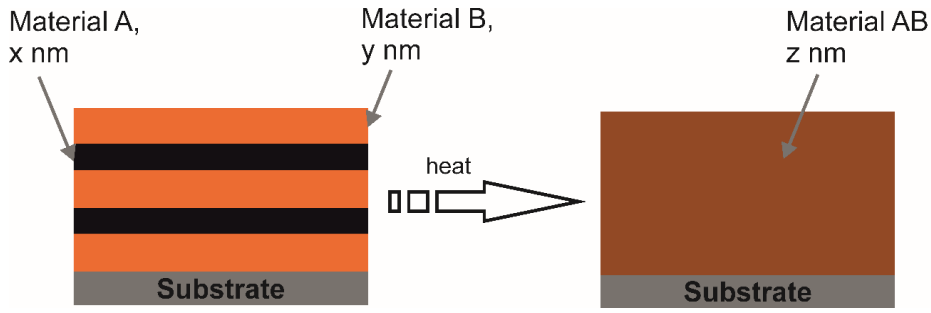

Figure 12: Ternary materials can be obtained from ALD-made thin film stacks with post-deposition annealing.

A third way of depositing ternary materials by ALD is to use single-source precursors (Figure 13).[74] In CVD literature, single-source precursors are complexes which deposit all the required film elements, including, for example, oxygen via the thermal decomposition of the precursor.[69, 103] However, in ALD the use of additional anion sources, such as water, is needed to maintain the self-limiting growth mechanism. In ALD, single-source precursors are viewed as complexes combining either multiple metals[104] or a metal with a nonmetal,[102] preferably in the stoichiometry desired for the deposited ternary or quaternary material. Thus, by using single-source precursors ternary materials can be deposited in a four-step cycle in a similar fashion as binary materials.[102, 104–108] For example, strontium tantalate $SrTa_2O_6$ films have been deposited using a heteroleptic double metal alkoxide precursor $SrTa_2(OEt)_{10}(dmae)_2$ and water,[105] and lithium silicate Li_2SiO_3 has been deposited using a lithium silylamide precursor in combination with ozone.[76, 109] However, this method has not been used very extensively in ALD because the stringent precursor property demands are difficult to meet with very large and complicated complexes.[69, 108, 110] In contrast, in CVD many examples of this method have been produced.[103, 107, 108, 111] For this thesis, a literature review was made to study the possibility of using double metal alkoxides as single-source precursors for lithium multicomponent oxides.[I]

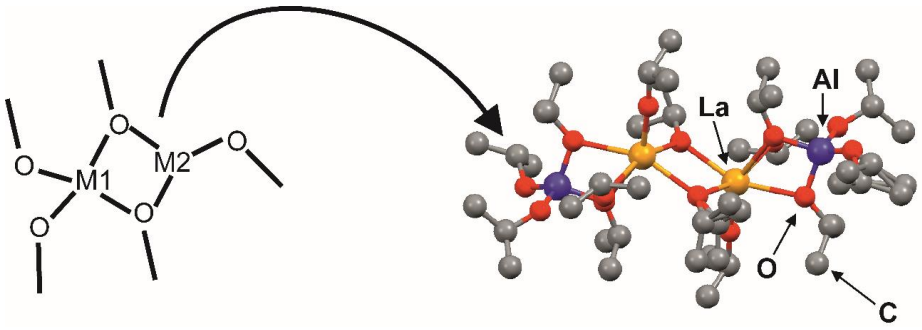

Figure 13: A schematic, and an atomic model of a bimetallic, single-source alkoxide precursor $[LaAl(O^iPr)_6(HO^iPr)]_2$. This compound has been used to deposit ternary lanthanum aluminum oxide by liquid injection ALD.[108, 111] Hydrogen atoms have been omitted for clarity.

3.2 Atomic layer deposition of metal fluorides

Fluoride materials have been of interest to ALD chemists since the beginning of the 1990s. In the very beginning, doping electroluminescent materials with fluorine was studied,[112] and soon after the first report on depositing CaF_2, ZnF_2 and SrF_2 was published.[79] For the first two decades, metal fluorides were studied because of their optical properties, namely low refractive indices and low absorption in the UV range.[58] However, with the rise of lithium-ion battery related ALD research, the potential of metal fluorides in batteries has also been recognized.[47, 80, 88, 113] Table 4 summarizes reported ALD fluoride processes, except those containing lithium, namely $LiF^{II, III}$ [81, 114] and Li_3AlF_6[V, 47] that will be covered in the next subchapter on ALD of lithium containing materials.

Table 4: ALD processes reported for fluoride materials.

Material	Precursors	T_{Dep}, °C	Growth rate, Å/cycle	Ref.
MgF_2	$Mg(thd)_2$ + Hhfac + O_3	N.A.	0.38	115
MgF_2	$Mg(EtCp)_2$ + HF - py	150	0.4	81
MgF_2	$Mg(EtCp)_2$ + HF	100–250	Varies, 0.6 at 100 °C	116
MgF_2	$Mg(thd)_2$ + TiF_4	250–400	Varies, 1.6 at 250 °C	84
MgF_2	$Mg(thd)_2$ + TaF_5	225–400	Varies, 1.1 at 225–250 °C	87

Material	Precursors	T_{Dep}, °C	Growth rate, Å/cycle	Ref.
CaF_2	$Ca(thd)_2$ + HF	300–400	0.2 at 320–400 °C	79
CaF_2	$Ca(hfac)_2$ + O_3	300	0.3	115
CaF_2	$Ca(thd)_2$ + Hhfac + O_3	250–350	0.4	115
CaF_2	$Ca(thd)_2$ + TiF_4	300–450	Varies, 1.6 at 300–350 °C	83
SrF_2	$Sr(thd)_2$ + HF	260–320	Varies, 0.6 at 300 °C	79
ZrF_4	TEMAZ + HF - py	150	0.9	81
ZrF_4	$Zr(O^tBu)_4$ + HF - py	150	0.6	81
HfF_4	TDMAH + HF - py	150	0.8	81
MnF_2	$Mn(EtCp)_2$ + HF - py	150	0.4	81
ZnF_2	$Zn(Ac)_2 \cdot 2H_2O$ + HF	260–320	0.7 at 260–300 °C	79
ZnF_2	DEZ + HF - py	150	0.7	81
AlF_3	$AlCl_3$ + TiF_4	160–340	Varies, 0.75 at 240 °C	IV
AlF_3	TMA + HF - py	75–300	Varies, 1.0 at 150 °C	80
AlF_3	TMA + HF	100–200	Varies, 1.2 at 100 °C	82
AlF_3	TMA + TaF_5	125–350	Varies, 1.9 at 125 °C	88
YF_3	$Y(thd)_3$ + TiF_4	175–325	Varies, 1.3–1.5 at 200–300 °C	86
LaF_3	$La(thd)_3$ + Hhfac + O_3	N.A.	0.49	115
LaF_3	$La(thd)_3$ + TiF_4	225–350	Varies, 5.2 at 225–250 °C	85
AlW_xF_y	TMA + WF_6	200	1–1.5	113

The ZnF_2, SrF_2 and CaF_2 films, reported in the first paper on ALD of fluorides in 1994, were deposited using HF as the fluorine source.[79] The HF gas was generated in the reactor *in situ* by thermal decomposition of NH_4F. Thus, there was no need to handle gaseous HF. An added benefit of this method was that excess HF can be condensed inside the reactor as ammonium fluoride, without the gas entering and damaging the pump. Metal thd-complexes were used as precursors for strontium and calcium, and zinc fluoride was deposited using zinc acetate. All

the films were close to stoichiometric and polycrystalline, with carbon impurities of the order of 0.5 at%. For the calcium and strontium fluoride processes, the growth rates decreased with increasing deposition temperatures, as has been since observed for many other fluoride processes.[II, IV, 80]

The work on fluoride deposition using HF has been continued by Hennessy *et al.*, who have deposited magnesium and aluminum fluoride films using anhydrous HF with bis(ethylcyclopentadienyl)magnesium and TMA.[82, 116] The magnesium fluoride showed growth rates of 0.6 to 0.3 Å/cycle in the deposition temperature range of 100 to 250 °C.[116] AlF_3 showed a similar decrease in growth rate, being 1.2 Å/cycle at 100 °C and 0.5 Å/cycle at 200 °C.[82] The MgF_2 films were crystalline and showed small amounts of carbon and oxygen impurities and a slight fluorine deficiency in X-ray photoelectron spectroscopy (XPS) measurements.[116] All the AlF_3 films were amorphous, with 1–2 at% of oxygen.[82] The aluminum fluoride films were stoichiometric based on the XPS measurements. The anhydrous HF required an unconventionally long purging time to obtain good film uniformity. It was speculated that multilayer physisorption might be the cause for this effect. However, it has been reported that MgF_2 does not readily adsorb HF during the ALD growth process.[81]

A number of metal fluorides have recently been deposited by Lee *et al*. using HF, including AlF_3,[80] LiF, ZrF_4, ZnF_2 and MgF_2.[81] To mitigate the safety concerns of anhydrous, gaseous HF, HF was generated from a mixture containing 30 w% of pyridine and 70 w% HF ("*Olah's reagent*"). The mixture is in equilibrium with gaseous HF, with no pyridine detected in the gas phase, and provides a safer alternative to pure, anhydrous HF.[80, 81] Metal precursors used included a diethylcyclopentadienyl complex for magnesium, a silylamide for lithium and alkylamide for zirconium. All processes resulted in saturation at 150 °C, with growth rates below 1 Å/cycle. All films, except AlF_3 and ZnF_2, were crystalline. Generally, the films contained less than 2 at% of oxygen impurities, as determined with XPS. Only ZrF_4 contained some carbon impurities in addition to the oxygen. The films appeared somewhat fluorine deficient, however this is speculated to be a result of preferential fluorine sputtering during the XPS measurement.[80, 81] In AlF_3 deposition from TMA and HF, an interesting etching reaction was observed: above 250 °C the precursor pulses etch AlF_3 in a non-self-limiting manner.[80, 82] We have also noted an etching reaction taking place during AlF_3 deposition, as will be discussed in chapter 5.2.2.[IV]

The deposition of many metal fluorides has been studied using TiF_4 as the fluorine source, including materials such as MgF_2, LaF_3 and CaF_2.[83–86] TiF_4 is a relatively safe alternative to HF, since it is a solid at room temperature. Still, it possesses relatively high volatility and

thermal stability, combined with high reactivity, making it a good ALD precursor. The use of TiF_4 is made possible by a net ligand exchange reaction with a metal thd-complex:

$$4M(thd)_x\,(g) + xTiF_4\,(g) \rightarrow 4MF_x\,(s) + xTi(thd)_4\,(g)$$

Also other volatile side products, such as $TiF_x(thd)_{4-x}$ can form. Recently, this precursor was demonstrated to work also with a metal chloride as the metal precursor.[IV]

Generally, metal fluorides deposited using TiF_4 as the fluorine source show a decrease in the growth rate as the deposition temperature is increased.[83] This decrease has been proposed to be due to a decrease in the TiF_x adsorption density, but this has not been verified experimentally. The film growth shows saturation with respect to the fluorine precursor, but the metal precursor can show both poor[84, 86] and good saturation,[85] depending on the material studied (Figure 14). Titanium is found as an impurity in all the films, but usually in only very small amounts.[83, 84] Still, this impurity can limit the UV transmittance of these films. The amount of impurities decreases as the deposition temperature is increased, but at the same time film roughness increases, resulting in more scattering of UV-light.[84–86]

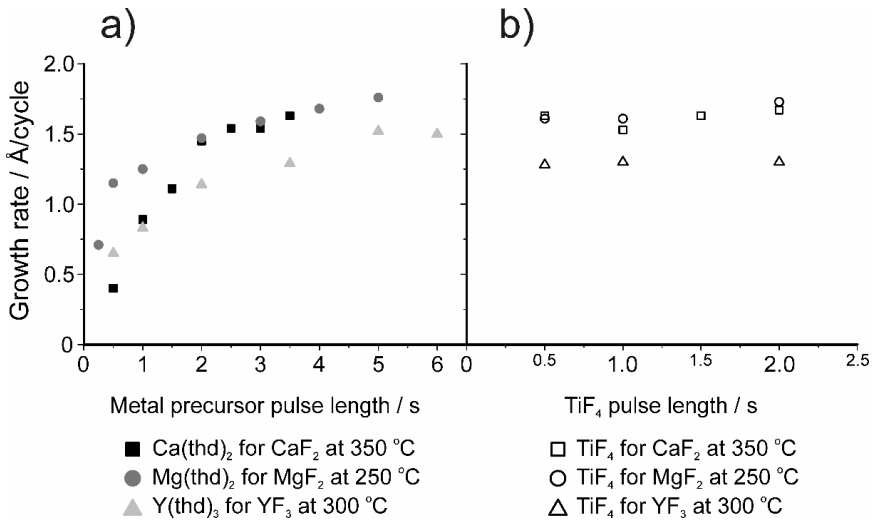

Figure 14: Saturation curves for metal fluoride deposition utilizing TiF_4 as the fluorine source, exhibiting the less than ideal saturation of the metal thd-complexes. a) Metal-thd precursor saturation for CaF_2, MgF_2 and YF_3 deposition b) TiF_4 saturation for CaF_2, MgF_2 and YF_3 deposition. Data obtained from refs [83], [84] and [86].

In an effort to obtain even purer metal fluoride films for optical applications, deposition of MgF_2 has been studied using TaF_5 as the fluorine source.[87] The growth process is very similar to that using TiF_4, although with TaF_5 saturation with respect to the $Mg(thd)_2$ pulse length is observed. The films contained less metal impurities than those deposited with TiF_4, and in addition the films were much smoother at high deposition temperatures.[84, 87] This resulted in improved optical properties.

Jackson *et al.* have attempted to combine the methods reported above for the deposition of AlF_3 by using TMA and TaF_5 as precursors.[88] This method is somewhat questionable, as it has been reported that combining TMA with metal halides leads to metal carbide deposition.[117–119] In addition, a metathesis reaction between TMA and TaF_5 should produce pentamethyl tantalum, which has been reported to be unstable.[120, 121] Indeed, also in this case significant amounts of TaC_x were deposited at elevated temperatures.[88] At 125 °C, the amount of tantalum impurity was decreased, and the process showed ALD-like behavior. The films contained approximately 20 at% of oxygen, meaning the process is unable to deposit good quality AlF_3. Despite the large amount of impurities, depositing this material onto a high-voltage lithium-ion battery cathode material led to significant improvements in its rate performance.

Similarly to Jackson *et al*., Park *et al*. used TMA with WF_6 to deposit an amorphous composite fluoride, composed of AlF_3 and metallic W and WC_x.[113] The material was studied as an artificial SEI-layer for $LiCoO_2$ and was found to improve the cycling properties of the cathode material. It appeared that the composite nature increased the conductivity of the fluoride layer while still retaining its chemical inertness.

Putkonen *et al*. provided other interesting pathways for avoiding the use of HF in fluoride deposition by depositing metal fluorides through oxide chemistry.[115] They found that by using the fluorinated β-diketonate precursor $Ca(hfac)_2$ and ozone as precursors, CaF_2 is deposited instead of the expected $CaCO_3$. The films had a growth rate of 0.3 Å/cycle at 300 °C and were close to stoichiometric, although approximately 5 at% of oxygen was present in the films. The more interesting approach to CaF_2 used a non-fluorinated metal precursor, such as $Ca(thd)_2$, in combination with ozone and the Hhfac molecule. First, $Ca(thd)_2$ was pulsed onto the substrate, followed by an ozone pulse, resulting in $CaCO_3$ deposition. Then Hhfac, which is known to adsorb to surfaces, was pulsed, followed again by an ozone pulse. Hhfac is broken down on the surface, providing fluoride ions which react with the calcium ions, resulting in a conversion reaction and turning $CaCO_3$ into CaF_2. This process provided a growth rate of 0.4 Å/cycle between 250 and 350 °C, which is close to the rate of $CaCO_3$ deposition from $Ca(thd)_2$ and ozone in similar conditions. The CaF_2 films were polycrystalline and close to stoichiometric, and the amount of oxygen was below the detection limit of Rutherford backscattering spectroscopy (RBS). The same approach was reported to be successful also for MgF_2 and LaF_3 deposition.

3.3 Atomic layer deposition of lithium containing materials

Lithium containing materials are, naturally, essential in the formulation of a lithium-ion battery. These materials are quite a new addition to the ALD family, as the first paper on the subject was published in 2009.[122] Since then, this area of research has expanded very rapidly. Putkonen *et al.* reported in the first paper studies on different possible ALD lithium precursors, which included alkoxides, alkyls, amides and β-diketonates.[122] The most suitable ALD precursors ended up being lithium *tert*-butoxide (LiO^tBu) and lithium 2,2,6,6-hexamethyl-3,5-heptanedionate (Lithd), which have been used in numerous ALD processes. Later, also lithium hexamethyldisilazide (LiHMDS, also known as lithium bis(trimethyl silyl)amide), a well-known organometallic synthesis starting material, was shown to be suitable for ALD purposes.[75–77] The advantages of using LiHMDS include a much lower evaporation temperature compared to LiO^tBu and Lithd, and its potential as a single-source precursor for lithium silicate deposition.[76]

Due to the mobility and reactivity of Li^+ ions, atomic layer deposition of lithium containing materials has shown to be somewhat different from most other ALD processes. Next, the properties of ALD processes for both binary and ternary lithium containing materials are covered, with emphasis on the growth reactions.

3.3.1 Binary materials

A natural starting point in the ALD research on lithium materials was the deposition of different binaries. Both lithium carbonate and oxide deposition have been studied in multiple publications, and later materials such as silicates and phosphates have gained interest. Binary lithium materials deposited by ALD have been collected in Table 5.

Table 5: ALD processes reported for binary lithium containing materials, i.e. materials with lithium being the only metal ion.

Material	Precursors	T_{Dep}, °C	Growth rate, Å/cycle	Ref.
Li_2O/LiOH	LiO^tBu + H_2O	225[123, 124] 225–300[125]	2.2 at 225 °C[124]	122–125
Li_2O/Li_2CO_3	LiO^tBu + O_2 plasma	225–300	N.A.	125
Li_2CO_3	Lithd + O_3	180–300	0.30 at 180–225 °C	122

Material	Precursors	T_{Dep}, °C	Growth rate, Å/cycle	Ref.
Li_2CO_3	$LiO^tBu + H_2O + CO_2$	225	0.8 at 225 °C	123
Li_2CO_3	LiHMDS + H_2O + CO_2	89–428	0.35 at 140–240 °C	75
Li_2CO_3	LiTMSO + H_2O + CO_2	175–300	0.5 at 225 °C	126
Li_3N	LiHMDS + NH_3	167, 332	0.95 at 167 °C	75
Li_2SiO_3	LiHMDS + O_3	150–400	Varies, 0.9 at 250 °C	76, 109
Li_xSi_yO	LiTMSO + O_3 + H_2O	175–300	1.55 at 200–300 °C	126
Li_3PO_4	LiO^tBu + TMPO	225–300[77] 250–350[127]	0.7 at 225–275 °C,[77] 0.69 at 300 °C[127]	77, 127
Li_3PO_4	LiHMDS + TMPO	275–350	Varies, 0.6 at 300 °C	77
LiPON	LiHMDS + DEPA	250–350	0.7 at 270–310 °C	78
LiPON	$LiO^tBu + H_2O$ + TMPO + N_2 plasma	250	1.05	128
Li_2S	$LiO^tBu + H_2S$	150–300	1.1 at 150–300 °C	129
LiF	LiHMDS + HF - py	150	0.5	81
LiF	$LiO^tBu + WF_6$	150–300	N.A.	114
LiF	$LiO^tBu + MoF_6$	150–300	2.6	114
LiF	Lithd + TiF_4	250–350	1.0 at 325 °C	II
LiF	$Mg(thd)_2$ + Lithd + TiF_4	300–350	1.4 at 325 °C	III
LiF	MgF_2 + Lithd	275–325	N.A.	III
LiTP	Lithd + TPA	200–280	3.0 at 200 °C, decreases with T_{Dep}	130
Li_2Q	LiHMDS + HQ	105–280	4.6 at 120 °C, decreases with T_{Dep}	131

Oxides, such as Al_2O_3 and TiO_2, are often considered as the model materials for atomic layer deposition. However, in the case of lithium even the deposition of the simple binary oxide Li_2O is a challenge. In the first lithium ALD paper, Putkonen *et al.* reported that reacting lithium *tert*-butoxide with water resulted in rough films which reacted in air.[122] The first paper reported little analysis of these films, but it was postulated that the material forming during the deposition was either Li_2O or LiOH. Lithium oxide readily reacts with water, forming LiOH. Lithium hydroxide is hygroscopic, and both the oxide and hydroxide react with ambient carbon dioxide to form lithium carbonate.[125] This was verified by the results of Cavanagh *et al.* a year after the initial report.[123] They followed the oxide deposition process with a quartz crystal microbalance (QCM) and noted that during an excessively long purge time the film lost a considerable amount of its mass. This can be explained as water desorption from a $LiOH \cdot H_2O$ film. Other groups have observed similar mass losses, and attributed them to water loss from unhydrated LiOH, resulting in Li_2O formation.[124, 125] *In situ* FTIR (Fourier transform infrared spectroscopy) provided evidence for LiOH formation during the growth process, as a sharp absorption peak at 3672 cm^{-1} was observed, which can originate from hydroxyl stretching vibrations in unhydrated LiOH. [123] *Ex situ* FTIR measurements showed that the films converted to Li_2CO_3 upon exposure to air.[123] Kozen *et al.* continued the studies on LiO^tBu and water a few years later using ultra-high vacuum (UHV) equipment and *in situ* XPS.[125] They noticed that films deposited at 225 °C were composed almost entirely of LiOH, whereas Li_2O with a hydroxylated surface layer was formed at 240 °C and above. The Li : O ratio was 1 : 1 at 225 °C, consistent with LiOH formation, and increased to 2 : 1 at higher temperatures. LiOH films could also be dehydrated, and formed Li_2O upon annealing at 300 °C.[124]

Since Li_2O/LiOH has a tendency to form Li_2CO_3 in air, it comes as no surprise that the carbonate can be easily deposited by ALD using combustion reactions with ozone. Putkonen *et al.* were the first to report also the deposition of this material.[122] They used Lithd as the lithium precursor, and showed that the process can be used to deposit Li_2CO_3 between 180 and 300 °C. The process had an ALD window between 180 and 225 °C, with a growth rate of 0.3 Å/cycle. The process showed good ALD behavior also in that the growth rate saturated with a 0.8 s Lithd pulse at 225 °C. The resulting films were crystalline and had a high roughness. Time-of-flight elastic recoil detection analysis (ToF-ERDA) measurements revealed that the films were very close to stoichiometric, the composition being $Li_{1.9}CO_{2.9}$ at a deposition temperature of 185 °C.

Due to the reactivity of Li_2O/LiOH, carbonate films can also be deposited by taking advantage of the conversion reaction of Li_2O/LiOH with carbon dioxide.[75, 123, 125, 126] Conversion of LiOH films has been reported to be much faster than that of Li_2O films at 225 °C.[125] The carbonate can be deposited by the pulsing sequences of $LiO^tBu + H_2O + CO_2$,[123, 125] LiHMDS + H_2O + CO_2,[75] and LiTMSO + H_2O + CO_2 (LiTMSO = lithium trimethyl silanolate). The growth rate of the film deposited with the *tert*-butoxide process was calculated from QCM data as 0.8

Å/cycle at 225 °C, assuming the film has the same density as bulk Li_2CO_3.[123] *Ex situ* FTIR and XPS measurements confirmed the presence of Li_2CO_3, with the exact composition being $Li_{1.7}CO_{2.5}$. For the silylamide process, a similar pulsing sequence was used in the temperature range of 89–428 °C.[75] An ALD-window was found approximately between 140 and 240 °C, with a growth rate of 0.35 Å/cycle. Between 89 and 380 °C, the films appeared very close to stoichiometric, as determined with XPS. The films were rough, and oriented in the (002) direction on silicon (100). The trimethyl silanolate process is very similar to the other two, producing a growth rate of approximately 0.5 Å/cycle at 225 °C.[126] The deposition temperature range was limited to 175–300 °C by the silanolate evaporation and decomposition temperatures. The resulting films were crystalline and similarly oriented as those deposited using the silylamide precursor.

In addition to thermal ALD processes, Kozen *et al.* have deposited a Li_2CO_3/Li_2O mixture film using LiO^tBu and oxygen plasma as precursors.[125] The mixture films could be deposited between 225 and 300 °C. The ratios of the two materials were reported to be independent of deposition temperature and plasma dose, however no information on the actual ratios was given. In this process the carbonate formation is a result of incomplete combustion reactions between the lithium precursor and the plasma-excited species.

Østreng *et al.* deposited Li_3N using LiHMDS and ammonia as precursors between 167 and 332 °C.[75] To facilitate the deposition and *ex situ* analyses, MoN_x films were used both as a buffer layer on the soda lime and titanium substrates and as a capping layer on the lithium nitride to protect the film from ambient air. The process showed saturation with both precursors and a linear relationship between film thickness and the number of deposition cycles at 167 °C. At 332 °C a mixed α- and β-phase film was deposited, with also some LiOH and Li_2CO_3 present. Due to the use of the silylamide precursor, approximately 6 at% of silicon impurity was found with XPS.

The silylamide precursor LiHMDS also provides a convenient route to lithium silicate deposition.[76, 109] Using ozone as the other precursor, LiHMDS can be combusted to lithium silicate in a similar manner as single-source precursors are used for the deposition of ternary materials. The process exhibited good ALD behavior at 250 °C, with saturation of both precursors seen, and the growth rate increased linearly with the number of cycles. However, no ALD window was present, the growth rate increasing from approximately 0.3 Å/cycle at 150 °C to 1.7 Å/cycle at 400 °C. This increase was explained with subsequent reaction mechanism studies:[109] The HMDS-ligand of the metal precursor reacts with surface hydroxyl groups, decomposing to different side products. Some of these are unreactive in the process but can still block active sites from the desired $-Si(CH_3)_3$ groups. At higher temperatures the decomposition

of the ligand to -$Si(CH_3)_3$ is enhanced, and in addition desorption of unreactive products is faster. The deposited films were amorphous below 400 °C and showed only small amounts of carbon and hydrogen impurities, as determined by ERDA.[76] Notably, no nitrogen was detected in the film despite the lithium precursor being a silylamide. The Li : Si and Si : O ratios changed with deposition temperature, but at 250 °C the film composition was $Li_2SiO_{2.9}$ which is very close to the lithium metasilicate Li_2SiO_3. The changing Li : Si ratios could be explained with the same reaction mechanism as the increasing growth rate: at higher temperatures more $Si(CH_3)_3$-groups are adsorbed on the surface and then decomposed to SiO_2 during the ozone pulse, resulting in a decreasing lithium to silicon ratio.[109]

Lithium silicate was later deposited also using LiTMSO.[126] In order to obtain good quality films, both an ozone and a water pulse was needed after the metal precursor pulse. It was postulated that the water generates hydroxyl groups on the surface of the silicate film, which are beneficial for LiTMSO adsorption. All the films were amorphous, and the growth rate remained constant at 1.5 Å/cycle between 200 and 300 °C. Films deposited at low temperatures had significant hydrogen contents of 14 at%. The amounts of both lithium and silicon increased with increasing deposition temperatures, but the Li : Si ratio remained at 2 : 1.

LiPON, currently the most often used solid lithium-ion electrolyte material, was undoubtedly the motivator for the atomic layer deposition studies on lithium phosphate films. Li_3PO_4 can be deposited using either LiO^tBu or LiHMDS as the lithium source and TMPO (trimethyl phosphate) as the phosphate precursor (Figure 15).[77, 127] The LiO^tBu + TMPO process showed a constant growth rate of approximately 0.7 Å/cycle between 225 and 275 °C.[77] However, no complete saturation was observed. The films were slightly crystalline, and showed decreasing impurity levels at higher deposition temperatures in ERDA measurements. At 300 °C, the film composition was $Li_{2.6}PO_{3.7}$. The process utilizing LiHMDS is less than ideal, as the film growth rate varies strongly with deposition temperature, being 0.4 Å/cycle at 275 °C and 1.3 Å/cycle at 350 °C. At 300 °C, these films were close to stoichiometric lithium phosphate, being $Li_{2.8}PO_{3.9}$ as determined by ERDA. However, using LiHMDS as the lithium precursor led to higher carbon and hydrogen impurities than in the LiO^tBu process. Regardless of the lithium precursor, the phosphate films crystallized into the orthorhombic Li_3PO_4 phase during high temperature X-ray diffraction (HTXRD) measurements. Wang *et al.* and Létiche *et al.* have studied the Li_3PO_4 process using LiO^tBu and TMPO in an effort to measure the lithium-ion conductivity of these films.[127, 132] Wang *et al.* reported an increasing growth rate as a function of the deposition temperature at 250–325 °C, which might be a result of the somewhat unsaturative behavior of the process.[77] Electrochemical impedance spectroscopy showed that the films had rather good conductivities when deposited at 300 °C: $3.3 \cdot 10^{-8}$ S/cm was extrapolated for a film with a composition of $Li_{2.8}PO_z$ (as determined by XPS).[127] Similarly, Létiche *et al.* reported conductivities as high as $4.3 \cdot 10^{-7}$ S/cm for Li_3PO_4 deposited at 300 °C.

These results are rather surprising, as it can be called common knowledge that lithium phosphate is no match for its nitrogen-doped counterpart LiPON, with conductivities of 10^{-6}–10^{-8} S/cm.[24] It appears that the small film thicknesses play a role in these high ionic conductivitites.[132] Li_3PO_4 layers have already been studied also in contact with electrode materials,[133, 134] and it has been found that although the phosphate layer can decrease the electrode capacity, capacity retention is increased due to less transition metal dissolution and more stable SEI formation.[133]

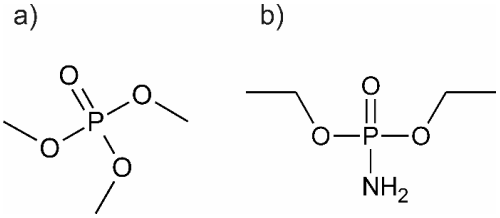

Figure 15: The structures of two phosphorus precursors used to deposit lithium phosphate and LiPON. a) TMPO, or trimethyl phosphate and b) DEPA, or diethyl phosphoramidate.

Recently, the deposition of LiPON was achieved both by thermal and plasma-enhanced ALD.[78, 128] In the PEALD process, LiO^{t}Bu was used as the lithium source, combined with a pulsing sequence of water, TMPO and nitrogen plasma.[128] Deposition of Li_2O/LiOH before exposure to TMPO resulted in less carbon impurities as compared to the process used by Hämäläinen *et al.* for Li_3PO_4. By using nitrogen plasma after the TMPO pulse, nitrogen could be incorporated into the films, causing the amorphization of the crystalline Li_3PO_4. In the thermal ALD process, the problem of nitrogen-phosphorous bond formation was resolved by using diethyl phosphoramidate or DEPA, a phosphate precursor with an amine group (Figure 15).[78] By using DEPA with LiO^{t}Bu, nitrogen contents as high as 9.7 at% were achieved. However, this process led to high carbon impurities from 9.9 to 13.3 at%, compared to virtually none in the plasma process.[128] Both processes deposited conformal coatings on demanding substrates as required from a potential solid electrolyte material. In addition, very good electrochemical properties were realized, with ionic conductivities of $1.45 \cdot 10^{-7}$ S/cm for the plasma process (5 at% nitrogen contents) and $6.6 \cdot 10^{-7}$ S/cm for the thermal process (9.7 at% nitrogen).[78, 128] The plasma-deposited LiPON has already been studied as a protecting layer for a conversion lithium-ion battery electrode. It was found that the LiPON layer enhanced the capacity retention of the electrode by providing both a high lithium-ion conductivity and mechanical support during cycling.[135]

Lithium sulfide, Li_2S, has also been deposited by ALD.[129] As with Li_2O,[125] working with this material requires inert atmosphere during sample handling to prevent reactions with ambient air. Li_2S has been deposited using LiO^{t}Bu and hydrogen sulfide between 150 and 300 °C.

Unlike most lithium containing processes, this one produced a constant growth rate over the whole deposition temperature range studied. The refractive index of the films was much lower than the value for bulk crystalline Li_2S, indicating a lower density of the films. The films were amorphous, and could not be crystallized with annealing in inert atmosphere. Both X-ray fluorescence (XRF) and XPS gave a Li : S ratio of 2 : 1, with no carbon contamination in the Li_2S layer. Thus, the reaction between the precursors was very efficient. The Li_2S films produced high capacities of 800 mAh/g and a Coulombic efficiency of ~ 100% in electrochemical testing, indicating that the material could be used as a cathode in lithium-sulfur batteries. However, film thickness had a large effect on the capacity, with thicker films producing smaller capacities per gram, as Li_2S is rather insulating. In addition, reactions with the copper current collector affected the charge-discharge profiles, indicating the formation of Cu_xS.

We have reported multiple ways for the deposition of lithium fluoride by ALD using solid precursors.[II, III] These results will be summarized in Chapters 5.2.1 and 5.3.1. LiF has also been deposited using LiHMDS and a HF-pyridine mixture, as was summarized for a number of other fluorides in the previous chapter.[81] LiF was deposited at 150 °C with a growth rate of 0.5 Å/cycle. The films had a refractive index of 1.37 and contained no O, C, N or Si impurities, as determined with XPS. The films were crystalline, and showed the same fluorine deficiency as other metal fluorides deposited with the same method. Similar to our method of using metal fluorides as fluorine sources, Mane *et al.* have reported on the deposition of LiF using LiO^tBu and either WF_6 or MoF_6 as the fluorine source.[114] Film growth took place between 150 and 300 °C, with amorphous films being deposited at the lowest temperature. Using MoF_6 the films had a growth rate of 2.6 Å/cycle. The films showed a 1 : 1 ratio of Li and F, with very small amounts of oxygen and carbon impurities. Most importantly, metal impurities were not detected with XPS.

In addition to purely inorganic materials, ALD can also be used to deposit hybrid materials using organic molecules as the second precursor.[136] Lithium terephthalate (LiTP, Figure 16) has been deposited using Lithd and terephthalic acid as precursors between 200 and 280 °C.[130] This material has been proposed as a possible Li-ion battery anode material due to its high theoretical capacity of 300 mAh/g and a low potential of 0.8 V (vs. Li^+/Li).[137] The ALD process for LiTP showed saturation, but no ALD window or constant growth rate as a function of the number of cycles. The changing growth rate, accompanied by changes in the film density, could be related to the island growth mechanism of the film. The films were crystalline already as deposited, which is unusual for ALD-made hybrid films. The films were electrochemically active and showed high rate capabilities with good capacity retention. The properties of the films could further be enhanced by a protective LiPON layer on top of the electrode.

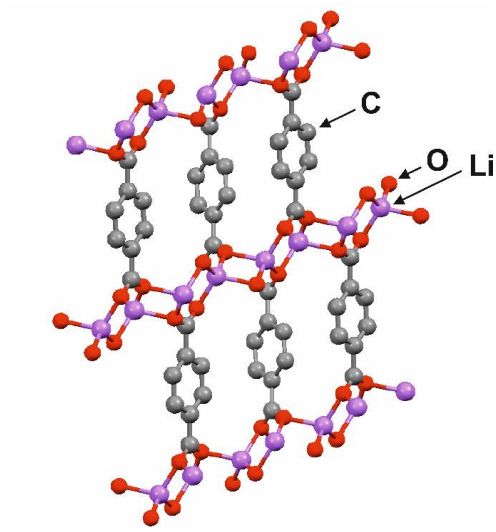

Figure 16: Structure of lithium terephthalate (space group P21/c). Hydrogen atoms have been omitted for clarity. Figure modified from ref. [138].

The work on lithium containing hybrid materials was continued by Nisula *et al.* with their experiments on dilithium 1,4-benzenediolate, Li_2Q.[131] The process used LiHMDS and hydroquinone as precursors, and deposited films between 105 and 280 °C. For *ex situ* analyses, the films needed to be protected with a thin Al_2O_3 film against contact with the ambient. Saturation was observed for both precursors, and all films were crystalline as-deposited with a low density of 1.2 g/cm^3. The crystal structure of the films resembled that of the sodium and potassium analogs, however with larger *a* and *b* lattice parameters. If no protection layer was used, a reaction in air occurred, with changes apparent both in grazing incidence X-ray diffraction (GIXRD) and FTIR measurements. Interestingly, the original crystal structure could be regained after exposure to air by a heating treatment and capping with alumina. Nisula *et al.* explain this as water absorption and release from coordinatively unsaturated lithium sites in the crystal structure.

3.3.2 Ternary and quaternary materials

Table 6 encompasses lithium containing ternary and quaternary materials deposited by ALD. The convention "Li_xM_yO" is used to describe the materials, since often many different metal stoichiometries have been obtained. For the deposition of lithium containing ternary materials, the subcycle method is commonly used. Thus, in most papers results on lithium contents as a function of subcycle ratio are reported. Most often the $LiO^tBu + H_2O$ process is used, despite its controllability problems. However, Lithd and LiHMDS are becoming increasingly more common precursors in these processes. Due to the reactivity of lithium oxide and mobility of the lithium-ion, already a small amount of lithium subcycles can lead to very large lithium contents in the deposited films. Because these materials are primarily of interest as lithium-ion battery materials, electrochemical characterizations are also often reported.

There seems to be no universally accepted way of reporting data on both the growth rates of lithium containing ternary films and the lithium contents. For this thesis, an attempt has been made to express growth rates per binary cycle. For a film deposited by using a pulsing scheme of x subcycles of material X and y subcycles of material Y for z supercycles, the growth per binary cycle is calculated by dividing the film thickness by $z \cdot (x+y)$. Therefore, the growth rates from some papers have been modified accordingly. For some papers, this modification was impossible due to the lack of information on the pulsing ratio. In these cases, the growth rate will be expressed per supercycle. For the lithium contents, mostly metal ratios of the type Li : M will be reported. However, due to their better translation into figures, metal ratios have also been expressed as cation percentages, or Li/(Li+M), where M is the contents of the other metal in the ternary film.

Table 6: ALD processes reported for ternary and quaternary lithium containing materials, i.e. materials with lithium being accompanied by other metal ions.

Material	Precursors	T_{Dep}, °C	Growth rate, Å/binary cycle	Notes	Ref.
Li_xAl_yO	$LiO^tBu + H_2O$ + TMA + O_3/H_2O	225	1.4 with Li:Al pulsing ratio 1:1[140]	Water absorption evident, pulsing ratio may or may not affect metal ratio	124, 139–141
Li_xAl_yO	LiTMSO + H_2O + TMA + O_3	175–300	1.0 with Li:Al pulsing ratio 1:1	Growth rate constant over temperature range	126, 142

Material	Precursors	T_{Dep}, °C	Growth rate, Å/binary cycle	Notes	Ref.
Li_xCo_yO	LiO^tBu + $CoCp_2$ + O_2 plasma	325	1.0 with Li:Co pulsing ratio 1:1	Metal ratio has a large effect on electrochemical activity	143, 144
$Li_xFe_yPO_4$	LiO^tBu + $FeCp_2$ + O_3 + TMPO + H_2O	300	0.85 with Li:Fe pulsing ratio 1:5.	Fe_2O_3 and PO_x subcycles before Li_2O subcycle	145
$Li_xFe_yPO_4$	Lithd + $Fe(thd)_3$ + O_3 + TMPO + H_2O	250	N.A.	Fe_2O_3 and PO_x subcycles before Li_2O subcycle	146
Li_xMn_yO	LiO^tBu/LiHMDS + $Mn(EtCp)_2$ + H_2O	250 for LiO^tBu; 200 for LiHMDS	Varies with pulsing ratio	Non-uniform films	147
Li_xMn_yO	LiHMDS + H_2O + $Mn(thd)_3$ + O_3	225	N.A.	Non-uniform, amorphous films	147
Li_xMn_yO	Lithd + $Mn(thd)_3$ + O_3	225	0.2 with Li:Mn pulsing ratio 1:19	Low pulsing ratio results in large amount of Li in films	147
Li_xMn_yO	LiO^tBu + H_2O or Lithd + O_3	225	N.A.	Li_2O/LiOH or Li_2CO_3 deposited onto MnO_2	147
Li_xV_yO	LiO^tBu + H_2O or Lithd + O_3	225	N.A.	Li_2O/LiOH or Li_2CO_3 deposited onto V_2O_5	147
Li_xTi_yO	LiO^tBu + $TiCl_4$ + H_2O	225	1.8 with Li:Ti pulsing ratio 1:2	Films air sensitive, low metal ratio	148
Li_xTi_yO	LiO^tBu + $Ti(O^iPr)_4$ + H_2O	225,[148] 250[149]	0.7 with Li:Ti pulsing ratio 1:1,[148] 0.6 with ratio 4:5[149]	$Li_4Ti_5O_{12}$ phase obtained on annealing	148–150
Li_xTi_yO	Lithd + O_3 + $TiCl_4$ + H_2O	225	N.A.	Layer of Li_2CO_3 on top of TiO_2, annealed in air	VI

Material	Precursors	T_{Dep}, °C	Growth rate, Å/binary cycle	Notes	Ref.
Li_xNb_yO	LiHMDS + $Nb(OEt)_5$ + H_2O	235	0.6 with Li:Nb pulsing ratio 1:2	Nb_2O_5 used to passivate reactor between depositions	151
Li_xNb_yO	Lithd + O_3 + $Nb(OEt)_5$ + H_2O	225	N.A.	Layer of Li_2CO_3 on top of Nb_2O_5, annealed in air	VI
Li_xTa_yO	LiO^tBu + $Ta(OEt)_5$ + H_2O	225	0.7 with Li:Ta pulsing ratio 1:6.	High amount of Li and C in films (XPS)	152
Li_xTa_yO	Lithd + O_3 + $Ta(OEt)_5$ + H_2O	225	N.A.	Layer of Li_2CO_3 on top of Ta_2O_5, annealed in air	VI
$Li_xLa_yTi_zO$	LiO^tBu + $La(thd)_3$ + $TiCl_4$ + O_3 + H_2O	225	Varies with pulsing ratio	TiO_2 and La_2O_3 subcycles before Li_2O subcycle	153
$Li_xAl_ySi_zO$	LiO^tBu + TMA + TEOS + H_2O	290	1.0 with Li:Al pulsing ratio 6:10	Al_2O_3 and Li_2O subcycles before SiO_2 subcycle	154
$Li_xLa_yZr_zO$:Al	LiO^tBu + $La(FMAD)_3$ + TDMAZ + TMA + O_3	225	1.0 with Li:La:Zr:Al ratio 8:28:12:1	Ionic conductivity $1.2 \cdot 10^{-6}$ S/cm at 100 °C for amorphous film	155
Li_xAl_yS	LiO^tBu + TDMA-Al + H_2S	150	0.5 with Li:Al ratio 1:1	Ionic conductivity $2.5 \cdot 10^{-7}$ S/cm at RT	156
Li_xAl_yF	LiHMDS + TMA + HF-py	150	0.45 with Li:Al pulsing ratio 1:1	Ionic conductivity $7.5 \cdot 10^{-6}$ S/cm at RT	47
Li_xAl_yF	Lithd + $Al(thd)_3$ + TiF_4	250–350	N.A.	AlF_3 deposition onto LiF films	V
Li_xAl_yF	$AlCl_3$ + TiF_4 + Lithd	250–300	N.A.	Lithd exposure on AlF_3 films	V

The problems of the Li_2O/LiOH process using LiO^tBu and water as precursors are evident when the material is mixed with Al_2O_3 in an effort to deposit lithium aluminate, a material that could be used as a buffer layer between solid electrolytes and electrodes.[124, 139, 141] With a 1 : 1 pulsing ratio of $LiO^tBu + H_2O$ and $TMA + O_3$, Aaltonen *et al.* reported a growth rate of 2.8 Å/supercycle at 225 °C for the amorphous aluminate, resulting in a growth rate of 1.4 per binary cycle.[139] The growth rate per supercycle is very high, especially while considering the Al_2O_3 growth rate of ~ 1 Å/cycle under similar conditions and using the same precursors.[157] Comstock and Elam reported that the growth rate is highly dependent on the pulsing ratio of the two binary oxide materials, although their process differed in that instead of ozone they used water also after the TMA pulse.[124] With Li : Al pulsing ratios smaller than 1 : 1, the growth was reported to be stable. QCM studies revealed that water absorbed readily into both Li_2O and Li_xAl_yO during the film growth, affecting the growth rate.[124, 139] Long enough purge times after the water pulse can be used to better control the growth. With higher Li : Al pulsing ratios, the hygroscopicity of both LiOH and Li_xAl_yO start playing a role in the growth process, leading to larger amounts of adsorbed water and thus to larger amounts of aluminum oxide deposited in very thin films.[124] The composition of the films deposited using TMA and ozone was $Li_{1.6}Al_{1.0}O_z$ by inductively coupled plasma mass spectrometry (ICP-MS), and a surface composition of $Li_{2.2}Al_{1.0}O_z$ was obtained with XPS.[139] XPS also revealed carbon impurities on the surface, indicating the formation of Li_2CO_3. Comstock and Elam found in their study a lithium cation percentage of 55% in a 1 : 1 ratio film.[124] The lithium-ion conductivity of the aluminate was reported to be $9 \cdot 10^{-4}$ S/cm at 400 °C with a rather high activation energy of 2.9 eV.[139] Later, a conductivity of $5.6 \cdot 10^{-8}$ S/cm at room temperature with a much lower activation energy of 0.56 eV was reported by Park *et al.*.[141]

Interestingly, Miikkulainen *et al.*[140] obtained somewhat different results for lithium aluminate films deposited using the same process as Aaltonen *et al.* at 225 °C. They obtained crystalline β-$LiAlO_2$ films with thicknesses of 200–400 nm. For these films the pulsing ratio of Li_2O/LiOH and Al_2O_3 seemed to have no effect on the growth rate or the lithium content: approx. 56–59 cation-% of lithium ended up in the film, regardless of the pulsing ratio (Figure 17). It was postulated that these differences in the deposition process originate from the much higher film thicknesses used in these studies, compared to those of both Aaltonen *et al.* and Comstock and Elam.[124, 139] However, similarly to the results of Comstock and Elam,[124] it was reported that pulsing ratios higher than Li : Al = 2 : 1 led to uncontrollable growth and nonuniform films.

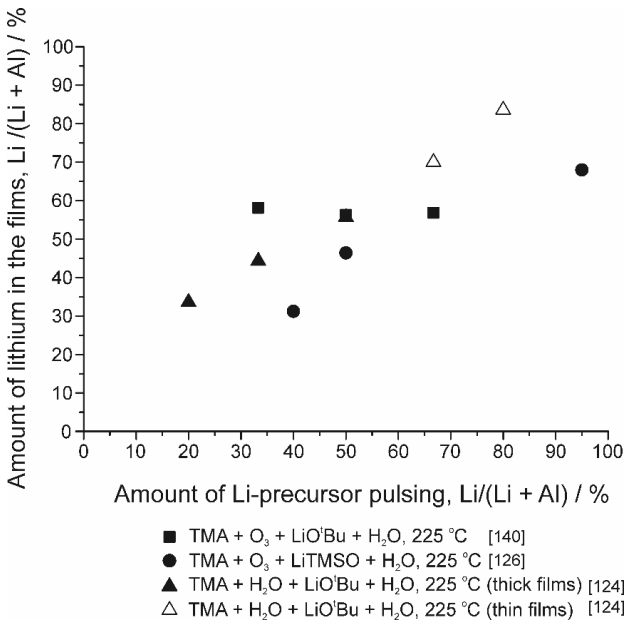

Figure 17: The amount of lithium cations deposited into a lithium aluminate film as a function of the amount of lithium subcycles using different ALD chemistries at 225 °C. Data obtained from refs [124], [126] and [140].

Later, Ruud *et al.* reported their results on using LiTMSO to deposit lithium aluminate.[126] They found that both the growth rate and the refractive index of the films remained relatively stable across the studied deposition temperature range of 175–300 °C, being 1 Å/binary cycle and 1.58, respectively. For films with subcycle pulsing ratio of 1 : 1, the composition of the films was constant at Li : Al = 1 : 1 at all deposition temperatures. The films were amorphous, but could be crystallized with annealing. Unlike in the thick films deposited by Miikkulainen *et al.*, using LiTMSO made it possible to change the metal ratio in the films simply by using larger numbers of subcycles for the lithium component (Figure 17): ratios from Li : Al = 1 : 2.2 to 2.1 : 1 were obtained. Films with a metal ratio 1 : 1.2 were studied with electrochemical impedance spectroscopy (EIS), both in in-plane and cross-plane geometries.[142] Conductivities of the order of 10^{-10} S/cm were obtained for both modes, with activation energies of 0.7–0.8 eV. The cross-plane geometry provided better reproducibility of the results.

As discussed in Chapter 2.2, lithium cobalt oxide $LiCoO_2$ is currently the most often used cathode material in lithium-ion batteries. Despite this, only two reports from one group on the deposition of $LiCoO_2$ by ALD can be found in the literature.[143, 144] It can be postulated that the challenges in cobalt oxide deposition have had an effect on the research of the lithiated material.

The reported $LiCoO_2$ process makes use of oxygen plasma combined with $CoCp_2$ and LiO^tBu.[143, 144] The deposition supercycle consists of Co_3O_4 and Li_2CO_3 subcycles, and the effect of different pulsing ratios on film properties was studied. The process showed saturation with both metal precursors with Li : Co = 1 : 1 pulsing ratio, and the film thickness increased fairly linearly with the number of cycles when using a 1 : 4 pulsing ratio. After annealing the films showed the hexagonal phase of $LiCoO_2$ in both Raman and GIXRD. Electrochemical characterization revealed that a 12% capacity loss was evident between charge and discharge cycles. For a 1 : 4 pulsing ratio film the capacity was only about 60% of the theoretical value. For a 1 : 2 ratio film, the capacity was even lower, which might be explained by the higher impurity contents in this film. With the 1 : 4 pulsing ratio the films were $Li_{1.2}CoO_{3.5}$, as determined by elastic backscattering.[144]

The potential cathode material lithium iron phosphate, $LiFePO_4$, has also been the subject of ALD studies.[145, 146] The material has been deposited at 300 °C on silicon substrates using ferrocene and ozone as precursors for the Fe_2O_3 subcycle, trimethylphosphate and water for PO_x and lithium *tert*-butoxide and water for the Li_2O/LiOH subcycle.[145] Iron oxide and the phosphate were pulsed after one another for five cycles, after which one cycle of Li_2O/LiOH was applied. The resulting films were amorphous and showed a linear increase in thickness as a function of deposited supercycles. The material could also be deposited onto carbon nanotubes (CNTs).[145] Also on this substrate the material was amorphous, but crystallization was observed after annealing in argon at 700 °C for 5 hours. The Fe : P ratio in the annealed film was 0.9, as determined by energy-dispersive X-ray spectroscopy (EDX). Unfortunately, no information on the lithium contents is given. The $LiFePO_4$ film deposited onto CNTs showed good electrical performance, with clear redox peaks in a cyclic voltammetry (CV) curve at 3.5 V and 3.3 V (vs Li/Li^+) and a discharge capacity of 150 mAh/g at 0.1 C.[145] Encouragingly, the material could maintain a discharge capacity of 120 mAh/g at 1 C-rate even after 2000 cycles.

$LiFePO_4$ has also been deposited using metal-thd complexes.[146] Pulsing Lithd and ozone between subcycles of $Fe(thd)_3 + O_3$ and $TMPO + O_3 + H_2O$ resulted in stoichiometric $LiFePO_4$ when the fraction of Li_2CO_3 subcycles was 37.5%. The as-deposited films were amorphous but could be crystallized in 10/90 H_2/Ar atmosphere at 500 °C. These films were reported to show poor electrical conductivity, as is to be expected with this material.[16] However, very little additional information was given. It should be noted that the same research group has also published an ALD process for the de-lithiated cathode material $FePO_4$.[158] They reported an initial electrochemical capacity of 159 mAh/g for the as-deposited, amorphous 46 nm thick $FePO_4$ film. The capacity increased to 175 mAh/g after 230 charge-discharge cycles, and after 600 cycles the capacity was still 165 mAh/g.

Lithium manganese spinel $Li_xMn_2O_4$ is an interesting cathode material for lithium-ion batteries due to its low volume change during (de)lithiation, high voltage and environmentally benign elements. The material has been deposited by ALD by Miikkulainen *et al.* using various methods.[147] Firstly, bis(ethylcyclopentadienyl)manganese has been used as the manganese precursor in combination with water. Both LiO^tBu and LiHMDS were tested as the lithium source. However, all these experiments led to films with surprisingly low growth rates, high nonuniformity and only low amounts of lithium. In further studies, $Mn(thd)_3$ and ozone were used as precursors for manganese oxide and this process was combined with the LiHMDS + H_2O process. However, also these films were nonuniform, which is why they began to use the Lithd + O_3 process for lithium incorporation. Interestingly, even with exceedingly small amounts of Li_2CO_3 subcycles, high Li^+ incorporation was achieved, with only a 5% Li_2CO_3 pulsing leading to a Li : Mn ratio of 1 : 1. This was in fact the maximum content of lithium obtained: using larger numbers of lithium carbonate subcycles led to an increase in film nonuniformity. To achieve the stoichiometric amount of lithium for $LiMn_2O_4$, already 1% of lithium carbonate pulsing was enough. All the films showed the crystalline spinel phase already as-deposited, with MnO_2 impurities present in the films with the lowest lithium concentrations. Crystalline spinel $LiMn_2O_4$ was also obtained by using LiO^tBu and water as precursors, however little else was reported on this process.

The lithium manganese spinel process is special in that while the growth rate of the films stays rather constant at below 0.3 Å/cycle, the lithium content increases very rapidly and reaches a high value already with very small Li-subcycle numbers.[147] This indicates that the mechanism of this process differs significantly from more conventional ternary ALD processes. Another clue about the mechanism was given by ToF-ERDA elemental depth profiles, which were very uniform, but with a lithium deficiency on the film surface. To achieve such high lithium concentrations, either more than one monolayer should be deposited in one subcycle, or the growth should include a bulk component in addition to the normal surface reactions. Multilayer growth could be assumed to lead to lithium excess on the film surface, since lithium carbonate was always the last material deposited. Therefore, the bulk must be playing a role in the deposition process. Miikkulainen *et al.* postulated that the reduction needed for manganese to move from +IV in MnO_2 to +III/+IV in $LiMn_2O_4$ takes place during the Lithd pulse, which affects not only the film surface but also deeper parts of the film.[147] The following ozone pulse removes organic residues from the surface and re-oxidizes the topmost manganese ions on the surface. This reaction then drives lithium-ions deeper into the film, resulting in a uniform elemental distribution with a slightly lithium deficient surface.

Miikkulainen *et al.* continued their studies on $LiMn_2O_4$, using both LiO^tBu and water, and Lithd and ozone exposure on MnO_2 at 225 °C.[147] Interestingly, 110 nm of manganese oxide could be converted to the spinel phase with only 100 cycles of lithium carbonate applied on top of the

film. The carbonate was not present in the X-ray diffractogram, meaning the reaction resembles that of Nb_2O_5 in paper VI. Lithiation was achieved to some extent also without ozone pulses, and in this respect the results here resemble the conversion results in papers III and V. The manganese oxide films lithiated with LiO^tBu and water in a similar manner showed the best electrochemical storage properties, with a capacity of 230 mAh/g at 50μA. The capacity retention was very good up to 550 cycles at 200 μA. Similarly to $LiMn_2O_4$, vanadium oxide V_2O_5 could also be lithiated by pulsing either LiO^tBu and water or Lithd and ozone on top of the oxide film.[147] Using the diketonate precursor, lithium contents as high as 15 at% were obtained with only 100 cycles of the Li_2CO_3 process applied on the 200 nm oxide film.

Lithium titanate spinel, $Li_4Ti_5O_{12}$, has been the subject of ALD studies because of its attractive properties as a possible anode material (Chapter 2.2). Attempts on its deposition have been made using both titanium tetrachloride $TiCl_4$[148] and titanium tetra-*iso*-propoxide $Ti(O^iPr)_4$ as precursors.[148–150] In both cases, LiO^tBu has been used as the lithium source, and water was used as the oxygen source. Titanate films deposited using $TiCl_4$ reacted rapidly in air.[148] The films were amorphous as determined with X-ray diffraction and showed only very small amounts of lithium in ERDA measurements. In contrast, when using $Ti(O^iPr)_4$ as the titanium source and applying a long pulse time for this precursor, uniform titanate films with higher lithium contents could be deposited.[148] These films also reacted with air, however the reaction was much slower than when using $TiCl_4$ as the titanium precursor. The growth rate of the films did not depend much on the pulsing ratio of the two metal precursors, being approximately 0.7 Å/cycle at 225 °C.[148] In another report using the same precursors, the growth rate was said to be slightly different at 0.6 Å/cycle at 250 °C.[149] For the process at 225 °C, ERDA measurements revealed that the lithium contents of the films could be easily tuned over a wide range by changing the metal pulsing ratio.[148] For example, with 33% of lithium cycles the film stoichiometry was $Li_{1.19}Ti_1O_{2.48}$ and the carbon and hydrogen impurity contents were low. XPS and ERDA revealed that in this material lithium was enriched on the film surface, most likely forming a carbonate layer: carbonate peaks were visible both in FTIR and XPS.[148, 150] Despite the carbonate formation, the films showed the $Li_4Ti_5O_{12}$ spinel phase in XRD measurements also in the as-deposited state. The crystallinity could be improved by annealing in nitrogen at 640–700 °C. Annealed titanate films showed electrochemical activity, but the capacity remained low at 40 mAh/g.[150] However, this low value might be related to uncertainties in the calculation of film mass. For the film deposited at 250 °C, the Li : Ti ratio was reported as 2 : 1 with 44% lithium pulsing,[149] which could indicate Li_2TiO_3 formation, a well-known impurity phase for $Li_4Ti_5O_{12}$.[VI, 159] After annealing in argon at 850 and 950 °C, also these films showed XRD peaks belonging to $Li_4Ti_5O_{12}$.[149]

Lithium niobate, $LiNbO_3$, has gained interest mostly as an optical material and due to its ferroelectric properties, although it can also show reasonable ionic conductivities.[160–162] The

material has been deposited using LiHMDS, niobium ethoxide $Nb(OEt)_5$ and water as precursors.[151] Higher Li : Nb pulsing ratios led to higher lithium contents in the films, as expected (Figure 18). A 1 : 1 ratio resulted in a film with the Li : Nb ratio being 2.8 : 1 as determined by ToF-ERDA. The refractive index of the films decreased as the contents of lithium increased, which reflects the low refractive index of Li_2O. In films deposited with a lithium pulsing ratio higher than 1 : 5, annealing in air at 650 °C for 5 minutes resulted in crystalline $LiNbO_3$. With a 1 : 2 pulsing ratio the films appeared phase pure, and grew epitaxially on Al_2O_3 (001), Al_2O_3 (012) and $LaAlO_3$ (012).

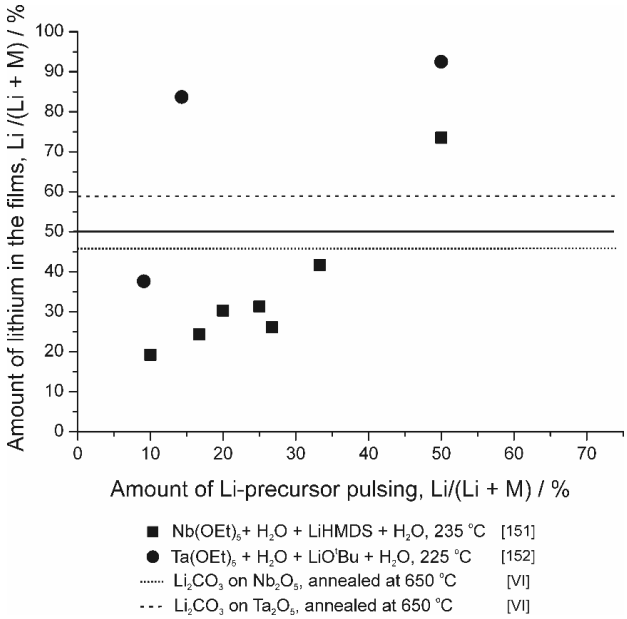

Figure 18: The amount of lithium cations deposited into lithium niobate and tantalate films as a function of the amount of lithium containing subcycles. Data points obtained from refs [151] and [152]. The solid line depicts the correct metal stoichiometry of $LiTaO_3$ and $LiNbO_3$. The dotted and dashed lines represent the stoichiometries obtained for the lithium niobate and tantalate, respectively, in paper VI.

Lithium tantalate, similarly to lithium niobate, is an interesting ferroelectric material.[163, 164] Its amorphous form has also been suggested as a possible solid electrolyte material for lithium ions.[152, 162, 165] The material has been deposited by ALD using LiO^tBu, $Ta(OEt)_5$ and water as precursors at 225 °C.[152] The film growth rate depended on the cycle ratio of the two binary processes, being 0.74 Å/binary cycle with a Li : Ta pulsing ratio of 1 : 6. Similarly, the lithium contents of the films changed drastically with changing pulsing ratio (Figure 18). Both X-ray absorption near edge structure (XANES) and XPS measurements revealed that the binding environment of tantalum in the films was similar to that of tantalum in stoichiometric $LiTaO_3$. However, in the films deposited with the highest tantalum oxide pulsing ratios, there was also

some Ta-O-Ta bonding present, indicating a Ta_2O_5 phase. XPS also revealed some carbonate formation on the film surface. Less carbonate was formed onto the surface of films deposited with high numbers of tantalum oxide subcycles, indicating that Ta_2O_5 was offering some protection for the lithium in the film against reactions with carbon dioxide in air. A lithium tantalate film with a composition of $Li_{5.1}TaO_x$ was studied with EIS.[152] The film showed a room temperature lithium-ion conductivity of $1.2 \cdot 10^{-8}$ S/cm, which increased to $9.0 \cdot 10^{-7}$ S/cm at 100 °C. The material has been used as a protective layer on lithium nickel cobalt manganese oxide cathodes.[165] With 5 supercycles of $LiTaO_3$ (pulsing ratio Li : Ta = 1 : 6), enhancements in both electrode capacity and cycling ability were obtained.

As discussed in Chapter 2.2.2, an amorphous solid electrolyte could be more beneficial than a crystalline one for lithium-ion batteries: amorphous films are (inherently) isotropic conductors, meaning the conductivity is the same in all directions. In addition, no grain boundaries exist in amorphous materials, which could lead to smaller electron migration and hence a better insulator ability. The first truly quaternary lithium material deposited by ALD was lithium lanthanum titanate (LLT), reported by Aaltonen *et al.* in 2010.[153] The thin films were deposited by combining binary ALD processes for TiO_2, La_2O_3 and Li_2O/LiOH and were amorphous as deposited. In this work $TiCl_4$ was used as the titanium precursor, and it was found that applying the Li_2O/LiOH subcycle after the TiO_2 cycle resulted in rougher and more nonuniform films than when lithium was pulsed after the La_2O_3 subcycle. This is a clear indication that the pulsing order can have a large effect on the deposition of quaternary materials. Because reactivity problems were also observed in the deposition of lithium titanate using $TiCl_4$,[148] the chloride precursor might be playing a large, thus far unknown role in these processes. These problems could be related to LiCl formation, for example. For the LLT deposition, a pulse sequence where 3 cycles of La_2O_3 were applied after one TiO_2 cycle was used, and the number of lithium subcycles was varied. Interestingly, the amount of lithium in the film was found not to linearly follow the number of Li_2O/LiOH subcycles. This could mean that reactivity of LiO^tBu is lower on a Li_2O/LiOH surface compared to its reactivity on a La_2O_3 surface, a somewhat similar conclusion as was made in the deposition experiments on lithium aluminate.[124] Despite this, saturation as a function of the LiO^tBu pulse length was observed.[153] The maximum lithium content reached with this pulsing scheme was approximately 20 at%. The lanthanum content stayed constant in all experiments, but the contents of titanium decreased as a function of the increased lithium contents. Under saturative conditions, the film composition, as determined by ToF-ERDA, was $Li_{0.32}La_{0.30}TiO_z$. Interestingly, secondary ion mass spectrometry (SIMS) depth profiling revealed that lithium was somewhat concentrated onto the film-substrate interface, whereas in many cases lithium has been reported to preferably reside on the outer surface of the film.[148, 151] The films could by crystallized by annealing in oxygen. The XRD measurement matched well with reported peak positions for $Li_{0.33}La_{0.557}TiO_3$, however four peaks could not be identified.[153]

$Li_xAl_ySi_zO$, another amorphous solid electrolyte, has been studied by Perng *et al.*.[154] The material belongs to the lithium aluminosilicate family, which includes materials with high lithium-ion conductivities with various metal ratios.[22] Lithium aluminosilicate was deposited by ALD using a pulsing sequence of Al_2O_3 from TMA and water, Li_2O/LiOH from LiO^tBu and water and SiO_2 from TEOS (tetraethyl orthosilicate) and water.[154] With a pulsing sequence of 10 : 6 : 4 the growth rate of the films increased linearly with the number of supercycles. The lithium contents of the films, as determined by synchrotron ultraviolet photoemission spectroscopy (UPS), increased with increasing lithium oxide pulsing ratio, but showed quite a lot of scattering. The deposited films were shown to be pinhole free and had ionic conductivities between 10^{-7} and 10^{-9} S/cm at room temperature, depending on the lithium content. Higher lithium contents led to higher conductivities, but also increased the activation energy. It should be noted that the film thicknesses used in these experiments were very small, 10 nm and under. Higher thicknesses led to a lower ionic conductivity.

Kazyak *et al.* have taken on the impressive task of depositing the garnet oxide $Li_7La_3Zr_2O_{12}$ by ALD.[155] This crystalline material is known to have a lithium-ion conductivity close to 10^{-3} S/cm at room temperature.[166] In order to stabilize the desired cubic phase at room temperature, the material was doped with alumina.[155] This resulted in an ALD process combining 8 subcycles of Li_2O, 28 subcycles of La_2O_3, 12 subcycles of ZrO_2 and 1 Al_2O_3 subcycle at 225 °C to obtain an amorphous film with metal ratios Li : La : Zr : Al = 52 : 27 : 19 : 2 (ideal composition 54 : 26 : 17 : 2). Interestingly, despite using ozone as the oxygen source for all subcycles, no Li_2CO_3 or $La_2(CO_3)_3$ formation was evident, based on XPS results. The thickness of the films increased linearly with the number of supercycles, and good conformality was also obtained. The ionic conductivity of the as-deposited, amorphous film was $1.2 \cdot 10^{-6}$ S/cm at 100 °C and did not differ for in-plane and through-plane measurements. By extrapolation, the conductivity was 10^{-8} S/cm at RT. The films could be crystallized to the cubic $Li_7La_3Zr_2O_{12}$ phase with annealing at 555 °C in inert atmosphere. A lithium-excess in the film and an extra lithium source was needed during the annealing due to lithium loss from the film. The annealed films had an island morphology, which prevented reliable conductivity measurements.

Although the majority of published ternary lithium ALD processes are for oxide materials, sulfides and fluorides have been studied as well.[47, 156] Lithium aluminum sulfide Li_xAl_yS has been deposited using subcycles of Li_2S[129] and Al_2S_3. Using a 1 : 1 subcycle ratio resulted in a Li : Al ratio of 2.9 : 1 in films deposited at 150 °C, as determined with ICP-MS. Evaluation of the metal ratio from QCM data, assuming stoichiometric growth, resulted in a metal ratio of 3.5 : 1, which is reasonably close to the value from ICP-MS. The ternary sulfide growth was linear as a function of cycles, with a reported growth rate of 0.50 Å/cycle. The growth rate during the Li_2S subcycle seemed somewhat lower in the ternary process than the one reported for the binary process.[129] This difference was not commented on in ref. [156], but it most likely

originates from different starting surfaces. A 50 nm Li_xAl_yS film was measured to have a room temperature ionic conductivity of $2.5 \cdot 10^{-7}$ S/cm, which is quite reasonable for an ALD-made material.[78, 128, 152, 154, 156] The sulfide was studied as an artificial SEI-layer on metallic Li, and it was found to effectively stabilize the interface between the metal anode and an organic liquid electrolyte.[156] In addition, the coating decreased lithium metal dendrite formation during cycling, which considerably improves the safety of lithium metal anodes.

Multicomponent, lithium containing fluorides have not been studied widely in ALD.[47, V] Still, Li_3AlF_6, which is a possible electrolyte material for lithium-ion batteries,[45] has been deposited using multiple processes. Results on this material from paper V will be reported in Chapter 5.3.2. Li_3AlF_6 has also been deposited using subcycles of AlF_3 and LiF using TMA and HF-pyridine and LiHMDS and HF-pyridine as precursors.[47] One subcycle of AlF_3 and one subcycle of LiF were used at 150 °C, and crystalline Li_3AlF_6 was obtained with a growth rate of 0.9 Å/cycle.[47] The films had a Li : Al ratio of 2.7 : 1, as determined with ICP-MS, and carbon, silicon and oxygen impurities were below the XPS detection limit. The films had an ionic conductivity of $7.5 \cdot 10^{-6}$ S/cm at room temperature, which is similar to the first reports from the literature on thermally evaporated amorphous films.[44, 45] Interestingly, changing the pulsing ratio to three subcycles of AlF_3 and one LiF resulted in the same metal ratio in the as-deposited film as a pulsing ratio of 1 : 1, hinting at a similar conversion reaction as we have seen in papers III and V.

4. Experimental

4.1 Film deposition

All thin films studied in this thesis were deposited using a hot-wall, flow-type F-120 ALD reactor (ASM Microchemistry Oy). The films were deposited onto 5 cm × 5 cm Si(111) and Si(100) substrates, terminated with native SiO_2. The pressure in the reactor during depositions was of the order of 5 mbar. Pulsing of the metal precursors was done by inert gas valving. For the LiF deposition experiments, the nitrogen used as the carrier and purge gas was produced by a domnick hunter G2100E nitrogen generator. For the rest of the experiments, the nitrogen was obtained from liquid N_2, with impurity levels less than 3 ppm of H_2O and O_2 each.

All the precursors were evaporated inside the reactor from open glass boats. In the LiF studies, $Mg(thd)_2$ (magnesium bis(2,2,6,6-tetramethyl-3,5-heptanedionate), Volatec Oy, Finland), Lithd (lithium 2,2,6,6-tetramethyl-3,5-heptanedionate, either from Strem Chemicals Inc. or Volatec Oy) and TiF_4 (Strem Chemicals Inc.) were evaporated at 110, 180, and 130–135 °C, respectively. For the AlF_3 deposition, $AlCl_3$ (Alfa Aesar GmbH & Co.) was evaporated at 80 °C and TiF_4 at 135 °C. For depositing Li_2CO_3 for the solid state reactions, Lithd (Volatec Oy) was evaporated at 192 °C. Ozone, generated by a Wedeco GmbH Modular 4 HC ozone generator, had a concentration of 100 g/Nm^3. Ozone was dosed into the reactor from the main flow using needle and solenoid valves.

AlF_3 films were crystallized by annealing in a tube furnace in N_2 flow (purity 5.0). For the solid state reactions of papers VI and VII, a muffle furnace was used for annealing the films in air.

4.2 Film characterization

Film thicknesses were evaluated both by UV-Vis reflectance spectroscopy using a Hitachi U2000 spectrophotometer, and by X-ray reflectivity (XRR) measurements, conducted with a PANalytical X'Pert Pro MPD X-ray diffractometer.

Crystallinity of the films was assessed by GIXRD measurements with the same PANalytical X'Pert Pro MPD X-ray diffractometer. *In situ* high temperature XRD (HTXRD) measurements were also conducted using an Anton-Paar HTK1200N oven.

Film morphology was examined both by field-emission scanning electron microscopy (FESEM) with a Hitachi S4800 FESEM instrument, and by atomic force microscopy (AFM) with a Multimode V AFM equipped with a Nanoscope V controller (Veeco Instruments). For roughness analysis with AFM, the samples were measured in tapping mode in air using a phosphorous-doped silicon probe (RTESP) delivered by Veeco Instruments. The FESEM instrument was also utilized in the determination of film thicknesses in papers VI and VII.

Adhesion of the films to the Si substrate was evaluated qualitatively by the Scotch tape test.

The composition of the samples was analyzed with ERDA and ToF-ERDA. The beam was selected depending on the material under study. Energy-dispersive X-ray spectroscopy (EDX) (Oxford INCA 350 Energy spectrometer connected to the Hitachi S-4800 FESEM instrument) was also used for composition analyses in some cases.

X-ray photoelectron spectroscopy (XPS) was used to study the surface composition of AlF_3 films in more detail. Mg K_α X-rays were produced by Omicron DAR 400 source (75 W), and the photoelectrons were analyzed by an Argus spectrometer with a 20 eV pass energy.

5. Results and Discussion

5.1 Search for lithium containing double metal alkoxides [I]

As already mentioned, single-source precursors are one of the three common methods used in depositing multicomponent thin films by ALD.[74, 105] Since many of the most promising lithium-ion battery materials are multicomponent oxides, a literature review was conducted on lithium containing double metal alkoxides.[I] These complexes, also called heterometallic alkoxides, are formed from alcohols and at least two different metal ions, with lithium being one of the metals in the present case. Lithium double metal alkoxides can be synthesized in similar ways as double metal alkoxides in general, including simply reacting two metal alkoxides in a solvent or using metallic lithium and a metal alkoxide in an alcohol medium.[167]

Lithium can form a large number of different types of complexes, since it can have coordination numbers from 2 to 8.[168] However, in double metal alkoxides lithium usually has a coordination number of 4 or 3. Lithium can take part in different ring structures, cages, heterocubanes and even polymers. Four member rings are the most common structural features found in these complexes. Lithium is especially prone to form cage complexes with other alkaline metals, and heterocubanes with metals such as zinc and titanium.

As was discussed in Chapter 3, highly volatile and thermally stable precursors are needed for ALD.[69] In double metal alkoxides, the most important factors influencing volatility are the molecular mass of the complex and the polar nature of the metal-ligand bonds.[110] Volatile double metal alkoxides can be obtained by using sterically shielding, simple alkoxo ligands. Fluorine substituents can further enhance volatility, whereas aryloxo ligands generally lead to low volatility.[110] During the literature survey it was noticed that in most studies dealing with lithium double metal alkoxides, no volatility information was available. This is possibly due to the complexes being mostly aimed as sol-gel precursors. In the sol-gel method, the solubility properties of complexes are more important than their volatility and thermal stability. When sublimation or other volatility experiments were reported, it was often noted that lithium double metal alkoxides are not particularly volatile or thermally stable. Therefore, we have concluded that, in the end, most of these complexes might not prove useful for ALD. Our own experimental results on lithium titanium and lithium tantalum double metal alkoxides corroborate these results.[169] Particularly, our ALD experiments with $LiTi(O^tBu)_5$ showed that the liquid precursor decomposed during heating, most likely to LiO^tBu and $Ti(O^tBu)_4$, resulting in only TiO_2 deposition when reacted with water. More promising results on volatility were obtained with complexes including β-diketonate ligands. However, the lower reactivity of β-diketonates, compared to pure alkoxides, might lead to lower reactivity with water in ALD

processes. The lower reactivity could be circumvented by using ozone as the oxygen source. However, this might lead to lithium carbonate deposition instead of the desired oxide material.[122]

Despite the low number of stable and volatile lithium double metal alkoxides in the literature, these complexes have already been utilized in both CVD and sol-gel depositions, where the limited thermal stability of the precursors is not as critical as in ALD.[I, 103] Therefore, these complexes do still have a place in the materials chemistry realm as precursors for depositing lithium containing multicomponent oxides.

5.2 Exploring ALD chemistries for metal fluoride deposition

As mentioned in Chapter 3.2, metal fluorides can be deposited by ALD using, for example, HF, TiF_4 or TaF_5 as the fluorine source.[79, 81, 83, 87] Due to the hazardous nature of HF and difficulties in its removal from exhaust gases, the metal containing solid fluorine precursors have been studied extensively in our laboratory. In this work, we have developed ALD processes for the deposition of LiF[II] and AlF_3[IV] exploiting the chemistry originally developed by Pilvi *et al*..[58]

5.2.1 LiF [II]

Lithium fluoride is an interesting optical material, with a band gap of approximately 14 eV and a low refractive index of 1.39 at 580 nm.[170, 171] However, our interest in this material stems in the first place from its possible use as a lithium-ion conducting material when combined with fluorides such as AlF_3 or NiF_2 (Figure 8).[44, 45, 49] Since no process for LiF was available in the literature, a new process was developed,[II] based on the earlier work by Pilvi *et al*..[83–86] Lithd and TiF_4 were used as precursors and the deposition temperature was varied between 250 and 350 °C. The upper temperature limit was set by Lithd decomposition at 375 °C. The lower limit was chosen so that the temperature gradient inside the reactor could be maintained approximately constant around the Lithd precursor kept at 180 °C.

The LiF process did not show a typical ALD-window of constant growth rate with deposition temperature (Figure 19b). Instead, the growth rate decreased with deposition temperature to 1 Å/cycle at 325 °C, and then increased slightly at 350 °C. The decrease of the growth rate with temperature has been postulated to originate from a decreased density of TiF_x-groups on the

growth surface.[83–85] The increased rate at 350 °C is more difficult to explain, as it is unlikely that precursor decomposition could explain the increase below 375 °C. Our growth rate was notably higher than the 0.5 Å/cycle obtained with LiHMDS and HF-pyridine.[81] Saturation of the growth was not found for Lithd at 325 °C, somewhat similarly as depicted in Figure 14 (Figure 19a). Pilvi *et al.* postulated that the reason for the non-saturative behavior might be either slow kinetics or an enhancement of metal precursor decomposition caused by the TiF_x-surface groups.[84] TiF_4, on the other hand, shows saturation type behavior between 0.5 and 2 s pulses. With longer pulse times, the growth rate increases linearly. Pilvi *et al.* did not observe such an increase, however they limited their studies generally to TiF_4 pulse times of 2 s or less (Figure 14).[83–86]

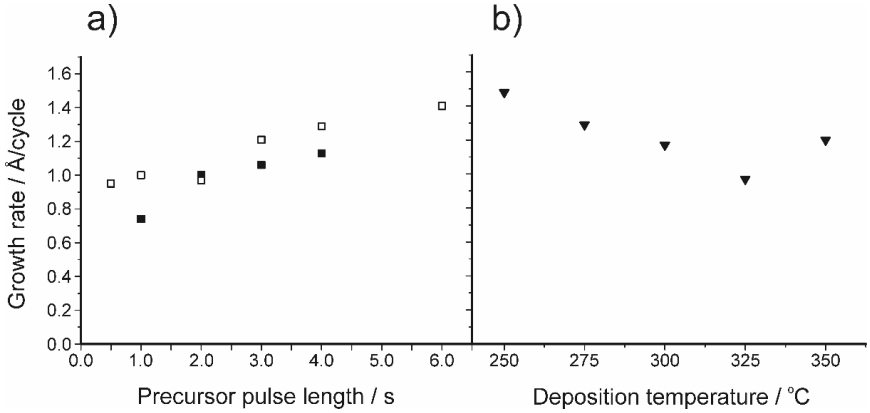

Figure 19: a) Growth rate of LiF films as a function of Lithd (black squares) and TiF_4 (white squares) pulse lengths at 325 °C. Purge times were 4 s. b) Growth rate of LiF films as a function of deposition temperature. Precursors were pulsed for 2 s and purged for 4 s.

All the films were highly crystalline, cubic LiF already as-deposited (Figure 20), with rms roughnesses increasing from 6.3 nm at 250 °C (111 nm film) to 20.6 nm at 350 °C (90 nm film). A similar trend has been seen with other fluorides deposited using TiF_4, showing increased grain sizes as the deposition temperature is increased.[84–86] The same phase was also obtained from LiHMDS and HF-pyridine depositions.[81] The films showed refractive index values between 1.37 and 1.43, the highest values obtained with long TiF_4 pulse times. This could be seen to indicate larger impurity contents with larger TiF_4 doses. However, no titanium impurities were found in the films with ERDA measurements (detection limit 0.1 at%). This in contrast to the previously reported fluoride processes, where the metal impurity from the fluorine precursor has been a problem especially at low temperatures.[84–86] In fact, the LiF films appear very pure in general, with the total amount of O, C and H impurities remaining well below 3 at%.

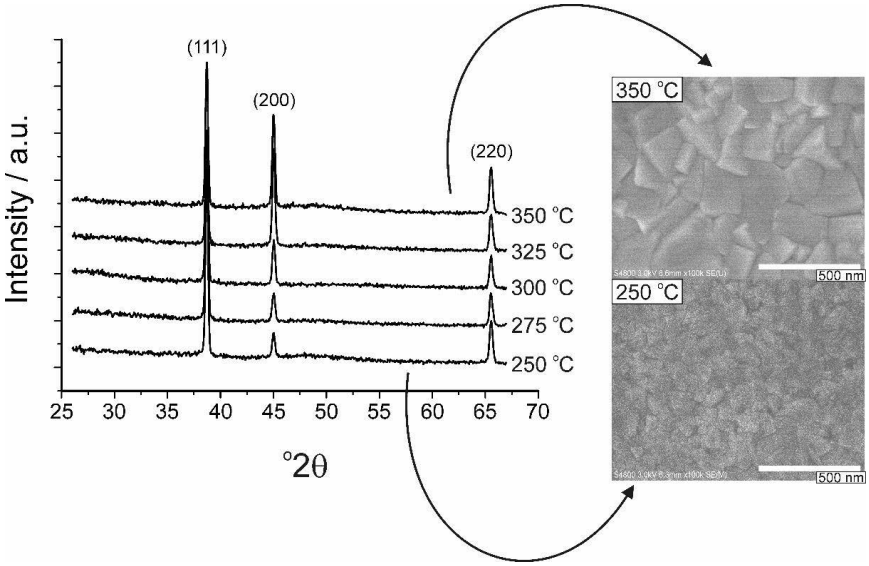

Figure 20: X-ray diffractograms of LiF films deposited at different temperatures, displaying the cubic LiF phase. FESEM imaging revealed that the morphology of the films changed with deposition temperature, higher temperatures producing larger grains.

5.2.2 AlF_3 [IV]

Aluminum fluoride is a similar material as LiF, with a wide variety of possible optical applications due to its high band gap and low refractive index.[82, 172–174] In addition, it is a potential artificial SEI-layer for protecting both cathodes and anodes.[40, 80, 88, 175–177] Thus, AlF_3 has become a much studied ALD material in the past few years.[IV, 80–82, 88] Encouraged by our results with LiF, we first studied $Al(thd)_3$ and TiF_4 as precursors for AlF_3. However, this precursor combination led to no film growth on silicon and aluminum oxide. Our assumption is that this lack of reactivity has to do with the presence of aluminum-oxygen bonds in the $Al(thd)_3$ complex. Further results on our experiments with $Al(thd)_3$ will be reported in Chapter 5.3.2.

$AlCl_3$ is a widely used ALD precursor, with no oxygen present in the molecule. In addition, $TiCl_4$ is a well-known, volatile ALD precursor,[74, 178] which is encouraging considering the expected ligand-exchange reaction taking place during the combination of $AlCl_3$ with TiF_4.

Thus, this combination was studied for the deposition of AlF_3. Film growth was observed between 160 and 340 °C.

The saturation of the growth rate was studied at 160, 200 and 240 °C (Figure 21a). TiF_4 shows similar behavior as in the LiF case,[II] with an increased growth rate with the longest pulse times. $AlCl_3$, on the other hand, shows an opposite trend, with growth rates decreasing as a function of pulse time. $AlCl_3$ vapor has been reported to enhance the volatility of AlF_3,[179] which might explain the etching-type behavior seen in this process. Moreover, the films deposited at higher temperatures showed a thickness profile perpendicular to the direction of the precursor vapor flow, with smaller thicknesses measured from the $AlCl_3$ inlet side of the substrate. Based on the saturation experiments, the $AlCl_3$ + TiF_4 deposition process is not ideal ALD. However, the process is controllable and reproducible. The film growth rate stays constant as a function of the number of deposition cycles at all temperatures studied (Figure 21b).

The AlF_3 growth rate shows no ALD-window, similarly to LiF.[II] Instead, the rate rapidly decreases as a function of temperature, from close to 3 Å/cycle at 160 °C to less than 0.3 Å/cycle at 340 °C. This might be related to a similar decrease in the surface density of active species as was hypothesized in the LiF process.[II] A similarly decreasing growth rate was observed in the AlF_3 process utilizing TMA and HF[80, 82] as precursors, although in that case the decrease was most likely a result of etching reactions at higher temperatures.[80] When AlF_3 was deposited using TMA and TaF_5, the growth rate increased with temperature due to TaC_x being deposited in addition to AlF_3.[88]

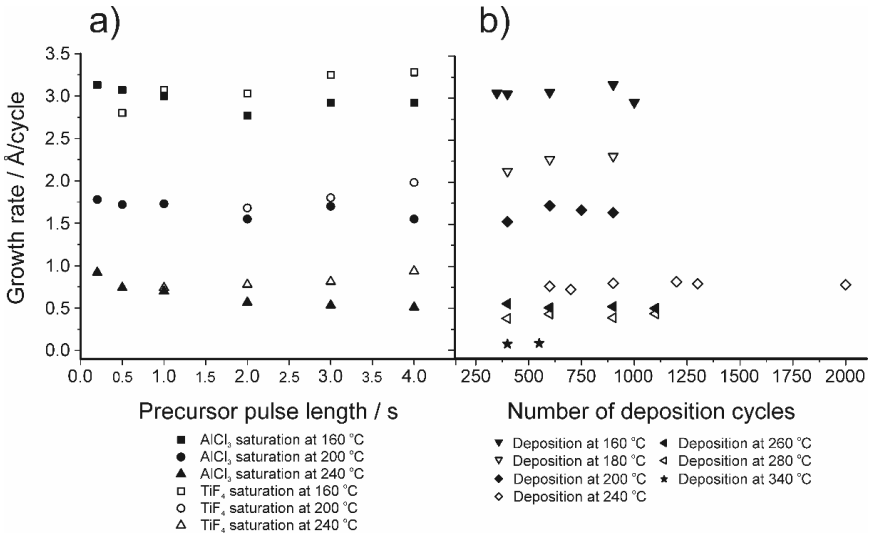

Figure 21: a) Growth rate of AlF_3 films as a function of $AlCl_3$ (black) and TiF_4 (white) pulse lengths at 160, 200 and 240 °C. Purge times were 3 s. b) Growth rate of AlF_3 films as a function of deposition cycles at various deposition temperatures. $AlCl_3$ pulse time was 0.5 s with a 1 s purge, TiF_4 pulse time was 1 s with a 1.5 s purge.

The as-deposited AlF_3 films show first signs of crystallinity at 280 °C. The amorphous films deposited at lower temperatures can be crystallized by annealing at 575 °C in nitrogen atmosphere. The resulting film is of the tetragonal phase. In contrast, films which show crystallinity already in the as-deposited state are hexagonal. The evolution of the crystallinity of the as-deposited films was followed with FESEM imaging (Figure 22). At 280 °C, globules are found on the otherwise smooth film surface, and the amount and size of these globules increase as thicker films are deposited. Both the smooth areas and the globules contain Al and F, as determined by EDX, and the globules also show up in AFM phase images, indicating that they could present the crystalline portion of the film. Due to the lower deposition temperatures of 100–200 °C, the films deposited using TMA and HF were reported to be amorphous.[80, 82]

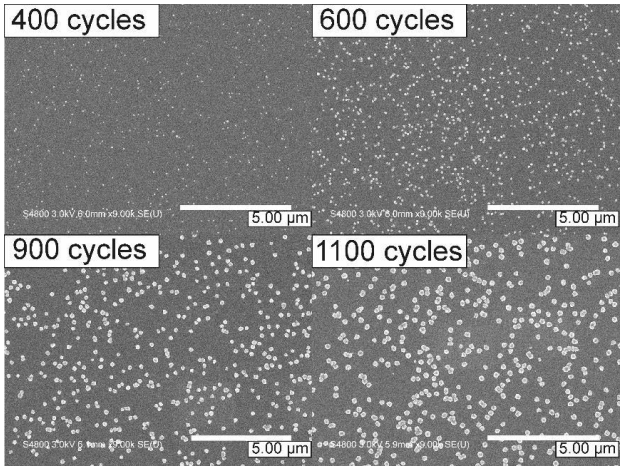

Figure 22: FESEM images of AlF_3 films deposited at 280 °C with different numbers of cycles.

ToF-ERDA measurements revealed that the films contain decreasing amounts of Cl and Ti impurities as the deposition temperature is increased, both being well below 1 at% at 280 °C. However, the H and O impurities showed the opposite trend, with films deposited at 280 °C containing up to 6 at% of oxygen. AlF_3 films were also studied with XPS and it was found that an aged sample, deposited at 280 °C, showed a higher contribution from oxygen than did a fresh sample deposited at the same temperature or a sample deposited at 160 °C (Figure 23). Based on the oxygen signals, the film deposited at lower temperatures shows possible formation of Al_2O_3 on the film surface. The films deposited at 280 °C more closely resemble either $Al(OH)_3$ or fluorohydroxides, indicating that the films might have absorbed moisture from the ambient during storage. Oxygen impurities of the order of 1–2 at% were also found in the AlF_3 films deposited using TMA and HF,[80, 82] and of the order of 20 at% in the films deposited with TMA and TaF_5.[88]

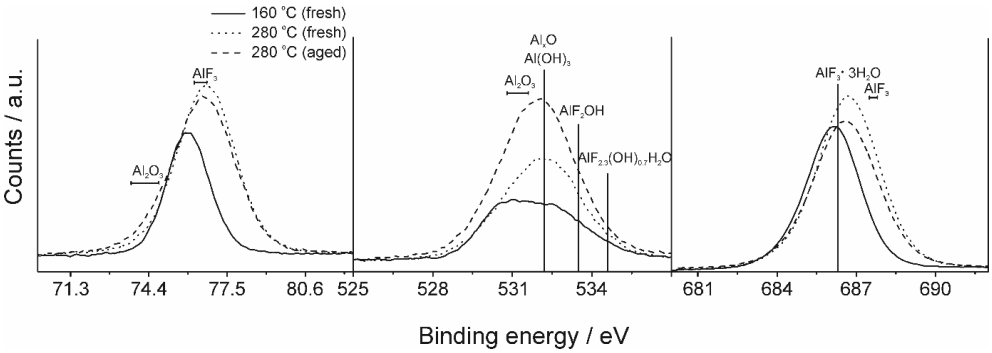

Figure 23: XPS spectra of AlF_3 thin films deposited at 160 and 280 °C.

5.3 Conversion reactions for metal fluoride deposition

Although the Lithd + TiF_4 process produces high quality LiF films, the process is quite challenging to control. To obtain uniform films, high doses of Lithd are needed, and the process appears to be very sensitive to the temperature gradient inside the reactor.[II] In an effort to further optimize the deposition of LiF, we discovered that lithium-ions show interesting reactivity when in contact with other fluoride materials. Thus, two new routes were discovered for the ALD of LiF: the sequential pulsing of $Mg(thd)_2$, Lithd and TiF_4, and the conversion reaction taking place between a MgF_2 film and Lithd.[III] A similar conversion reaction was also used to deposit Li_3AlF_6 mixture fluoride films.[V]

5.3.1 LiF [III]

The pulsing sequence $Mg(thd)_2$ + TiF_4 + Lithd + TiF_4 produces LiF thin films between 300 and 350 °C. Unlike the Lithd + TiF_4 process of paper II, this sequence shows both an ALD window between 325 and 350 °C and saturation with respect to both Lithd and TiF_4 (Figure 24). The growth rate at 325 °C was 1.4 Å/cycle, as opposed to 1 Å/cycle in the previous process. All the films were again highly crystalline, with the film roughnesses being 19–20 nm for 70–80 nm films regardless of the deposition temperature. ToF-ERDA measurements showed the films to be very pure LiF, with very minute amounts of Mg and Ti impurities. C and H formed the largest part of impurities, however both were below 1 at% in the deposition temperature range of 300–350 °C.

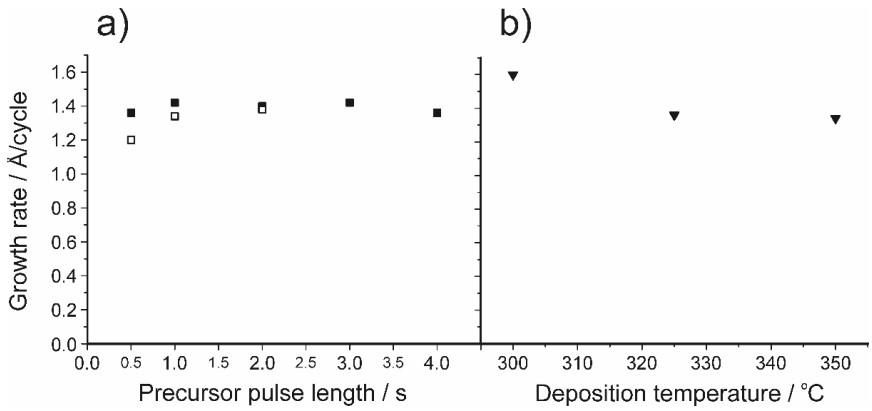

Figure 24: a) Growth rate of LiF films as a function of Lithd (black squares) and TiF_4 (white squares) pulse lengths at 325 °C. Purge times were 2 s. b) Growth rate of LiF films as a function of deposition temperature. $Mg(thd)_2$ was pulsed for 3 s, Lithd for 4 s and TiF_4 for 2 s, with 2 s purge times.

It is surprising that despite the use of $Mg(thd)_2$ in the pulsing sequence, no magnesium ended up in the LiF films. We have proposed a two step mechanism to explain the deposition process. First, $Mg(thd)_2$ and TiF_4 deposit MgF_2 as has been previously reported.[84] In the second step, Li^+ from Lithd replaces Mg^{2+} in the fluoride film and forms LiF. Magnesium leaves the films as $Mg(thd)_2$, because the low amounts of O, C and H impurities imply that virtually no ligand decomposition is occurring during the growth. This type of fluoride–to–β-diketonate ligand exchange might at first seem unexpected, however it has been reported that, for example, metal oxides can be dry etched using β-diketone vapors to form volatile β-diketonato complexes of metal ions.[180] After the removal of magnesium, Lithd adsorbs onto the formed lithium fluoride, and is converted to LiF during the last TiF_4 pulse.

To verify the conversion reaction occurring in the second step, we studied the conversion of MgF_2 films by pulsing only Lithd over them under ALD conditions. As it turned out, with high enough Lithd doses, MgF_2 films of 150 nm in thickness could be converted into LiF, with no indication of MgF_2 or Mg impurities in GIXRD, EDX and ToF-ERDA measurements (Figure 25). The lower the reaction temperature, the larger the Lithd dose needed to completely convert the MgF_2 film into LiF. Although the resulting LiF films were again highly crystalline as determined with GIXRD, they showed much smaller grain sizes and thus smaller roughnesses than the films deposited with either the two^{II} or four^{III} step LiF processes (Figure 26). In addition, the adhesion of the films to the silicon substrates was markedly improved. Our experiments proved that the conversion reaction with Lithd is not limited to the surface regions of MgF_2 films, but can in fact proceed very deep into the films. The high mobility and reactivity

of Li^+ seen in these experiments can well be playing a role in many processes used to deposit materials containing lithium, especially in the case of ternaries. For example, Miikkulainen *et al.* later reported similar results in their conversion experiments to form spinel $LiMn_2O_4$ using MnO_2 films and Lithd, as was already discussed in Chapter 3.3.2.[147] However, their conversion reaction also led to significant amounts of hydrogen and carbon impurities when no ozone was used after the Lithd pulse, as opposed to our very clean conversion reactions of MgF_2.

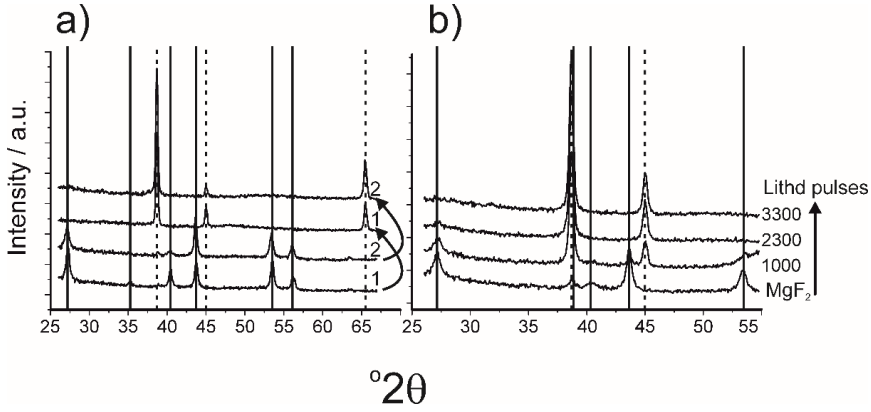

Figure 25: a) X-ray diffractograms of 1) 97 nm and 2) 126 nm MgF_2 films, which were converted to LiF through Lithd exposure at 325 °C using 500 pulses. b) X-ray diffractograms of a 158 nm MgF_2 film exposed to a successively larger number of Lithd pulses at 275 °C. The conversion from MgF_2 to LiF could be followed due to the slower reaction at lower temperature. The solid lines indicate MgF_2 peak positions, while the dashed lines denote LiF.

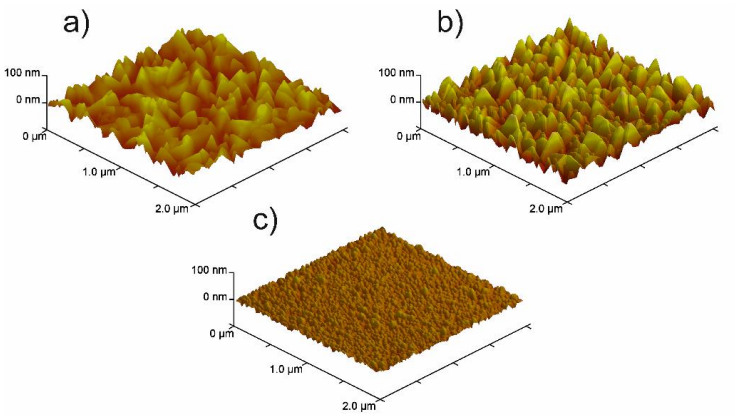

Figure 26: AFM images of LiF films deposited at 325 °C using three different processes. a) Lithd + TiF_4, thickness 73 nm, rms roughness 15.9 nm, b) $Mg(thd)_2$ + TiF_4 + Lithd + TiF_4, thickness 68 nm, rms roughness 20.1 nm, c) conversion from a MgF_2 film using Lithd, thickness 94 nm, rms roughness 4.8 nm.

Although the conversion of bulk layers goes against the basic principles of ALD, a few other processes have been reported which exhibit similar behavior to our LiF process.[115, 181–185] Especially interesting is the work of Thimsen *et al.*[183] who studied the effect of diethylzinc pulsing on Cu_2O films and bis(N, N´-disec-butylacetamidinato)dicopper(I) pulsing on ZnS. They found that diethylzinc can convert Cu_2S into ZnS and metallic copper. On the other hand, pulsing the copper(I)precursor onto ZnS led to Cu_2S films with no zinc impurities, indicating that zinc is removed into the vapor phase in a similar manner to our results.

5.3.2 Li_3AlF_6 [V]

As mentioned in Chapter 2.3.2, Li_3AlF_6 is a ternary fluoride, which has been reported to have a high lithium-ion conductivity.[44, 45, 47, 48, 186] Like metal fluorides in general, also Li_3AlF_6 has a large band gap, making it a possible solid electrolyte material for lithium-ion batteries.[187] The atomic layer deposition of Li_3AlF_6 was first reported in a conference presentation by Lee *et al.* in 2014[47] and these results were summarized in Chapter 3.3.2. As with the other fluorides in this work, we have deposited this material using only solid precursors.

The deposition of Li_3AlF_6 proved complicated when using the binary processes of papers II, III and IV: Uncontrollable conversion by Lithd to LiF was a threat to using the subcycle approach. More importantly, exposing LiF to $AlCl_3$ could result in undesirable LiCl deposition. Thus, attempts on depositing Li_3AlF_6 were made using two processes (Schemes 1 and 2). In Process 1, $Al(thd)_3$ and TiF_4 were pulsed onto LiF thin films in an ALD manner, and a conversion reaction to the mixture film Li_3AlF_6 took place already during the depositing process. In process 2, AlF_3 films were exposed to Lithd vapor in an ALD reactor in a similar way as described in Chapter 5.3.1 for MgF_2 and Lithd. In Process 1, $Al(thd)_3$ was used instead of $AlCl_3$ to avoid Li^+ contact with Cl^- from $AlCl_3$. In process 2, AlF_3 was deposited with the process described in Chapter 5.2.2, since in this case lithium ions would not be in contact with chlorine ions and thus no LiCl could form.

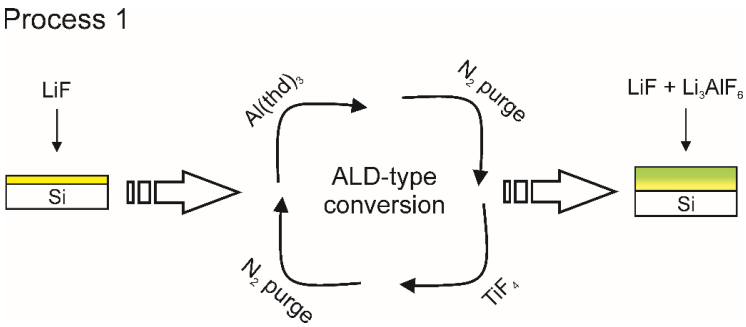

Scheme 1: Process 1 for depositing Li_3AlF_6 using ALD.

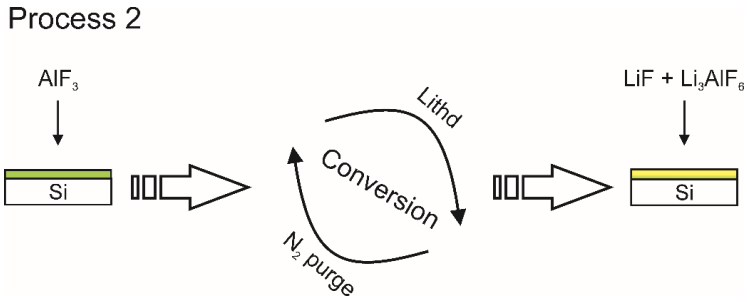

Scheme 2: Process 2 for depositing Li_3AlF_6 using a conversion reaction between AlF_3 and Lithd.

Although we had previously noted that $Al(thd)_3$ and TiF_4 did not produce AlF_3 on silicon substrates,[IV] a reaction did occur between these precursors when pulsed onto LiF films. The fluorides mixed together already during the deposition process, resulting in crystalline Li_3AlF_6 with crystalline LiF residues. High deposition temperatures together with long $Al(thd)_3$ pulses resulted in less LiF impurity in the film, as observed with GIXRD. However, these same conditions worsened the visual appearance of the films. ToF-ERDA revealed that even in the best samples, the amount of Al was very low, although Li_3AlF_6 was clearly visible in the X-ray diffractograms. In addition, the contents of titanium impurity was high. Thus, it was concluded that Process 1 was not efficient in depositing Li_3AlF_6.

Process 2 was developed based on the conversion reactions first noted between MgF_2 and Lithd. Approximately 50 and 100 nm thin films of AlF_3 were exposed to the lithium precursor at different temperatures and for different Lithd pulse numbers to determine whether good quality Li_3AlF_6 could form from this conversion reaction. GIXRD analyses show that amorphous AlF_3

transforms into monoclinic Li_3AlF_6 with Lithd exposure. Choosing a too large number of Lithd pulses resulted in crystalline LiF formation. The mechanism of the conversion is most likely similar to that discussed in Chapter 5.3.1, as the oxygen, carbon and hydrogen impurities were very small in the films after conversion, as determined with ToF-ERDA.

Despite crystalline Li_3AlF_6 being visible in the X-ray diffractograms, obtaining the correct Li : Al ratio was challenging. ToF-ERDA revealed that doubling the Lithd exposure from 20 to 40 pulses increased the Li : Al ratio from 0.93 : 1 to 7.9 : 1 for approx. 50 nm AlF_3 films (Figure 27). For 100 nm AlF_3 films exposed to 40 Lithd pulses, the ratio varied between 1.33 : 1 and 1.49 : 1. Thus, thinner films were much faster to convert than thicker ones, as was expected. The exposure temperature also played a role in the conversion. Just a 25 °C change from 250 °C to 275 °C increased the Li : Al ratio for a 40 pulse sample from 1.49 : 1 to 2 : 1. However, despite the still lithium deficient metal ratio, the 275 °C exposure temperature sample already contained a prominent amount of crystalline LiF based on GIXRD.

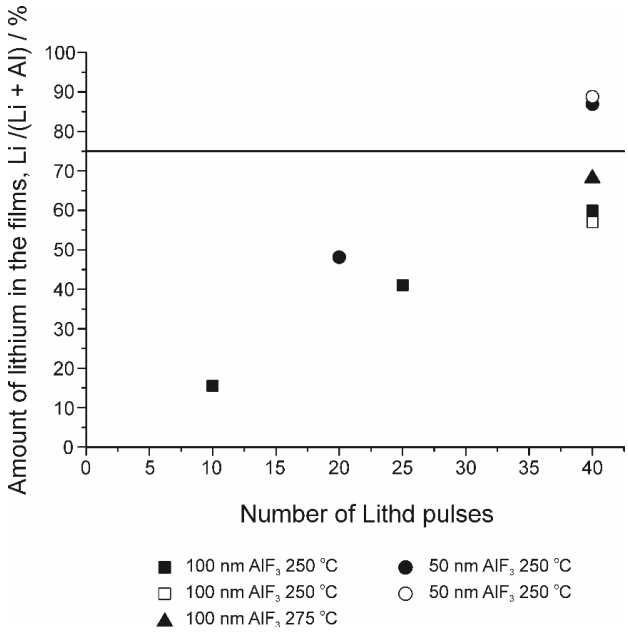

Figure 27. The amount of lithium cations in converted AlF_3 films as a function of the number of Lithd pulses. Black and white symbols denote samples prepared at different times but with using same parameters for exposure. Solid line illustrates the correct metal stoichiometry of Li_3AlF_6.

Even though LiF was a common impurity phase in our Li_3AlF_6, we deposited two AlF_3 films of 55 and 100 nm thickness onto platinum in order to study their electrical properties after exposure to Lithd. Platinum dots were electron-beam evaporated on top of the exposed films to act as top electrodes. It turned out that all our samples were in short-circuit. This is most likely a result of the morphology of the films after conversion, which is in quite contrast compared to the parent materials AlF_3 and LiF (Figure 28): it is possible that the evaporated platinum is deposited also on the inner parts of the very porous-looking mixture fluoride film, thus getting into contact with the bottom electrode. Such as spongy morphology is a definite drawback for using this process for the deposition of a solid-electrolyte material. However, this problem could possibly be solved by using a suitable barrier layer on top of Li_3AlF_6.

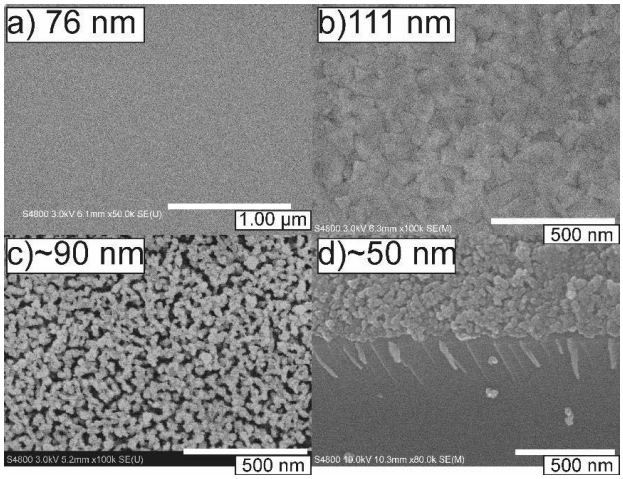

Figure 28: FESEM images of a) 76 nm amorphous AlF_3 film, b) 111 nm crystalline LiF film, c) ~ 90 nm crystalline Li_3AlF_6 film, d) ~50 nm crystalline Li_3AlF_6 film taken by tilting the sample.

Compared to the results of Li_3AlF_6 deposition using TMA, LiHMDS and HF-pyridine,[47] our films were always either lithium poor or lithium rich. In the work of Lee *et al.* a lower deposition temperature of 150 °C was used, which most likely prevented any large scale conversion reactions with excess LiF formation. Thus, they obtained films which were both crystalline and close to the correct stoichiometry. As already mentioned, they did notice that changing the ratio of the AlF_3 and LiF subcycles did not affect the metal ratio in the resulting films, indicating that some conversion is most likely taking place also in this process.[47]

5.4 Combining ALD and solid state reactions for lithium containing ternary oxides

As was discussed in Chapters 3.1.2 and 3.3.2, depositing ternary materials by ALD is not always straightforward, especially in the case of lithium containing materials. To overcome these difficulties, a new approach was developed. By combining the deposition of well-defined ALD materials, such as TiO_2 and Li_2CO_3, and solid state reactions caused by post-deposition annealing, we were able to obtain many different ternary lithium materials.[VI] By applying only on layer of each of the materials to be mixed, we effectively avoided problems such as changing growth rates on different surfaces.[68] In addition, by using the lithium carbonate process[122] instead of the oxide/hydroxide made from lithium *tert*-butoxide and water,[125] we obtained films with stable, ALD-type growth and saw no reactions of the as-deposited films in ambient air. We applied this method also to materials such as HfO_2, and found that with sufficient heating, lithium-ions can be mobile in HfO_2, even reacting with a layer underneath the hafnia.[VII]

5.4.1 Studies on solid state reactions between ALD-made Li_2CO_3 and Ta_2O_5, TiO_2, and Nb_2O_5 films [VI]

In these experiments, 3000 cycles of Lithd + O_3, resulting in approximately 28 nm of Li_2CO_3 on silicon, were applied onto approx. 50 nm ALD films of Ta_2O_5, TiO_2 and Nb_2O_5. These transition metal oxides were chosen based on the interesting properties of their lithium containing ternaries: $LiTaO_3$ and $LiNbO_3$ are ferroelectric materials with piezo- and pyroelectric properties,[160, 163, 188] and $Li_4Ti_5O_{12}$ is a potential lithium-ion battery anode material,[189, 190] as discussed in Chapter 2.2.1. After the Li_2CO_3 deposition, the Ta_2O_5 and TiO_2 films showed crystalline Li_2CO_3 on top of an either amorphous (Ta_2O_5, Figure 29) or crystalline (TiO_2) film. Interestingly, the film deposited onto Nb_2O_5 (Figure 29) was completely amorphous, indicating that some reaction between the oxide and the carbonate may have occurred already at the deposition temperature of 225 °C. This could be due to more facile redox-reactions of niobium, as compared to tantalum, for example.[191] The reaction seen with niobium oxide and lithium carbonate resembles that reported for the deposition of lithium manganese spinel.[147]

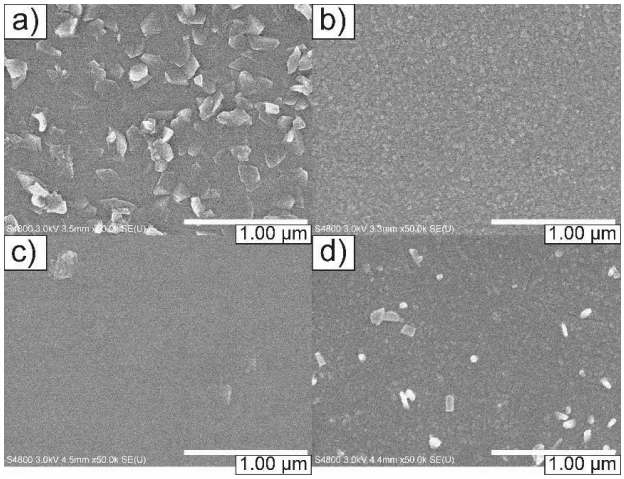

Figure 29: FESEM images of films deposited by applying 3000 cycles of Li_2CO_3 onto approximately 50 nm of Ta_2O_5 (a and b) and Nb_2O_5 (c and d). Figures a) and c) show the as-deposited films, while b) and d) are the same films after annealing for 2 hours at 650 °C in air.

All the films were post-deposition annealed in air at 650 °C and showed the formation of the respective lithium containing ternary oxides. ToF-ERDA measurements revealed that all the films were close to stoichiometric and contained very little carbon impurities after the annealing. The metal ions were very well mixed after annealing, as can be seen from ToF-ERDA depth profiles (Figure 30). Figure 18 shows our composition results on $LiTaO_3$ and $LiNbO_3$ compared to the subcycle methods used in refs [151] and [152]. In addition to $LiTaO_3$, the tantalum oxide sample also contained some crystalline Li_3TaO_4 as a result of a slight lithium excess in the films, as determined with ToF-ERDA. Lithium niobate crystallizes nicely at 650 °C and was very close to stoichiometric based on the ToF-ERDA measurements. Somewhat disappointingly, the titanium oxide sample did not form the desired spinel $Li_4Ti_5O_{12}$ phase. Instead, Li_2TiO_3 was formed, according to both GIXRD and ToF-ERDA. Li_2TiO_3 is commonly seen as an impurity phase in the synthesis of $Li_4Ti_5O_{12}$.[159, 192] The reason for the 2 : 1 phase was two-fold: Firstly, our annealing temperature of 650 °C was insufficient for the 4 : 5 phase to form. Secondly, we found that on TiO_2, the Li_2CO_3 grew in fact much thicker than on the other materials. The reason for the almost 4-fold increase in the growth rate remains unclear. Despite these challenges, we were able to witness the formation of $Li_4Ti_5O_{12}$ in an isothermal HTXRD measurement conducted at 670 °C on a sample with TiN as a barrier layer between silicon and 90 nm of TiO_2 (Figure 31). However, prolonged exposure to this temperature led to lithium silicate formation due to the lithium-ion mobility and reactivity with the underlying silicon substrate, despite the barrier.

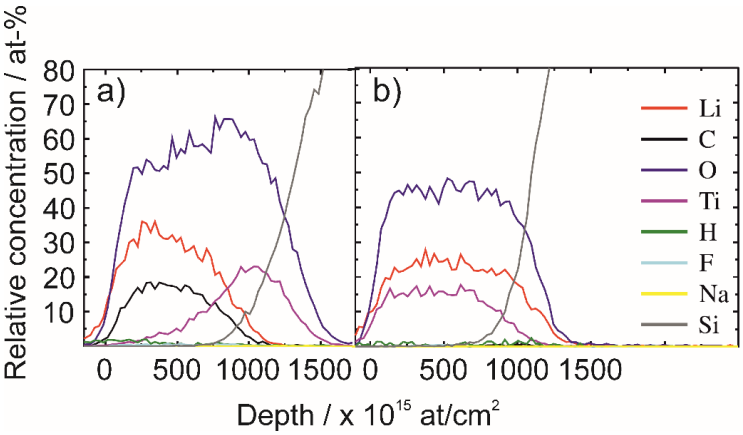

Figure 30: ToF-ERDA depth profiles of a film composed of 3000 cycles of Li_2CO_3 on top of 54 nm of TiO_2 a) before b) after annealing for 2 hours at 650 °C in air.

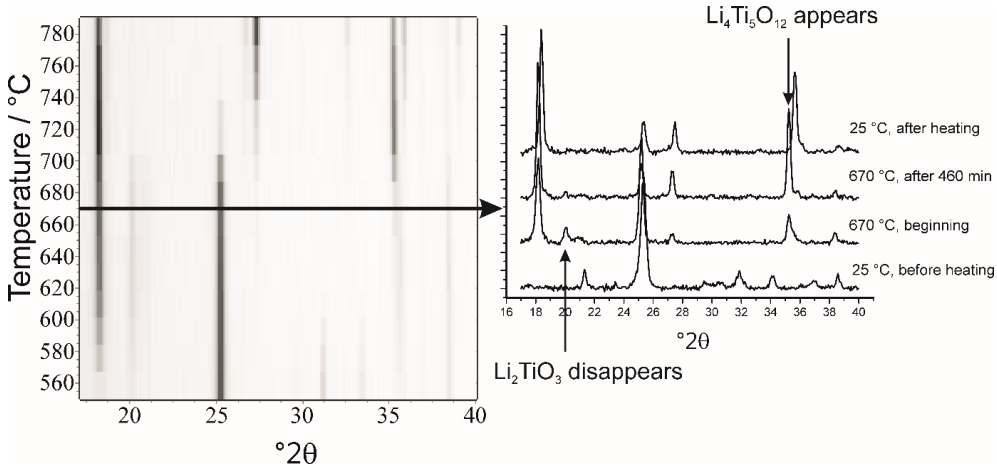

Figure 31: HTXRD of a Li_2CO_3 – TiO_2 – TiN film stack, measured in air. Above 750 °C the rutile phase of TiO_2 begins to form, accompanied by the destruction of TiN. Formation of $Li_4Ti_5O_{12}$ (appearance of a reflection at 35.3°) and disappearance of Li_2TiO_3 (decreasing peak at 20.4°) can be seen during an isothermal measurement at 670 °C.

With these experiments, we were able to prove that the simple combination of atomic layer deposited thin films and solid state reactions in air can be used to obtain ternary lithium containing oxides. We believe that this method simplifies greatly the deposition of these materials, and that it could further be used to deposit many other lithium containing ternaries in a similar fashion.

5.4.2 Studies on solid state reactions between ALD-made Li_2CO_3 and HfO_2, and ZrO_2 films [VII]

Experiments with hafnia and zirconia were conducted in a similar manner as those in paper VI. 3000 cycles of Li_2CO_3 were applied onto 50 nm of HfO_2 and 54 nm of ZrO_2, and the resulting stacks were annealed in air at various temperatures. In contrast to the results of paper VI, no crystalline ternary phases of hafnia[193] and zirconia[194–196] were observed during the annealing experiments (Figure 32). Instead, lithium diffused through the oxide layer, forming silicates with the single-crystalline silicon substrate likely with some help from the oxygen in air. The transition metal oxide film appeared to remain intact during the annealing, with no changes in phases detected with GIXRD. Based on the literature, higher annealing temperatures would be needed to form ternary lithium containing hafnium or zirconium oxides, similarly as was noticed for the deposition of $Li_4Ti_5O_{12}$ in paper VI.[197, 198]

The diffusion of lithium through hafnia was studied in more detail by annealing the film stack at various temperatures and measuring elemental depth profiles of the films by ToF-ERDA (Figure 33). It was found that after an anneal of 4 hours in air at 300 °C, lithium had not diffused into the hafnium oxide. After 2 hours at 400 and 500 °C the lithium carbonate layer was still present on top of the oxide. At 600 and 650 °C lithium diffusion had occurred, being more complete after 650 °C. The results were very similar with zirconia, the complete diffusion occurring at 650 °C. The ToF-ERDA measurements also revealed that after the annealing at 650 °C, all the films contained only very small amounts of impurities such as carbon and hydrogen.

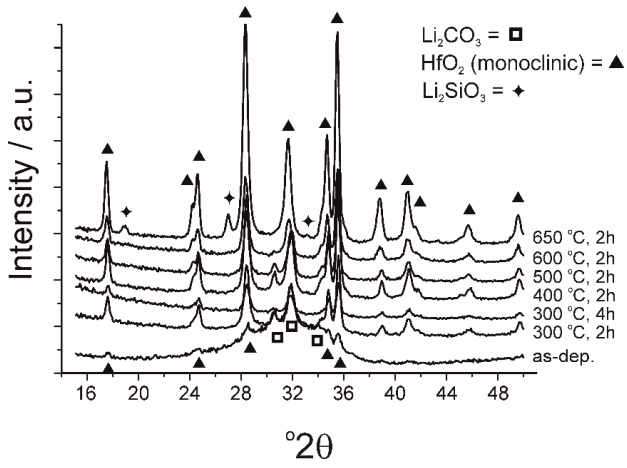

Figure 32: X-ray diffractograms of samples consisting of 3000 cycles of Li_2CO_3 on top of 50 nm of HfO_2 as-deposited and after annealing at various temperatures in air.

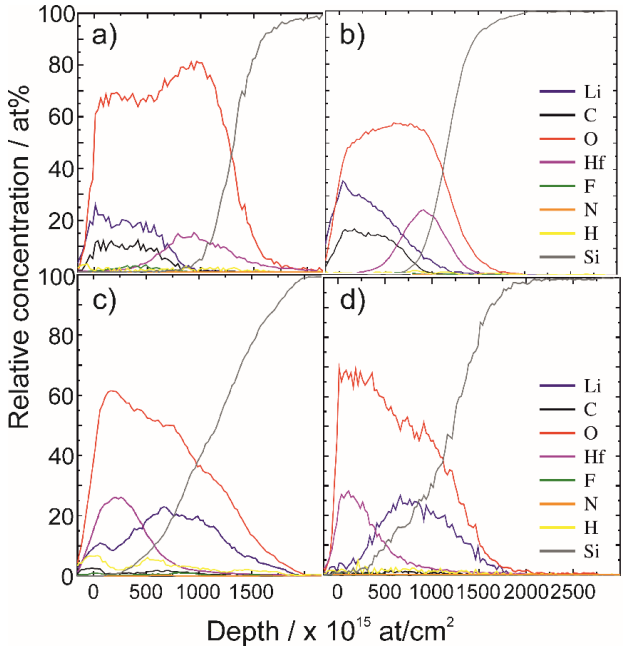

Figure 33: ToF-ERDA depth profiles of a Li_2CO_3/HfO_2 film stack a) as-deposited, b) after annealing at 500 °C, c) after annealing at 600 °C, and d) after annealing at 650 °C. All heat treatments were done in air and for 2 hours.

The morphology of the films changed drastically during annealing. The very rough Li_2CO_3 surface was converted to a much smoother surface, consisting of the transition metal oxide based on the elemental depth profiles (Figure 33). In contrast to the results reported in paper VI, the films showed some cracking after the annealing, the zirconia more so than the hafnia. This might be related to increased stress caused by the lithium silicate formation under the oxide films, and to the rather high amount of hydrogen impurity in the ALD-deposited zirconia film.

To further study the lithium diffusion through hafnia, a film stack consisting of a top layer of Li_2CO_3, a HfO_2 layer and a TiO_2 layer was deposited by ALD. After annealing in air at 650 °C for only 30 minutes, the stack showed formation of Li_2TiO_3 (Figure 34). Thus, lithium can be driven through the hafnium oxide film and into a possible electrode material, as would occur during battery operation with hafnia as a solid electrolyte. The hafnium and titanium oxide films do not mix during the annealing, as confirmed by GIXRD measurements, FESEM cross-section imaging and ToF-ERDA elemental depth profiles.

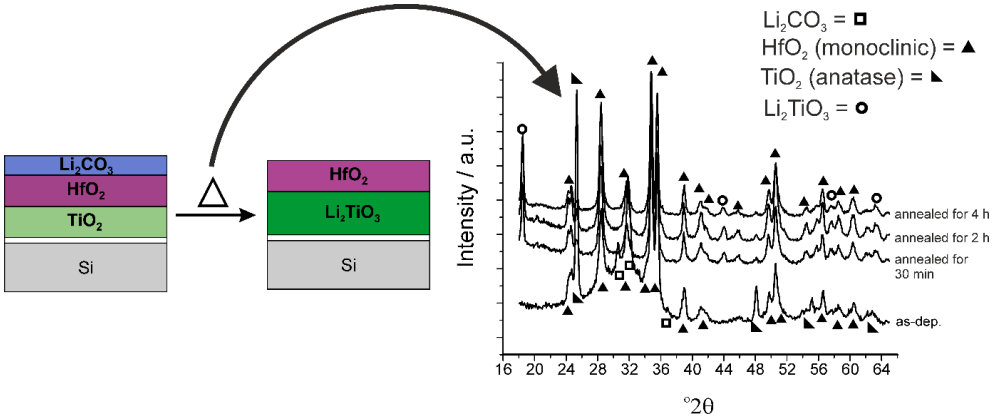

Figure 34: A stack composed of Li_2CO_3, HfO_2 and TiO_2 on top of a silicon substrate produces Li_2TiO_2 and HfO_2 after annealing at 650 °C in air as observed with GIXRD.

Based on these results, it is clear that lithium can diffuse through well-known insulating materials HfO_2 and ZrO_2 and react with an underlying material. Therefore, these oxides could prove useful in lithium-ion battery applications as solid electrolyte layers or protective coatings for electrodes.[199]

6. Conclusions and Outlook

The lithium-ion battery will most likely continue as one of the most important energy storage devices in the world. Its usage and continued development are supported by both the increasing utilization of renewable energy sources and the growth of the market for personal electronics. However, radical new designs for both materials and battery structures are needed to ensure that these batteries are applicable in a wide range of products also in the future. In addition, issues regarding battery safety are becoming even more important, requiring a radical move away from the current organic liquid electrolytes.

Atomic layer deposition can be one of the enabling technologies for the future all-solid-state 3D-batteries. As a technology that produces conformal, uniform, pin-hole free films with easy and accurate thickness control, ALD can be used to deposit thin films onto complicated structures, increasing the energy densities of current batteries. The combination of ALD and lithium-ion batteries has gained much interest in recent years, and as was summarized in this thesis, everything from active to protective battery layers have already been deposited by ALD.

The application of suitable thin film techniques is not enough to realize the perfect battery for future applications. New materials also need to be studied in order to obtain all the desired battery properties. For this end, fluorides could prove to be a useful class of battery materials. Especially, transition metal fluorides as cathodes, protective layers and solid electrolytes, in combination with LiF, will undoubtedly receive more research interest in the future. We have demonstrated that materials such as LiF and AlF_3 can be deposited by ALD, and our initial research efforts have been followed by publications from other groups. However, despite our success in depositing the binary materials, depositing the mixture fluoride Li_3AlF_6 proved challenging due to the reactivity of the lithium-ion.

The biggest challenges in ALD battery research come from depositing complicated, multimetal oxides and fluorides of lithium. The lithium-ion does not always behave in a self-limiting manner during the ALD film growth, resulting in, for example, unexpectedly high lithium contents in the films and interesting conversion reactions in the case of fluorides. We have demonstrated that some of these problems can be circumvented by depositing thick layers of materials by ALD and then annealing the resulting film stack. This process was used to deposit ternary oxide films, and could possibly be used to obtain even more complicated materials.

This thesis summarized the results of 7 papers and manuscripts from a wide range of research topics related to atomic layer deposited lithium-ion battery materials. For future work, it would be interesting to focus on studying other double metal complexes of lithium as possible ALD precursors, such as β-diketonates or heteroleptic compounds. Also, more work should be put into the deposition of transition metal fluorides, such as NiF_2 and VF_3, for solid electrolyte studies with LiF.

References

[1] http://www.nissanusa.com/electric-cars/leaf/charging-range/battery/ accessed 13th of Oct., 2016.

[2] http://qz.com/764723/tesla-has-maxed-out-what-its-current-batteries-can-do/ accessed 13th of Oct., 2016.

[3] C. Pillot, "The worldwide battery market 2011–2025", Batteries, 24.-26.2012, Nice, France.

[4] Bloomberg L.P. *Batteries Storing Power Seen as Big as Rooftop Solar in 12 Years* by A. Hirtenstein https://www.bloomberg.com/news/articles/2016-06-13/batteries-storing-power-seen-as-big-as-rooftop-solar-in-12-years accessed 13th of Oct., 2016.

[5] United States Department of Transportation, Pipeline and Hazardous Materials Safety Administration, http://phmsa.dot.gov/safetravel/batteries accessed 13th of Oct., 2016.

[6] United States Consumer Product Safety Commission, Recall number 16–266: Samsung Recalls Galaxy Note7 Smartphones Due to Serious Fire and Burn Hazards https://www.cpsc.gov/Recalls/2016/Samsung-Recalls-Galaxy-Note7-Smartphones/ accessed 13th of Oct., 2016.

[7] New York Times, *Why Samsung Abandoned Its Galaxy Note 7 Flagship Phone* by Brian X. Chen and Choe Sang-Hun, http://www.nytimes.com/2016/10/12/business/international/samsung-galaxy-note7-terminated.html accessed 13th of Oct., 2016.

[8] R. A. Huggins (**2009**). *Advanced Batteries: Materials Science Aspects*. New York, U.S.A: Springer.

[9] J.-M. Tarascon and M. Armand, *Nature* 414 (**2001**) 359–367.

[10] C. M. Hayner, X. Zhao, and H. H. Kung, *Annu. Rev. Chem. Biomol. Eng.* 3 (**2012**) 445–471.

[11] L. Baggetto, R. A. H. Niessen, F. Roozeboom, and P. H. L. Notten, *Adv. Funct. Mater.* 18 (**2008**) 1057–1066.

[12] J. W. Long, B. Dunn, D. R. Rolison, and H. S. White, *Chem. Rev.* 104 (**2004**) 4463–4492.

[13] B. Dunn, J. W. Long, and D. R. Rolison, *Electrochem. Soc. Interface* 17 (**Fall 2008**) 49–53.

[14] J. F. M. Oudenhoven, L. Baggetto, and P. H. L. Notten, *Adv. Energy Mater.* 1 (**2011**) 10–33.

[15] M. S. Whittingham, *Chem. Rev.* 104 (**2004**) 4271–4301.

[16] B. L. Ellis, K. T. Lee, and L. F. Nazar, *Chem. Mater.* 22 (**2010**) 691–714.

[17] Z. Chen, Y. Qin, K. Amine, and Y.-K. Sun, *J. Mater. Chem.* 20 (**2010**) 7606–7612.

[18] N. Nitta and G. Yushin, *Part. Part. Syst. Charact.* 31 (**2014**) 317–336.

[19] C.-M. Park, J.-H. Kim, H. Kim, and H.-J. Sohn, *Chem. Soc. Rev.* 39 (**2010**) 3115–3141.

[20] P. Poizot, S. Laruelle, S.Grugeon, L. Dupont, and J.-M. Tarascon, *Nature* 407 (**2000**) 496–499.

[21] H. Li, P. Balaya, and J. Maier, *J. Electrochem. Soc.* 151 (**2004**) A1878–A1885.

[22] V. Thangadurai and W. Weppner, *Ionics* 8 (**2002**) 281–292.

[23] V. Thangadurai and W. Weppner, *Ionics* 12 (**2006**) 81–92.

[24] H. Xia, H. L. Wang, W. Xiao, M. O. Lai, and L. Lu, *Int. J. Surf. Sci. Eng.* 3 (**2009**) 23–43.

[25] P. Knauth, *Solid State Ionics* 180 (**2009**) 911–916.

[26] J. W. Fergus, *J. Power Sources* 195 (**2010**) 4554–4569.

[27] G. G. Amatucci and N. Pereira, *J. Fluorine Chem.* 128 (**2007**) 243–262.

[28] M. Hu, X. Pang, and Z. Zhou, *J. Power Sources* 237 (**2013**) 229–242.

[29] J. Cabana, L. Monconduit, D. Larcher, and M. R. Palacín, *Adv. Mater.* 22 (**2010**) E170–E192.

[30] H. Li, G. Richter, and J. Maier, *Adv. Mater.* 15 (**2003**) 736–739.

[31] F. Badway, F. Cosandey, N. Pereira, and G. G. Amatucci, *J. Electrochem. Soc.* 150 (**2003**) A1318–A1327.

[32] H. Zhang, Y.-N. Zhou, Q. Sun, and Z.-W. Fu, *Solid State Sci.* 10 (**2008**) 1166–1172.

[33] M. Bervas, F. Badway, L. C.Klein, and G. G. Amatucci, *Electrochem. Solid-State Lett.* 8 (**2005**) A179–A183.

[34] E. Gonzalo, A. Kuhn, and F. García-Alvarado, *J. Power Sources* 195 (**2010**) 4990–4996.

[35] A. Basa, E. Gonzalo, A. Kuhn, and F. García-Alvarado, *J. Power Sources* 197 (**2012**) 260–266.

[36] A. Basa, E. Gonzalo, A. Kuhn, and F. García-Alvarado, *J. Power Sources* 207 (**2012**) 160–165.

[37] Y. Koyama, I. Tanaka, and H. Adachi, *J. Electrochem. Soc.* 147 (**2000**) 3633–3636.

[38] F. Amalraj, M. Talianker, B. Markovsky, L. Burlaka, N. Leifer, G. Goobes, E. M. Erickson, O. Haik, J. Grinblat, E. Zinigrad, D. Aurbach, J. K. Lampert, J.-Y. Shin, M. Schulz-Dobrick, and A. Garsuch. *J. Electrochem. Soc.* 160 (**2013**) A2220–A2233.

[39] S.-H. Lee, C. S. Yoon, K. Amine, and Y.-K. Sun, *J. Power Sources* 234 (**2013**) 201–207.

[40] Y.-K. Sun, M.-J. Lee, C. S. Yoon, J. Hassoun, K. Amine, and B. Scrosati, *Adv. Mater.* 24 (**2012**) 1192–1196.

[41] A. Tron, Y. D. Park, and J. Mun, *J. Power Sources* 325 (**2016**) 360–364.

[42] Y.-K. Sun, S.-W. Cho, S.-T. Myung, K. Amine, and J. Prakash, *Electrochim. Acta* 53 (**2007**) 1013–1019.

[43] F. Ding, W. Xu, D. Choi, W. Wang, X. Li, M. H. Engelhard, X. Chen, Z. Yang, and J.-G. Zhang, *J. Mater. Chem.* 22 (**2012**) 12745–12751.

[44] T. Oi, *Mat. Res. Bull.* 19 (**1984**) 1343–1348.

[45] T. Oi, *Mat. Res. Bull.* 19 (**1984**) 451–457.

[46] T. Oi, *Mat. Res. Bull.* 19 (**1984**) 1077–1082.

[47] Y. Lee, D. M. Piper, A. S. Cavanagh, M. J. Young, S.-H. Lee, and S. M. George, "*Atomic Layer Deposition of Lithium Ion Conducting $(AlF_3)(LiF)_x$ Alloys Using Trimethylaluminum, Lithium Hexamethyldisilazide and Hydrogen Fluoride-Pyridine*", 14th International Conference on Atomic Layer Deposition, 15.-18.6.2014, Kyoto, Japan.

[48] R. Miyazaki and H. Maekawa, *ECS Electrochem. Lett.* 1 (**2012**) A87–A89.

[49] J.-M. Dance and T. Oi, *Thin Solid Films* 104 (**1983**) L71–L73.

[50] Y. Kawamoto, J. Fujiwara, and C. Ichimura, *J. Non-Cryst. Solids* 111 (**1989**) 245–251.

[51] J. M. Reau, H. Kahnt, and M. Poulain, *J. Non-Cryst. Solids* 119 (**1990**) 347–350.

[52] J. Senegas, J. M. Reau, H. Aomi, P. Hagenmuller, and M. Poulain, *J. Non-Cryst. Solids* 85 (**1986**) 315–334.

[53] V. Trnovcová, P. P. Fedorov, Č. Bárta, V. Labaš, V. A. Meleshina, and B. P. Sobolev, *Solid State Ionics* 119 (**1999**) 173–180.

[54] V. Trnovcová, P. P. Fedorov, and I. Furár, *J. Rare Earths* 26 (**2008**) 225–232.

[55] B. Dieudonné, J. Chable, F. Mauvy, S. Fourcade, E. Durand, E. Lebraud, M. Leblanc, C. Legein, M. Body, V. Maisonneuve, and A. Demourgues, *J. Phys. Chem. C* 119 (**2015**) 25170–25179.

[56] N. I. Sorokin and B. P. Sobolev, *Crystallogr. Rep.* 52 (**2007**) 842–863.

[57] M. A. Reddy and M. Fichtner, *J. Mater. Chem.* 21 (**2011**) 17059–17062.

[58] T. Pilvi (**2008**), *Atomic Layer Deposition for Optical Applications: Metal Fluoride Thin Films and Novel Devices*. Academic Dissertation, University of Helsinki.
https://helda.helsinki.fi/handle/10138/21109

[59] Y. Lee (**2015**), *Atomic Layer Etching of Metal Oxides and Atomic Layer Deposition of Metal Fluorides*. Academic Dissertation, University of Colorado, Boulder.

[60] O. Nilsen, V. Miikkulainen, K. B. Gandrud, E. Østreng, A. Ruud, and H. Fjellvåg, *Phys. Status Solidi A* 211 (**2014**) 357–367.

[61] L. Ma, R. B. Nuwayhid, T. Wu, Y. Lei, K. Amine, and J. Lu, *Adv. Mater. Interfaces* 3 (**2016**) 1600564.

[62] X. Meng, X. Wang, D. Geng, C. Ozgit-Akgun, N. Schneider, and J. W. Elam, *Mater. Horiz.* 4 (**2017**) 133–154.

[63] X. Meng, X.-Q. Yang, and X. Sun, *Adv. Mater.* 24 (**2012**) 3589–3615.

[64] C. Guan and J. Wang, *Adv. Sci.* 3 (**2016**) 1500405.

[65] X. Meng and J. W. Elam, *ECS Trans.* 69 (**2015**) 39–57.

[66] M. Leskelä and M. Ritala, *Angew. Chem. Int. Ed.* 42 (**2003**) 5548–5554.

[67] S. M. George, *Chem. Rev.* 110 (**2010**) 111–131.

[68] R. L. Puurunen, *Chem. Vap. Deposition* 9 (**2003**) 249–257.

[69] M. Ritala and M. Leskelä (**2002**). *Atomic Layer Deposition*. In H. S. Nalwa (Ed.), *Handbook of Thin Film Materials, Volume 1: Deposition and Processing of Thin Films* (pages 103–159). San Diego, U.S.A: Academic Press.

[70] H. B. Profijt, S. E. Potts, M. C. M. van de Sanden, and W. M. M. Kessels, *J. Vac. Sci. Technol. A* 29 (**2011**) 050801-1–050801-26.

[71] P. R. Chalker, *Surf. Coat. Technol.* 291 (**2016**) 258–263.

[72] K. Väyrynen, V. Miikkulainen, K. Mizohata, V. Kilpi, and M. Ritala, "*Photo-ALD of Tantalum and Niobium Oxides*", 13th Baltic Conference on Atomic Layer Deposition, 28.-29.9.2015, Tartu, Estonia.

[73] M. Kariniemi, J. Niinistö, M. Vehkamäki, M. Kemell, M. Ritala, and M. Leskelä, *J. Vac. Sci. Technol. A* 30 (**2012**) 01A115-1–01A115-5.

[74] V. Miikkulainen, M. Leskelä, M. Ritala, and R. L. Puurunen, *J. Appl. Phys.* 113 (**2013**) 021301-1–021301-101.

[75] E. Østreng, P. Vajeeston, O. Nilsen, and H. Fjellvåg, *RSC Adv.* 2 (**2012**) 6315–6322.

[76] J. Hämäläinen, F. Munnik, T. Hatanpää, J. Holopainen, M. Ritala, and M. Leskelä, *J. Vac. Sci. Technol. A* 30 (**2012**) 01A106-1–01A106-5.

[77] J. Hämäläinen, J. Holopainen, F. Munnik, T. Hatanpää, M. Heikkilä, M. Ritala, and M. Leskelä, *J. Electrochem. Soc.* 159 (**2012**) A259–A263.

[78] M. Nisula, Y. Shindo, H. Koga, and M. Karppinen, *Chem. Mater.* 27 (**2015**) 6987–6993.

[79] M. Ylilammi and T. Ranta-aho, *J. Electrochem. Soc.* 141 (**1994**) 1278–1284.

[80] Y. Lee, J. W, DuMont, A. S. Cavanagh, and S. M. George, *J. Phys. Chem. C* 119 (**2015**) 14185–14194.

[81] Y. Lee, H. Sun, M. J. Young, and S. M. George, *Chem. Mater.* 28 (**2016**) 2022–2032.

[82] J. Hennessy, A. D. Jewell, K. Balasubramanian, and S. Nikzad, *J. Vac. Sci. Technol. A* 34 (**2016**) 01A120-1–01A120-6.

[83] T. Pilvi, K. Arstila, M. Leskelä, and M. Ritala, *Chem. Mater.* 19 (**2007**) 3387–3392.

[84] T. Pilvi, T. Hatanpää, E. Puukilainen, K. Arstila, M. Bischoff, U. Kaiser, N. Kaiser, M. Leskelä, and M. Ritala, *J. Mater. Chem.* 17 (**2007**) 5077–5083.

[85] T. Pilvi, E. Puukilainen, K. Arstila, M. Leskelä, and M. Ritala, *Chem. Vap. Deposition* 14 (**2008**) 85–91.

[86] T. Pilvi, E. Puukilainen, F. Munnik, M. Leskelä, and M. Ritala, *Chem. Vap. Deposition* 15 (**2009**) 27–32.

[87] T. Pilvi, E. Puukilainen, U. Kreissig, M. Leskelä, and M. Ritala, *Chem. Mater.* 20 (**2008**) 5023–5028.

[88] D. H. K. Jackson, M. R. Laskar, S. Fang, S. Xu, R. G. Ellis, X. Li, M. Dreibelbis, S. E. Babcock, M. K. Mahanthappa, D. Morgan, R. J. Hamers, and T. F. Kuech, *J. Vac. Sci. Technol. A* 34 (**2016**) 031503-1–031503-8.

[89] S. D. Elliot and O. Nilsen, *ECS Trans.* 41 (**2011**) 175–183.

[90] M. D. McDaniel, T. Q. Ngo, S. Hu, A. Posadas, A. A. Demkov, and J. G. Ekerdt, *Appl. Phys. Rev.* 2 (**2015**) 041301-1–041301-32.

[91] J. W. Elam, Z. A. Sechrist, and S. M. George, *Thin Solid Films* 414 (**2002**) 43–55.

[92] B. Marchand, P. Jalkanen, V. Tuboltsev, M. Vehkamäki, M. Puttaswamy, M. L. Kemell, K. Mizohata, T. Hatanpää, A. M. Savin, J. Räisänen, M. Ritala, and M. Leskelä, *J. Phys. Chem. C* 120 (**2016**) 7313–7322.

[93] S. Riedel, J. Neidhardt, S. Jansen, L. Wilde, J. Sundqvist, E. Erben, S. Teichert, and A. Michaelis, *J. Appl. Phys.* 109 (**2011**) 094101-1–094101-8.

[94] O. Nilsen, E. Rauwel, H. Fjellvåg, and A. Kjekshus, *J. Mater. Chem.* 17 (**2007**) 1466–1475.

[95] C. Murray and S. D. Elliott, *ACS Appl. Mater. Interfaces* 5 (**2013**) 3704–3715.

[96] Y. Gao, O. Zandi, and T. W. Hamann, *J. Mater. Chem. A* 4 (**2016**) 2826–2830.

[97] E. Thimsen, S. C. Riha, S. V. Baryshev, A. B. F. Martinson, J. W. Elam, and M. J. Pellin, *Chem. Mater.* 24 (**2012**) 3188–3196.

[98] A. Zolotaryov, S. Goetze, R. Zierold, D. Novikov, B. Birajdar, D. Hesse, and K. Nielsch, *Adv. Eng. Mater.* 12 (**2010**) 509–516.

[99] R. Mantovan, S. Vangelista, C. Wiemer, A. Lamperti, G. Tallarida, E. Chikoidze, Y. Dumont, and M. Fanciulli, *J. Appl. Phys.* 115 (**2014**) 17D907-1–17D907-3.

[100] A. Zolotaryov, S. Goetze, J. Bachmann, D. Goerlitz, D. Hesse, and K. Nielsch, *Adv. Eng. Mater.* 13 (**2011**) 330–335.

[101] E. Thimsen, S. V. Baryshev, A. B. F. Martinson, J. W. Elam, I. V. Veryovkin, and M. J. Pellin, *Chem. Mater.* 25 (**2013**) 313–319.

[102] J. Harjuoja, T. Hatanpää, M. Vehkamäki, S. Väyrynen, M. Putkonen, L. Niinistö, M. Ritala, M. Leskelä, and E. Rauhala, *Chem. Vap. Deposition* 11 (**2005**) 362–367.

[103] A. N. Gleizes, *Chem. Vap. Deposition* 6 (**2000**) 155–173.

[104] M. J. Saly, F. Munnik, and C. H. Winter, *J. Mater. Chem.* 20 (**2010**) 9995–10000.

[105] M. Vehkamäki, M. Ritala, M. Leskelä, A. C. Jones, H. O. Davies, T. Sajavaara, and E. Rauhala, *J. Electrochem. Soc.* 151 (**2004**) F69–F72.

[106] Y. J. Chung, D.-C. Moon, J. H. Han, M. Park, J. W. Park, T.-M. Chung, Y. K. Lee, and K. S. An, *Thin Solid Films* 564 (**2014**) 140–145.

[107] J. M. Gaskell, S. Przybylak, A. C. Jones, H. C. Aspinall, P. R. Chalker, K. Black, R. J. Potter, P. Taechakumput, and S. Taylor, *Chem. Mater.* 19 (**2007**) 4796–4803.

[108] J. M. Gaskell, A. C. Jones, H. C. Aspinall, S. Przybylak, P. R. Chalker, K. Black, H. O. Davies, P. Taechakumput, S. Taylor, and G. W. Critchlow, *J. Mater. Chem.* 16 (**2006**) 3854–3860.

[109] Y. Tomczak, K. Knapas, M. Sundberg, M. Leskelä, and M. Ritala, *J. Phys. Chem. C* 117 (**2013**) 14241–14246.

[110] W.A. Herrmann, N.W. Huber, and O. Runte, *Angew. Chem. Int. Ed. Engl.* 34 (**1995**) 2187–2206.

[111] T. D. Manning, Y. F. Loo, A. C. Jones, H. C. Aspinall, P. R. Chalker, J. F. Bickley, L. M. Smith, and G. W. Critchlow, *J. Mater. Chem.* 15 (**2005**) 3384–3387.

[112] E. Nykänen, P. Soininen, L. Niinistö, M. Leskelä, and E. Rauhala, Proceedings of 1994 International Workshop on Electroluminescence (**1994**) 437–444.

[113] J. S. Park, A. U. Mane, J. W. Elam, and J. R. Croy, *Chem. Mater.* 27 (**2015**) 1917–1920.

[114] A. Mane, J. Libera, and J. Elam, "*Atomic Layer Deposition of LiF Thin Films Using Lithium Tert-Butoxide and Metal Fluoride Precursors*", 16th International Conference on Atomic Layer Deposition, 24.-27.7.2016, Dublin, Ireland.

[115] M. Putkonen, A. Szeghalmi, E. Pippel, and M. Knez, *J. Mater. Chem.* 21 (**2011**) 14461–14465.

[116] J. Hennessy, A. P. Jewell, F. Greer, M. C. Lee, and S. Nikzad, *J. Vac. Sci. Technol. A* 33 (**2015**) 01A125-1–01A125-6.

[117] S. Haukka, *ECS Trans.* 3 (**2007**) 15–26.

[118] J. A. Klug, T. Proslier, J. W. Elam, R. E. Cook, J. M. Hiller, H. Claus, N. G. Becker, and M. J. Pellin, *J. Phys. Chem. C* 115 (**2011**) 25063–25071.

[119] M. Kaipio, M. Kemell, M. Vehkamäki, M. Mattinen, K. Mizohata, M. Ritala, and M. Leskelä, "*Atomic layer deposition of metal carbides – The $TiCl_4$/TMA process as an example*", 14th Baltic Conference on Atomic Layer Deposition, 2.-4.10.2016, St. Petersburg, Russia.

[120] Y. Chen, S. Ould-Chikh, E. Abou-Hamad, E. Callens, J. C. Mohandas, S. Khalid, and J.-M. Basset, *Organometallics* 33 (**2014**) 1205–1211.

[121] R. R. Schrock, and P. Meakin, *J. Am. Chem. Soc.* 96 (**1974**) 5288–5290.

[122] M. Putkonen, T. Aaltonen, M. Alnes, T. Sajavaara, O. Nilsen, and H. Fjellvåg, *J. Mater. Chem.* 19 (**2009**) 8767–8771.

[123] A. S. Cavanagh, Y. Lee, B. Yoon, and S. M. George, *ECS Trans.* 33 (**2010**) 223–229.

[124] D. Comstock and J. W. Elam, *J. Phys. Chem. C* 117 (**2013**) 1677–1683.

[125] A. C. Kozen, A. J. Pearse, C.-F. Lin, M. A. Schoeder, M. Noked, S. B. Lee, and G. W. Rubloff, *J. Phys. Chem. C* 118 (**2014**) 27749–27753.

[126] A. Ruud, V. Miikkulainen, K. Mizohata, H. Fjellvåg, and O. Nilsen, *J. Vac. Sci. Technol. A* 35 (**2017**) 01B133-1–01B133-8.

[127] B. Wang, J. Liu, Q. Sun, R. Li, T.-K. Sham, and X. Sun, *Nanotechnology* 25 (**2014**) 504007.

[128] A. C. Kozen, A. J. Pearse, C.-F. Lin, M. Noked, and G. W. Rubloff, *Chem. Mater.* 27 (**2015**) 5324–5331.

[129] X. Meng, D. J. Comstock, T. T. Fisher, and J. W. Elam, *ACS Nano* 8 (**2014**) 10963–10972.

[130] M. Nisula and M. Karppinen, *Nano Lett.* 16 (**2016**) 1276–1281.

[131] M. Nisula, J. Linnera, A. J. Karttunen, and M. Karppinen, *Chem. Eur. J.* 23 (**2017**) 2988–2992.

[132] M. Létiche, E, Eustache, J. Freixas, A. Demortière, V. De Andradem L. Morgenroth, P. Tilmant, F. Vaurette, D. Troadec, P. Roussel, T. Brousse, and C. Lethien, *Adv. Energy Mater.* 7 (**2017**) 1601402.

[133] J. Liu, B. Wang, Q. Sun, R. Li, T.-K. Sham, and X. Sun, *Adv. Mater. Interfaces* 3 (**2016**) 1600468.

[134] B. Wang, J. Liu, Q. Sun, B. Xiao, R. Li, T.-K. Sham, and X. Sun, *Adv. Mater. Interfaces* 3 (**2016**) 1600369.

[135] C.-F. Lin, M. Noked, A. C. Kozen, C. Liu, O. Zhao, K. Gregorczyk, L. Hu, S. B. Lee, and G. W. Rubloff, *ACS Nano* 10 (**2016**) 2693–2701.

[136] P. Sundberg and M. Karppinen, *Beilstein J. Nanotechnol.* 5 (**2014**) 1104–1136.

[137] M. Armand, S. Grugeon, H. Vezin, S. Laruelle, P. Ribière, P. Poizot, and J.-M. Tarascon, *Nat. Mater.* 8 (**2009**) 120–125.

[138] Personal communication from Mr. Mikko Nisula, Aalto University.

[139] T. Aaltonen, O. Nilsen, A. Magrasó, and H. Fjellvåg, *Chem. Mater.* 23 (**2011**) 4669–4675.

[140] V. Miikkulainen, O. Nilsen, H. Li, S. W. King, M. Laitinen, T. Sajavaara, and H. Fjellvåg, *J. Vac. Sci. Technol. A* 33 (**2015**) 01A101-1–01A101-7.

[141] J. S. Park, X. Meng, J. W. Elam, S. Hao, C. Wolverton, C. Kim, and J. Cabana, *Chem. Mater.* 26 (**2014**) 3128–3134.

[142] Y. Hu, A. Ruud, V. Miikkulainen, T. Norby, O. Nilsen, and H. Fjellvåg, *RSC Adv.* 6 (**2016**) 60479–60486.

[143] M. E. Donders, H. C. M. Knoops, W. M. M. Kessels, and P. H. L. Notten, *ECS Trans.* 41 (**2011**) 321–330.

[144] M. E. Donders, W. M. Arnoldbik, H. C. M. Knoops, W. M. M. Kessels, and P. H. L. Notten, *J. Electrochem. Soc.* 160 (**2013**) A3066–A3071.

[145] J. Liu, M. N. Banis, Q. Sun, A. Lushington, R. Li, T.-K. Sham, and X. Sun, *Adv. Mater.* 26 (**2014**) 6472–6477.

[146] K. B. Gandrud, A. Pettersen, O. Nilsen, and H. Fjellvåg, "*Growth of $LiFePO_4$ cathode material by ALD*", 10th International Conference on Atomic Layer Deposition, 20.-23.6.2010, Seoul, Korea.

[147] V. Miikkulainen, A. Ruud, E. Østreng, O. Nilsen, M. Laitinen, T. Sajavaara, and H. Fjellvåg, *J. Phys. Chem. C* 118 (**2014**) 1258–1268.

[148] V. Miikkulainen, O. Nilsen, M. Laitinen, T. Sajavaara, and H. Fjellvåg, *RSC Adv.* 3 (**2013**) 7537–7542.

[149] X. Meng, J. Liu, X. Li, M. N. Banis, J. Yang, R. Li, and X. Sun, *RSC Adv.* 3 (**2013**) 7285–7288.

[150] V. Miikkulainen, O. Nilsen, M. Laitinen, T. Sajavaara, and H. Fjellvåg, "*Atomic Layer Deposition of $Li_xTi_yO_z$ Films*", 12th International Conference on Atomic Layer Deposition, 17.-20.6.2012, Dresden, Germany.

[151] E. Østreng, H. H. Sønsteby, T. Sajavaara, O. Nilsen, and H. Fjellvåg, *J. Mater. Chem. C* 1 (**2013**) 4283–4290.

[152] J. Liu, M. N. Banis, X. Li, A. Lushington, M. Cai, R. Li, T.-K. Sham, and X. Sun, *J. Phys. Chem. C* 117 (**2013**) 20260–20267.

[153] T. Aaltonen, M. Alnes, O. Nilsen, L. Costelle, and H. Fjellvåg, *J. Mater. Chem.* 20 (**2010**) 2877–2881.

[154] Y.-C. Perng, J. Cho, S. Y. Sun, D. Membreno, N. Cirigliano, B. Dunn, and J. P. Chang, *J. Mater. Chem. A* 2 (**2014**) 9566–9573.

[155] E. Kazyak, K.-H. Chen, K. N. Wood, A. L. Davis, T. Thompson, A. R. Bielinski, A. J. Sanchez, X. Wang, C. Wang, J. Sakamoto, and N. P. Dasgupta, *Chem. Mater.* 29 (**2017**) 3785–3792.

[156] Y. Cao, X. Meng, and J. W. Elam, *ChemElectroChem* 3 (**2016**) 858–863.

[157] J. Kim, K. Chakrabarti, J. Lee, K.-Y. Oh, and C. Lee, *Mater. Chem. Phys.* 78 (**2003**) 733–738.

[158] K. B. Gandrud, A. Pettersen, O. Nilsen, and H. Fjellvåg, *J. Mater. Chem. A* 1 (**2013**) 9054–9059.

[159] Y. Shen, M. Søndergaard, M. Christensen, S. Birgisson, and B. B. Iversen, *Chem. Mater.* 26 (**2014**) 3679–3686.

[160] R. S. Weis and T. K. Gaylord, *Appl. Phys. A* 37 (**1985**) 191–203.

[161] D. Kip, *Appl. Phys. B* 67 (**1998**) 131–150.

[162] A. M. Glass, K. Nassau, and T. J. Negran, *J. Appl. Phys.* 49 (**1978**) 4808–4811.

[163] R. T. Smith, *Appl. Phys. Lett.* 11 (**1967**) 146–148.

[164] I. Tomeno and S. Matsumura, *Phys. Rev. B* 38 (**1988**) 606–614.

[165] X. Li, J. Liu, M. N. Banis, A. Lushington, R. Li, M. Cai, and X. Sun, *Energy Environ. Sci.* 7 (**2014**) 768–778.

[166] R. Murugan, V. Thangadurai, and W. Weppner, *Angew. Chem. Int. Ed.* 46 (**2007**) 7778–7781.

[167] K.G. Caulton and L.G. Hubert-Pfalzgraf, *Chem. Rev.* 90 (**1990**) 969–995.

[168] U. Olsher, R.M. Izatt, J.S. Bradshaw, and N.K. Dalley, *Chem. Rev.* 91 (**1991**) 137–164.

[169] M. Mäntymäki (**2010**) *Litiumin kaksoismetallialkoksidien valmistus ja käyttö ohutkalvojen lähdeaineena*. Master's Thesis, University of Helsinki.

[170] D. A. Lapiano-Smith, E. A. Eklund, F. J. Himpsel, and L. J. Terminello, *Appl. Phys. Lett.* 59 (**1991**) 2174–2176.

[171] H. H. Li, *J. Phys. Chem. Ref. Data* 5 (**1976**) 329–528.

[172] F. Bridou, M. Cuniot-Ponsard, J.-M. Desvignes, M. Richter, U. Kroth, and A. Gottwald, *Opt. Commun.* 283 (**2010**) 1351–1358.

[173] J. Sun, X. Li, W. Zhang, K. Yi, and J. Shao, *Appl. Opt.* 51 (**2012**) 8481–8489.

[174] D. König, R. Scholz, D. R. T. Zahn, and G. Ebest, *J. Appl. Phys.* 97 (**2005**) 093707-1–093707-9.

[175] G.-M. Song, Y. Wu, G. Liu, and Q. Xu, *J. Alloys Compd.* 487 (**2009**) 214–217.

[176] D.-J. Lee, K.-S. Lee, S.-T. Myung, H. Yashiro, and Y.-K. Sun, *J. Power Sources* 196 (**2011**) 1353–1357.

[177] H. J. Lee, S. B. Kim, and Y. J. Park, *Nanoscale Res. Lett.* (**2012**) 7:16.

[178] M. Ritala, M. Leskelä, E. Nykänen, P. Soininen, and L. Niinistö, *Thin Solid Films* 225 (**1993**) 288–295.

[179] R. F. Krause Jr. and T. B. Douglas, *J. Phys. Chem.* 72 (**1968**) 3444–3451.

[180] F. Rousseau, A. Jain, T. T. Kodas, M. Hampden-Smith, J. D. Farr, and R. Muenchausen, *J. Mater. Chem.* 2 (**1992**) 893–894.

[181] M. Putkonen, T. Sajavaara, P. Rahkila, L. Xu, S. Cheng, L. Niinistö, and H. J. Whitlow, *Thin Solid Films* 517 (**2009**) 5819–5824.

[182] J. Ihanus, M. Ritala, M. Leskelä, and E. Rauhala, *Appl. Surf. Sci.* 112 (**1997**) 154–158.

[183] E. Thimsen, Q. Peng, A. B. F. Martinson, M. J. Pellin, and J. W. Elam, *Chem. Mater.* 23 (**2011**) 4411–4413.

[184] J. R. Bakke, J. T. Tanskanen, H. J. Jung, R. Sinclair, and S. F. Bent, *J. Mater. Chem.* 21 (**2011**) 743–751.

[185] I. Stassen, M. Styles, G. Grenci, H. Van Gorp, W. Vanderlinden, S. De Feyter, P. Falcaro, D. De Vos, P. Vereecken, and R. Ameloot, *Nat. Mater.* 15 (**2016**) 304–310.

[186] T. Oi and K. Miyauchi, *Mat. Res. Bull.* 16 (**1981**) 1281–1289.

[187] V. A. Pustovarov, I. N. Ogorodnikov, S. I. Omelkov, M. S. Molokeev, A. V. Kozlov, and L. I. Isaenko, *Opt. Mater.* 49 (**2015**) 201–207.

[188] Y. Tao, F. Gitmans, Z. Sitar, H. Pierhöfer, A. Kündig, I. Gamboni, and P. Günter, *Ferroelectrics* 201 (**1997**) 245–253.

[189] T.-F. Yi, L.-J. Jiang, J. Shu, C.-B. Yue, R.-S. Zhu, and H.-B. Qiao, *J. Phys. Chem. Solids* 71 (**2010**) 1236–1242.

[190] Y.-Q. Wang, L. Gu, Y.-G. Guo, H. Li, X.-Q. He, S. Tsukimoto, Y. Ikuhara, and L.-J. Wan, *J. Am. Chem. Soc.* 134 (**2012**) 7874–7879.

[191] N. N. Greenwood and A. Earnshaw (**1998**). *Chemistry of the Elements*, 2nd edition (pages 976–983). Oxford, UK: Butterworth Heinemann.

[192] H. Kleykamp, *Fusion Eng. Des.* 61–62 (**2002**) 361–366.

[193] Ya. V. Baklanova, A. V. Ishchenko, T. A. Denisova, L. G. Maksimova, B. V. Shulgin, V. A. Pustovarov, and L. V. Viktorov, *Opt. Mater.* 34 (**2012**) 1037–1041.

[194] Z. Miao, H. Ni, H. Zhang, C. Wang, J. Fang, and G. Yang, *J. Power Sources* 264 (**2014**) 147–154.

[195] Y. Xu, Y. Liu, Z. Lu, H. Wang, D. Sun, and G. Yang, *Appl. Surf. Sci.* 361 (**2016**) 150–156.

[196] Y. Dong, Y. Zhao, H. Duan, and J. Huang, *Electrochim. Acta* 161 (**2015**) 219–225.

[197] D. Cruz, H. Pfeiffer, and S. Bulbulian, *Solid State Sci.* 8 (**2006**) 470–475.

[198] J. Ida, R. Xiong, and Y. S. Lin, *Sep. Purif. Technol.* 36 (**2004**) 41–51.

[199] N. Yesibolati, M. Shahid, W. Chen, M. N. Hedhili, M. C. Reuter, F. M. Ross, and H. N. Alshareef, *Small* 10 (**2014**) 2849–2858.